Superfund Records Center
SITE: Centredale
BREAK: 3.7
OTHER:

Battelle
The Business of Innovation

US ARMY CORPS
OF ENGINEERS
New England District

Contract No. DACW33-01-D-0004
Delivery Order No. 01
November 2004

Final Technical Memorandum

Sediment Stability Study

Centredale Manor Restoration Project Superfund Site North Providence, Rhode Island

SDMS DocID 206723

FINAL TECHNICAL MEMORANDUM

Sediment Stability Study

Centredale Manor Restoration Project Superfund Site
North Providence, Rhode Island

CONTRACT NUMBER: DACW33-01-D-0004
DELIVERY ORDER NO. 01

Submitted to

Department of the Army
U.S. Army Corps of Engineers
North Atlantic Division
New England District

November 2004

Prepared by

Quantitative Environmental Analysis, LLC
Montvale, NJ

Under contract to

BATTELLE
397 Washington Street
Duxbury, MA 02332
(781) 934-0571

TABLE OF CONTENTS

1.0 INTRODUCTION 1-1
1.1 Objective and Approach 1-1
1.2 Report Organization 1-2

2.0 DATA-BASED STABILITY ANALYSES 2-1
2.1 Bulk Bed Property Data 2-1
2.1.1 Allendale Pond 2-1
2.1.2 Lyman Mill Pond 2-2
2.1.3 Comparison of Bulk Bed Properties 2-2
2.2 Geochronology Analyses 2-2
2.2.1 ^{210}Pb Data Analysis 2-2
2.2.2 ^{137}Cs Data Analysis 2-4
2.2.3 Comparison of Sedimentation Rates Based on ^{210}Pb and ^{137}Cs Data 2-5
2.3 Dioxin Bed Concentration Data 2-5
2.4 Dioxin Water-Column Concentration Data 2-5

3.0 MODEL-BASED STABILITY ANALYSES 3-1
3.1 Hydrodynamic Model Development 3-1
3.1.1 Geometry and Bathymetry 3-1
3.1.2 Boundary Conditions 3-1
3.1.3 Model Calibration 3-2
3.2 Rare Flood Simulations 3-3
3.2.1 Estimates of Flood Flow Rate 3-3
3.2.2 Estimating Bed Stability 3-3
3.2.3 Allendale Pond Results 3-4
3.2.4 Lyman Mill Pond Results 3-6
3.3 Sensitivity Analysis 3-7
3.3.1 Sensitivity Analysis: Bottom Roughness 3-7
3.3.2 Sensitivity Analysis: Erosion Potential Parameters 3-8
3.3.3 Sensitivity Analysis: Dry Density 3-9
3.4 Summary of Model Results 3-9
3.5 Model Limitations 3-10

4.0 CONCEPTUAL SITE MODEL FOR SEDIMENT TRANSPORT 4-1

5.0 CONCLUSIONS RELATED TO BED STABILITY 5-1

6.0 REFERENCES 6-1

LIST OF TABLES

Table 2-1. Average Content of Clay/Silt, Sand and Gravel in Allendale and Lyman Mill Ponds 2-1
Table 2-2. Estimated Sedimentation Rates Based on ^{210}Pb Data. 2-3
Table 2-3. Estimated Ranges of Sedimentation Rates. 2-4
Table 2-4. Spatial Extent of Zones Used in Non-Resuspending Dioxin Flux Analysis. 2-6
Table 2-5. Statistics for Dioxin Concentration in Five Zones (Oct-Nov 1999 Data). 2-6
Table 2-6. Statistics for Dioxin Load in Five Zones (Oct-Nov 1999 Data) 2-7
Table 3-1. Flow Rates for Rare Flood Simulations. 3-3
Table 3-2. Resuspension Parameters Used in Scour Depth Analysis. 3-4
Table 3-3. Potential Scour Areas in Allendale Pond. 3-5

Table 3-4. Areas of Potential Significant Scour in Allendale Pond....3-5
Table 3-5. Impacts of Bed Scour in Allendale Pond....3-6
Table 3-6. Potential Scour Areas in Lyman Mill Pond....3-6
Table 3-7. Areas of Potential Significant Scour in Lyman Mill Pond....3-6
Table 3-8. Impacts of Bed Scour in Lyman Mill Pond....3-7
Table 3-9. Sensitivity to Bottom Roughness Variation: Allendale Pond, 100-Year Flood....3-8
Table 3-10. Sensitivity to Bottom Roughness Variation: Lyman Mill Pond, 100-Year Flood....3-8
Table 3-11. Sensitivity of Erosion Mass to Erosion Parameters (100-Year Flood)....3-9

Appendix A: Figures

ABBREVIATIONS AND ACRONYMS

1940-TH	1940 time horizon
95% CI	95 percent confidence interval
cfs	cubic feet per second
COC	Chemical-of-concern
CSM	Conceptual site model
D50	50th percentile (median) particle diameter
D90	90th percentile particle diameter
EFDC	Environmental Fluid Dynamics Code
FEMA	Federal Emergency Management Agency
FIS	Flood Insurance Study
FS	Feasibility Study
QEA	Quantitative Environmental Analysis, LLC
RI	Remedial Investigation
TEQ	Toxic Equivalency Quotient
USACE	United States Army Corps of Engineers
USEPA	United States Environmental Protection Agency
USGS	United States Geological Survey

1.0 INTRODUCTION

The U.S. Environmental Protection Agency (USEPA) Region I and U.S. Army Corps of Engineers (USACE) New England District are conducting a Remedial Investigation and Feasibility Study (RI/FS) for the Centredale Manor Restoration Project Superfund Site (i.e., the site), located in North Providence, Rhode Island. As part of the RI/FS, a sediment stability study was conducted at the site. The results of that study are presented in this report.

A sediment stability evaluation is used to assess the impacts of sediment erosion, transport, and deposition processes on surficial sediment bed and water column concentrations of a chemical-of-concern (COC) within a river channel. Thus, a general understanding of sediment transport processes is important when conducting a sediment stability study. Stability evaluations consider both the hydrodynamic forces that induce sediment resuspension and properties of the sediment bed that influence erosion rates. Erosion from a sediment bed occurs through two modes of transport: 1) bed load transport, which is the near-bed transport of sand and gravel; and 2) suspended load transport, which is resuspension of clay, silt and fine sand into the water column. The eroded sediment particles eventually deposit, or return to the sediment bed, at a different location.

The assessment of the efficacy of remedial alternatives for contaminated sediment deposits generally includes a sediment stability analysis. Determining whether a sediment deposit is stable or unstable typically involves evaluating the impact of sediment transport processes on COC concentrations in the bioavailable layer and the associated effects of remedial alternatives on mitigating those impacts. Erosion potential of the overlying portion of the sediment bed will determine whether or not the elevated COC concentrations become bioavailable at some point in the future. Re-exposure of the elevated concentrations to the bioavailable layer may occur due to bed elevation changes occurring over two time scales: 1) net erosion during a high-energy event (e.g., flood in a river); and 2) long-term bed degradation (e.g., changes on decadal time scales). Another process that must be considered is natural recovery, which is the burial of high-concentration COC deposits by subsequent deposition of low-concentration COC (i.e., cleaner) sediment. Erosion, transport, and deposition, and therefore natural recovery, are generally both temporally and spatially variable within a contaminated sediment site.

Erosion is caused by physical forces on the sediment bed. These forces are typically generated by two hydrodynamic processes: current velocity and surface waves. These processes induce erosion by applying a shear stress (i.e., force per unit area) on the sediment bed that exceeds the critical value for the bed to remain in place (i.e., critical shear stress). The sediment bed resists erosion through a combination of gravitational force on particles, physical structure of the bed, and cohesive forces holding the bed together. These cohesive forces depend on various sediment physical properties, including bulk density, mineralogy, grain size distribution, gas content, and organic content.

1.1 Objective and Approach

Sediment stability is an important issue when considering the efficacy of various remedial alternatives at the site. While this study considers site-specific issues or questions, the primary issues that this study focuses on, with respect to remedial alternative evaluation, are:

- Potential for short- and long-term sediment transport processes to re-distribute bed contaminants within Allendale and Lyman Mill Ponds and downstream of Lyman Mill Dam.

- The impact of sediment transport processes on the natural recovery rate of bed concentrations in the surface layer.

The specific questions addressed in this sediment stability evaluation are as follows:

- What is the impact of floods of various magnitudes on surficial dioxin TEQ concentrations in Allendale and Lyman Mill Ponds?
    - What scour depth will be caused by floods of various magnitudes?
    - Where is scour likely to occur within the ponds?

- What effect will different remedial alternatives have on mitigating the impacts of a rare (i.e., 100-year) flood?

A two-phased approach was used to address these questions as described in the Final Sediment Stability Work Plan (Quantitative Environmental Analysis [QEA] 2004). In Phase I, site data were compiled, analyzed and synthesized to develop a coherent understanding of sediment transport in the study area. The results of the data synthesis task were used to develop a Conceptual Site Model (CSM) for sediment transport. A CSM is an important component of a sediment stability analysis because consistency must be maintained between the CSM and the results of quantitative and qualitative sediment stability analyses. The sediment transport CSM is a qualitative description of the processes (e.g., deposition and erosion) and system characteristics (e.g., upstream and tributary sediment loads, spatial distribution of bed properties) that control sediment dynamics within the study area.

In Phase II, a hydrodynamic model was developed and applied. The hydrodynamic model was used to evaluate the potential impacts of a range of floods on bed stability. Impacts of floods with 5-, 10-, 25-, 50- and 100-year return periods were investigated. For each flood simulation, two methods were used to analyze the potential impacts on bed stability: 1) comparison of bottom shear stress and current velocity to critical values for those parameters; and 2) estimation of scour depth.

1.2 Report Organization

This report consists of six sections and one appendix, as follows:

Section 1:	Introduction
Section 2:	Data-Based Stability Analyses
Section 3:	Model-Based Stability Analyses
Section 4:	Conceptual Site Model for Sediment Transport
Section 5:	Conclusions Related to Bed Stability
Section 6:	References
Appendix A:	Figures

2.0 DATA-BASED STABILITY ANALYSES

The main objective of the data-based analyses presented in this section is to develop an understanding of data and processes related to bed stability in Allendale and Lyman Mill Ponds. The primary data sets used in these analyses were collected in May 2003 and include data on bulk bed properties, radioisotope activities and dioxin concentrations. In addition, dioxin water-column concentration data obtained during a low-flow period in October-November 1999 were analyzed to develop an understanding of bed fluxes from the pond under non-resuspending conditions.

2.1 Bulk Bed Property Data

Sediment core samples were collected in Allendale and Lyman Mill Ponds during May 2003. Core sample locations are shown on Figures 2-1 and 2-2. Bulk bed property data from these samples were evaluated to develop a general understanding of the type of sediment in the ponds and associated physical properties. A detailed mapping of sediment bed type, i.e., delineation of cohesive and noncohesive bed areas, within the two ponds is not possible at the present time due to technical difficulties associated with the side-scan sonar survey conducted during October 2002 (Shields 2003).

2.1.1 Allendale Pond

The sediment bed in Allendale Pond is generally composed of cohesive sediment, i.e. muddy sediment with some sand and gravel. Surface-layer sediment (i.e., approximately top 6-12 inches) in Allendale Pond is primarily composed of fine-grained cohesive sediment with sandy sediment found in the deeper portions of the bed. Core logs presented in Corcoran (2004) show that, generally, surficial sediment is classified as peat. Grain size distribution data for surficial sediments were collected from 15 cores, with 13 cores being classified as cohesive sediment. A core was classified as cohesive if it met the following criteria: median particle diameter (D_{50}) < 250 µm and clay/silt content > 15 percent (Ziegler and Nisbet 1994). The two cores classified as noncohesive had D_{50} values of 900 and 23,500 µm (cores CMS-SD-4214 and CMS-SD-4208, respectively), with clay/silt content less than 3 percent.

Frequency distributions of four bulk bed properties for the 13 surficial cores classified as cohesive are shown on Figure 2-3: organic matter content, dry (bulk) density, median particle diameter (D_{50}), and 90th percentile particle diameter (D_{90}). Organic matter content ranges from about 23 to 57 percent, with a median value of 33 percent. Dry (bulk) density of surficial layer sediment has an average value of 0.76 g/cm^3, with a range of 0.47 to 1.11 g/cm^3. The 95 percent confidence interval (95% CI) about the mean value is 0.63 to 0.89 g/cm^3. For the 13 cohesive cores, D_{50} values range from 10 to 113 µm and the clay/silt content varies from 39 to 98 percent.

In addition to the surficial data described above, grain size distribution information was collected from deeper segments of sediment cores in both ponds. Frequency distributions of clay/silt, sand and gravel content of surficial and subsurface Allendale Pond sediments are presented on Figure 2-4. Average contents of the three sediment classes are listed in Table 2-1.

Table 2-1. Average Content of Clay/Silt, Sand and Gravel in Allendale and Lyman Mill Ponds.

Sediment Type	Allendale Pond	Lyman Mill Pond
Clay/silt	41	67
Sand	49	30
Gravel	10	3

2.1.2 Lyman Mill Pond

The Lyman Mill Pond bed is primarily composed of cohesive sediment. Core logs indicate that the upper 6-12 inches of the bed is generally classified as muck, with coarser material occurring deeper in the bed (Corcoran 2004). Figure 2-5 presents frequency distributions of bed property data measured in surface-layer samples from cores collected from this pond. The median value of organic matter content is approximately 25 percent, with most of the data ranging from about 18 to 27 percent (one sample has an organic content of 60 percent). The mean dry density value of surficial sediment is 0.59 g/cm^3, with the 95% CI varying from 0.47 to 0.71 g/cm^3. Seven cores with grain distribution data are classified as cohesive sediment. The D_{50} values of surficial sediment in these cores range from 7 to 122 μm, with clay/silt content varying between 26 and 99 percent. Frequency distributions of clay/silt, sand and gravel content of Lyman Mill Pond sediments (all depths) are presented on Figure 2-6. Average contents of the three sediment classes are listed in Table 2-1.

2.1.3 Comparison of Bulk Bed Properties

The sediment bed in Lyman Mill Pond is generally finer (i.e., more clay/silt and less sand/gravel) than the bed in Allendale Pond. A large fraction of the coarse sediment (sand and gravel) entering the upstream pond (Allendale) will be deposited in that pond; the sand content of the suspended sediment load entering Lyman Mill Pond will be significantly less than the sand content flowing into Allendale Pond. This situation is typical for a river with a series of impoundments, such as occurs within the study area.

2.2 Geochronology Analyses

The radioisotopes cesium-137 (^{137}Cs) and lead-210 (^{210}Pb) are used to age-date sediments and to establish sedimentation rates in estuarine and freshwater systems (Olsen et al. 1978, Orson et al. 1990). Cesium-137 concentrations in sediments are derived from atmospheric fallout from nuclear weapons testing. The first occurrence of ^{137}Cs in sediments generally marks the year 1954, while peak concentrations correspond to 1963 (Simpson et al. 1976). Based on these dates, long-term average sedimentation rates can be computed by dividing the thickness of sediment between the sediment surface and the buried ^{137}Cs peak by the number of years between 1963 and the time of core collection (e.g., 41 years for a core collected in 2004).

Radon-222 (^{222}Rn) is a volatile, short-lived intermediate daughter of uranium-238 (^{238}U), a naturally-occurring radioisotope found in the earth's crust. Lead-210, which is a decay product of atmospheric ^{222}Rn, is present in sediments primarily as a result of recent atmospheric deposition. Sedimentation rates can be estimated using ^{210}Pb sediment data because of two facts. First, ^{210}Pb is deposited on the earth's surface at an approximately constant rate related to the volatilization rate of ^{222}Rn from the earth's surface. Second, the activity of ^{210}Pb in sediment decreases exponentially as a function of its decay half-life of 22.3 years. Thus, sedimentation rate can be estimated by analyzing the vertical profile of ^{210}Pb activity in a sediment core (Olsen et al. 1978, Orson et al. 1990, Robbins 1978).

Ten of the sediment cores collected in the two ponds during May 2003 were analyzed for radioisotopes (i.e., ^{210}Pb and ^{137}Cs activity). Nine cores are from Allendale Pond and one core is from Lyman Mill Pond (LPX-SD-4201, Figure 2-2). A preliminary evaluation of sedimentation rates for the cores was conducted by USACE (Corcoran 2004). The analyses presented in this section expand upon the USACE analysis, with an emphasis on evaluating uncertainty in the estimated sedimentation rates.

2.2.1 ^{210}Pb Data Analysis

The ^{210}Pb activity measured in a sediment core is the total activity ($^{210}Pb_T$), which is composed of two components: 1) unsupported ^{210}Pb ($^{210}Pb_u$), which represents ^{210}Pb due to atmospheric deposition; and 2) supported ^{210}Pb ($^{210}Pb_s$), which is background ^{210}Pb activity in the sediment. Sedimentation rate analysis

uses unsupported ^{210}Pb activity data. Thus, the first step in the analysis is to determine $^{210}Pb_s$ for a core in order to calculate $^{210}Pb_u$:

$$^{210}Pb_u = {}^{210}Pb_T - {}^{210}Pb_s \qquad (2\text{-}1)$$

Average values of $^{210}Pb_s$ were determined for each core (see Table 2-2). Data points used to calculate the average value in each core are shown as open circles on the left-hand panels of Figures 2-7 to 2-16.

Table 2-2. Estimated Sedimentation Rates Based on ^{210}Pb Data.

Core Number	Average $^{210}Pb_s$ Activity (pCi/g dry)	QEA Estimated Sedimentation Rate (cm/yr)	USACE Estimated Sedimentation Rate (cm/yr)
CMS-SD-4204	2.1	0.17	0.23
CMS-SD-4206	1.7	0.24	0.29
CMS-SD-4209	1.0	0.65	0.49
CMS-SD-4210	1.2	2.8	0.64
CMS-SD-4212	0.95	0.34	0.34
CMS-SD-4213	0.97	0.43	0.43
CMS-SD-4218	1.3	0.68	0.40
CMS-SD-4219	0.52	0.90	0.33
CMS-SD-4222	0.95	0.76	0.52
LPX-SD-4201	0.56	0.30	0.33

The next step in the analysis is to evaluate the vertical profile of $^{210}Pb_u$ (unsupported) activity, which is presented for each of the ten cores on the left-hand panels of Figures 2-7 to 2-16. Unsupported $^{210}Pb_u$ activity data are transformed to $\ln(^{210}Pb_u)$ and plotted as a function of depth in the sediment bed (d_{bed}). A linear regression analysis of $\ln(^{210}Pb_u)$ versus d_{bed} (in feet) is conducted and the slope of the regression line (m) is determined. Sedimentation rate (^{Pb}R) is calculated using:

$$^{Pb}R = -0.948/m \qquad (2\text{-}2)$$

where ^{Pb}R has units of cm/yr.

The estimated sedimentation rates for the ten cores range from 0.17 to 2.8 cm/yr (Table 2-2). Table 2-2 also includes sedimentation rates determined from the USACE analysis (Corcoran 2004). Comparison of the QEA and USACE results indicate that significant differences in estimated rates exist for several of the cores. These differences are primarily due to the choice of $^{210}Pb_u$ data points used in the regression analysis. Because an objective method for picking a unique set of $^{210}Pb_u$ data points for the regression analysis does not exist, professional judgment must be used to select these data points.

Differences in the QEA and USACE sedimentation rate results illustrate the uncertainty inherent in the analysis of ^{210}Pb data. While each rate presented in Table 2-2 may be thought of as the 'best' estimate of average sedimentation rate for a particular core, the uncertainty associated with that 'best' estimate should be quantified. Thus, the following procedure was developed for evaluating uncertainty in the sedimentation rate analysis.

For each core, a total of N $^{210}Pb_u$ data points were used in the regression analysis to determine m and ^{Pb}R. For convenience, the sedimentation rate determined from the regression analysis conducted with N data points is denoted as $^{Pb}R_N$. Because a large portion of the uncertainty in results is due to the subset of data

points used in the regression analysis, the variability in ^{Pb}R is estimated by creating N sub-samples, with each sub-sample consisting of (N-1) data points. A sub-sample is generated by removing one data point from the original group of N values. This process is repeated until each data point has been removed one time. For each of the sub-samples from a particular core, the regression analysis is conducted and a regression slope is determined, producing N values of m (i.e., m_n for n = 1, N). Statistical analysis of m_n yields a 95% CI for m for each core. The range of sedimentation rates for a particular core was estimated by using the upper- and lower-bound values of the 95% CI for m in Equation (2-2). The resulting ranges of sedimentation rates are tabulated in Table 2-3.

Table 2-3. Estimated Ranges of Sedimentation Rates.

Core Number	Sedimentation Rate Range: ^{210}Pb Analysis (cm/yr)	Sedimentation Rate Range: ^{137}Cs Analysis (cm/yr)
CMS-SD-4204	0.11 → 0.30	0.33 → 0.52
CMS-SD-4206	0.20 → 0.31	NA
CMS-SD-4209	0.63 → 0.96	0.48 → 1.04
CMS-SD-4210	1.55 → 7.29	0.56 → 1.12
CMS-SD-4212	0.26 → 0.45	0.26 → 0.52
CMS-SD-4213	0.53 → 0.59	0.56 → 0.82
CMS-SD-4218	0.53 → 0.84	0.67 → 1.04
CMS-SD-4219	0.58 → 1.41	NA
CMS-SD-4222	0.73 → 1.02	0.33 → 0.74
LPX-SD-4201	0.26 → 0.35	0.11 → 0.45

NA = no analysis due to non-interpretable ^{137}Cs profile

2.2.2 ^{137}Cs Data Analysis

The average sedimentation rate based on location of the peak ^{137}Cs concentration in a core (^{Cs}R, in cm/yr) is calculated using:

$$^{Cs}R = d_p / 40 \qquad (2\text{-}3)$$

where d_p is depth of the peak concentration (cm) and 40 years is the lapsed time period between 1963 and core collection in 2003. Vertical profiles of ^{137}Cs activity are presented on the middle panels of Figures 2-7 to 2-16. Examination of these profiles shows that peak ^{137}Cs concentrations are evident in eight of the ten cores, with cores CMS-SD-4206 and CMS-SD-4219 having non-interpretable profiles. The ^{137}Cs peaks, however, are generally not well defined or highly resolved, i.e., relatively large vertical distances exist between sample points in the core. Thus, the average sedimentation rate cannot be estimated with a high-degree of accuracy based on the depth of the ^{137}Cs peak.

The uncertainty in the location of the ^{137}Cs peak in a core is addressed as follows. As with the ^{210}Pb uncertainty analysis, the ^{137}Cs data are used to determine a range of sedimentation rates for a particular core. The first step in the analysis is to identify the peak ^{137}Cs concentration ($^{137}Cs_{peak}$) in a core. This value represents the average activity in a sediment segment that is typically 0.05 ft (1.5 cm) thick. Vertical spacing between segments is generally greater than 0.05 ft. The next step is to define the 1963 time horizon in a core as the zone in which the maximum ^{137}Cs concentration exists. This zone (i.e., 1963 time horizon) is assumed to extend from the lower-edge of the segment immediately above $^{137}Cs_{peak}$ to the upper-edge of the segment immediately below $^{137}Cs_{peak}$ (see middle panels of Figures 2-7 to 2-16); the 1963 time horizon extends from d_{lower} to d_{upper} in the core. Finally, these two depths are used in Equation (2-3) to calculate a range for ^{Cs}R in a particular core. The results of this analysis are tabulated in Table 2-3.

2.2.3 Comparison of Sedimentation Rates Based on ^{210}Pb and ^{137}Cs Data

Independent estimates of sedimentation rate are provided by the ^{210}Pb and ^{137}Cs analyses. Combining the estimated rates from these two approaches yields an improved understanding of the depositional environment in Allendale and Lyman Mill Ponds. Frequency distributions of upper- and lower-bound estimates of sedimentation rates based on the ^{210}Pb and ^{137}Cs analyses (see Table 2-3) in Allendale Pond are presented on Figure 2-17. Note that the results for core CMS-SD-4210 are excluded from Figure 2-17 because those results are exceptionally high, inconsistent with ^{137}Cs results for that core, and, hence, are considered to be unreliable. These results indicate that, generally, the ^{210}Pb and ^{137}Cs analyses produce consistent upper- and lower-bound estimates of sedimentation rate. Median values of lower- and upper-bound sedimentation rates are about 0.5 and 0.8 cm/yr, respectively. While there is variability in sedimentation rate in Allendale Pond, with an approximate overall range of 0.1 to 1.5 cm/yr, a reasonable estimate of a representative (or average) range of sedimentation rate for this pond is 0.5 to 0.8 cm/yr.

2.3 Dioxin Bed Concentration Data

Sediment samples from the geochronology cores discussed in Section 2.2 were also analyzed for dioxin concentrations. For convenience, dioxins in this analysis are expressed as toxic equivalency quotient (TEQ) concentration. Vertical profiles of dioxin TEQ concentration in the ten geochronology cores are displayed on the right-hand panel of Figures 2-7 to 2-16. In general, maximum TEQ concentrations in the cores are less than 20 µg/kg, with the exception of core CMS-SD-4213 (maximum of approximately 50 µg/kg). In addition, maximum concentrations usually occur in the upper 1 ft (30 cm) of the core.

Chemical manufacturing activities at the Centredale Manor site began in approximately 1940. Therefore, it is reasonable to assume that negligible dioxin concentrations will occur below the 1940 time horizon (1940-TH) in the sediment bed. Thus, determining the 1940-TH in the sediment bed may provide useful information for developing certain remedial alternatives for Allendale and Lyman Mill Ponds.

The depth of the 1940-TH is calculated by multiplying sedimentation rate by the time period between 1940 and 2003. Uncertainty in the estimated sedimentation rate, however, must be incorporated into the time horizon, which is accomplished by using the ranges listed in Table 2-3. This approach yields the 1940-TH ranges, based on the ^{210}Pb and ^{137}Cs analyses, shown on Figures 2-7 to 2-16 (represented as the cross-hatched zones on the figures). Examination of these figures shows that the 1940-TH is relatively thick in some cores (approximately 1 ft) due to uncertainty in sedimentation rate. The range of 1940-TH depths in Allendale Pond is indicated on Figure 2-18, which presents the frequency distributions of minimum and maximum depths of the 1940-TH. These results indicate that a representative estimate for the 1940-TH in Allendale Pond is a depth between 1 and 2 ft.

2.4 Dioxin Water-Column Concentration Data

Water column samples were collected at various locations in the study area during October and November 1999 (TTNUS 2000). Flow rates in the river during the water column sampling ranged from about 25 to 110 cubic feet per second (cfs). The average flow rate at the U.S. Geological Survey (USGS) Centredale gaging station is approximately 73 cfs (USGS 1996). Thus, the sampling was carried out during low to moderate flow conditions during which it is expected that sediment resuspension does not occur. Under non-resuspending conditions, COC flux (e.g., dioxin flux) from the bed to the water column occurs due to a combination of various processes, including diffusion, bioturbation and groundwater flux. To evaluate the validity of the assumption that dioxin is not being added to the water column via bed erosion, the correlation between total dioxin water-column concentration and flow rate during the 1999 sampling period is shown on Figure 2-19. If significant bed erosion were occurring, it is expected that dioxin water-column concentration would increase with increasing flow rate; no increase in concentration

with flow rate is evident during the sampling period. Therefore, this data set may be used to evaluate non-resuspension loading of dioxin to the water column within the study area.

Significant variation in dioxin water-column concentrations occurred within the study area during the 14 days that samples were collected between October 25 and November 10, 1999; total dioxin concentrations ranged from 11 to 8,900 pg/L. The spatial distribution of total dioxin concentration during the low-flow sampling period in 1999 is shown on Figure 2-20. Examination of this spatial distribution suggests that the study area may be separated into five zones, which are defined in Table 2-4 and shown on Figures 2-21 and 2-22. Frequency distributions of total dioxin concentrations in the five zones are shown on Figure 2-23, while statistics for concentrations in each zone are tabulated in Table 2-5. These results indicate an interesting spatial pattern in total dioxin concentration. A significant increase in dioxin concentration occurs between Zones 1 and 2 (i.e., from the upstream area to the source/upstream portion of Allendale Pond area), with average concentrations increasing from 27 to 1,160 pg/L. Moving from Zone 2 to 3 (i.e., from upstream portion to downstream portion in Allendale Pond), concentrations decrease to levels observed in Zone 1. In Zone 4 (i.e., upstream portion of Lyman Mill Pond), dioxin water-column concentrations increase again (average value of 105 pg/L). Similar to the pattern in Allendale Pond, concentrations in Zone 5 decline to values comparable to Zone 1 and 3 concentrations.

Table 2-4. Spatial Extent of Zones Used in Non-Resuspending Dioxin Flux Analysis.

Zone	General Description	Distance Upstream from Lyman Mill Dam (ft)
1	Upstream area	0 → 1,500
2	Source area and upstream portion of Allendale Pond	1,500 → 4,300
3	Downstream portion of Allendale Pond	4,300 → 5,300
4	Upstream portion of Lyman Mill Pond	5,300 → 7,300
5	Downstream portion of Lyman Mill Pond	7,300 → 9,000

Table 2-5. Statistics for Dioxin Concentration in Five Zones (Oct-Nov 1999 Data).

Zone	No. Observations	Average (pg/L)	Standard Deviation (pg/L)	95% CI (pg/L)
1	3	27	7.1	9 → 45
2	8	1,160	3,130	0 → 3,800
3	5	28	9.9	16 → 40
4	9	105	99	29 → 180
5	5	22	14	5 → 39

Dioxin loads were calculated by multiplying the observed dioxin water-column concentration by the daily-average flow rate for the day of sample collection. The calculated water-column loads have a spatial pattern that is similar to the one observed for water-column concentrations (Figure 2-24). Higher loads occur in Zones 2 and 4, while lower loads are observed in Zones 1, 3 and 5. Dioxin loads range from about 2 to 870 mg/day during this low-flow period. Frequency distributions of dioxin loads in the five zones are shown on Figure 2-25; load statistics are listed in Table 2-6.

Table 2-6. Statistics for Dioxin Load in Five Zones (Oct-Nov 1999 Data).

Zone	No. Observations	Average (mg/day)	Standard Deviation (mg/day)	95% CI (mg/day)
1	3	4.6	1.2	1.6 → 7.6
2	8	115	310	0 → 380
3	5	6.0	2.2	3.3 → 8.7
4	9	17	18	3 → 31
5	5	4.2	2.5	1.1 → 7.3

Results of the water-column load analysis provide insights about dioxin loading to the water column during non-resuspending conditions in the study area. First, dioxin loads of approximately 110 and 11 mg/day, on average, are added to the water column in Zones 2 and 4, respectively. It assumed that the sediment bed is a source of the dioxin loading to the water column in Zones 2 and 4; mass transfer of pore water from the bed to water column (due to non-resuspension processes such as diffusion, bioturbation and groundwater advection) is probably the main source of dioxin. Another possible source of dioxin in Zone 2 is contaminated groundwater discharge to the river in the vicinity of the Brook Village parking lot, where the dioxin TEQ concentration in groundwater was 4,180 pg/L in 2002 (Battelle 2003). Second, transport processes within Allendale and Lyman Mill Ponds appear to remove the increased loads (in Zones 2 and 4) such that loads in the downstream portions of each pond return to background levels. Background dioxin loads in the river appear to be approximately 4 mg/day. It is unclear what processes cause the removal of the loads added in Zones 2 and 4. Third, minimal increase in dioxin loading occurs between the upstream boundary of the study area and Lyman Mill Dam; minimal net export of dioxin from the two ponds occurs during low-flow, non-resuspending conditions. The validity of these hypotheses on low-flow dioxin loads should be tested with additional data. The October-November 1999 data set is limited, with only three to five samples in Zones 1, 3 and 5. Thus, uncertainty exists in the estimates of dioxin loads and the conclusions/insights developed from this analysis.

3.0 MODEL-BASED STABILITY ANALYSES

The primary objective of the modeling analyses is to estimate the potential impacts of rare floods on bed stability. This goal is accomplished by using a hydrodynamic model to predict current velocity and bottom shear stress in Allendale and Lyman Mill Ponds during rare floods. Information from the hydrodynamic model is used to estimate areas of potential erosion in the ponds and approximate scour depths within those areas.

3.1 Hydrodynamic Model Development

The hydrodynamic model used in this study is an enhanced version of the Environmental Fluid Dynamics Code (EFDC). This model (EFDC) is an USEPA-approved model which QEA has modified so as to make the model easier to use; the QEA version of EFDC is non-proprietary. EFDC is a sophisticated three-dimensional, time-dependent, boundary-fitted hydrodynamic model capable of simulating density-driven circulation in rivers, reservoirs, lakes, estuaries and coastal waters. The model has been extensively tested and applied to a wide range of aquatic systems. For this study, the model was used in two-dimensional, vertically-averaged mode, which is a valid approximation for the shallow, non-stratified flow conditions that exist in the two ponds during flood conditions; a two-dimensional model produces results that are sufficiently accurate for this study.

3.1.1 Geometry and Bathymetry

The modeling domain extends from an upstream boundary at the Route 44 Bridge to a downstream boundary at Lyman Mill Dam. Flow is constrained within the normal shoreline, i.e., in-bank flow conditions, of the river and ponds; effects of floodplain flow during over-bank floods are neglected in all simulations. This approximation produces conservative results, i.e., predicted current velocities are higher by neglecting floodplain effects. Bathymetric model inputs were developed from water depth data collected during the October 2002 geophysical survey (Shields 2003). These data were limited to Allendale and Lyman Mill Ponds. Bathymetric data are not available for the river channels upstream of the two ponds. As a first approximation, equilibrium water depths were assumed to be 1.2 and 0.72 m in the channels upstream of Allendale and Lyman Mill Ponds, respectively. This approximation is valid because the channels are not a focus of this study and uncertainty in channel bathymetry has minimal impact on model predictions in the ponds.

Two numerical grids were generated to represent the study area: 1) Allendale Pond (extending from the Route 44 Bridge to Allendale Dam), and 2) Lyman Mill Pond (extending from Allendale Dam to Lyman Mill Dam). The grids were constructed using 5-meter square grid cells to delineate the geometry and bathymetry of each pond. A total of 2,201 and 4,157 grid cells were used for Allendale and Lyman Mill Ponds, respectively.

3.1.2 Boundary Conditions

Flow rate is specified at the upstream (inflow) boundary of the model. Discharge data collected at the USGS gaging station at Centredale (located near the Route 44 Bridge) were used to specify the inflow boundary condition. It is assumed that tributary inflow within the study area is small compared to flow in the river (particularly during flood conditions) and, thus, can be neglected. Estimation of the magnitude of discharge during rare floods is discussed in Section 3.2.1.

Stage height (i.e., water surface elevation) as a function of flow rate at the dams is specified as the downstream boundary condition. No stage height data are available so a broad-crested weir formulation is used to estimate stage height at each dam (Roberson et al. 1998):

$$\eta = (Q / 3.3 L)^{0.67} \quad (3\text{-}1)$$

where η is depth of water over dam crest (ft), Q is flow rate (cfs) and L is length of dam crest (ft). Crest length of the Allendale and Lyman Mill Dams is 106 ft.

3.1.3 Model Calibration

The objective of calibrating the hydrodynamic model is to adjust effective bottom roughness (Z_o) such that agreement between observed and predicted stage height and current velocity is optimized. This model parameter (Z_o) affects bottom shear stress and, hence, current velocity and stage height.

Stage height and current velocity data are not available to calibrate and validate the hydrodynamic model. Lack of data made it necessary to investigate the following alternative method for calibrating the model. A Flood Insurance Study (FIS) was conducted by the Federal Emergency Management Agency (FEMA) for each pond. As part of the FIS, a one-dimensional (1-D) hydraulic model was developed and applied to Allendale and Lyman Mill Ponds. The 1-D model was used by FEMA to predict water surface elevation during a 100-year flood. Thus, it was envisioned that the two-dimensional (2-D) model used in the present study could be calibrated through use of the FIS 1-D model results.

An attempt was made to compare stage heights predicted by the 1-D and 2-D models during a 100-year flood. This attempt at calibrating the 2-D model, however, was problematic. Reasonable agreement between the 1-D and 2-D models was achieved for the spatial gradient in water surface elevation for Lyman Mill Pond. For Allendale Pond, however, the 1-D model predicted a high spatial gradient that the 2-D model could not reproduce. Closer examination of the discrepancy between the models revealed potential weaknesses with the FIS 1-D model. First, the reliability of the FIS 1-D model is uncertain because no information is available concerning model parameters or calibration results. It is likely that the 1-D model was not calibrated. Second, stage height at each dam during the 100-year flood for the 1-D model is approximately two times lower than the stage height estimated using Equation (3-1); stage height at the dam for the 1-D model appears to be unrealistically low. Third, the spatial gradient of the river channel (which is an input for the 1-D model) is approximately 10 times higher than the gradient estimated from topographic maps. Thus, it was concluded that the 2-D model could not be reliably calibrated through comparison to predictions of the FIS 1-D model.

Without a reliable method for calibrating the 2-D model, an objective approach for estimating Z_o is needed. This approach was developed as follows. Bottom shear stress (τ) is calculated using the quadratic stress formula (van Rijn 1993):

$$\tau = \rho_w C_f u^2 \quad (3\text{-}2)$$

where ρ_w is density of water, C_f is a bottom friction coefficient and u is depth-averaged velocity. The bottom friction coefficient depends on Z_o:

$$C_f = [2.5 \ln(0.5 h / Z_o)]^{-2} \quad (3\text{-}3)$$

where h is water depth. Now, the Nikuradse roughness height (k_s) depends on grain size distribution of the bed (van Rijn 1993):

$$k_s = 3 D_{90} \quad (3\text{-}4)$$

where D_{90} is the 90th percentile particle diameter. The Nikuradse and effective roughness heights are related as follows:

$$k_s = 24\, Z_o \qquad (3\text{-}5)$$

Thus, the effective roughness height in Equation (3-3) depends on D_{90}:

$$Z_o = D_{90} / 8 \qquad (3\text{-}6)$$

Grain size distribution data for the two ponds (see Section 2.1) are used to determine representative values of D_{90}; average values are 134 and 79 μm for Allendale and Lyman Mill Ponds, respectively.

3.2 Rare Flood Simulations

The hydrodynamic model was used to evaluate the potential impacts of rare floods on bed stability in Allendale and Lyman Mill Ponds. Five floods were simulated, corresponding to return periods of 5, 10, 25, 50 and 100 years.

3.2.1 Estimates of Flood Flow Rate

Historical flow rate data collected at the USGS gaging station at Centredale were used by USACE personnel to conduct a flood frequency analysis (M. Corcoran, personal communication, June 3, 2004). The results of this analysis are used in this study to define flow rates for floods with the following return periods: 5, 10, 25, 50 and 100 years. A summary of the flow rates associated with each flood return period is provided in Table 3-1.

Table 3-1. Flow Rates for Rare Flood Simulations.

Flood Return Period (years)	Flow Rate (cfs)
5	894
10	1,111
25	1,398
50	1,621
100	1,850

3.2.2 Estimating Bed Stability

The hydrodynamic model is used to evaluate the potential impacts of a range of floods on bed stability. Impacts of floods with 5-, 10-, 25-, 50- and 100-year return periods are investigated. For each flood simulation, two methods are used to analyze the potential impacts on bed stability: 1) comparison of bottom shear stress and current velocity to critical values of those parameters; and 2) estimation of scour depth.

Predicted current velocity is used to calculate bottom shear stress (τ), which is compared to a critical shear stress for erosion (τ_{cr}). Areas where the bottom shear stress is greater than the critical value (i.e., $\tau > \tau_{cr}$) correspond to areas that are subject to scour during a flood. Critical shear stress for cohesive sediment is variable and depends on the site-specific erosion properties of surficial sediments. Shaker studies of the resuspension properties of cohesive sediments in the Fox, Saginaw and Buffalo Rivers suggested an appropriate value for τ_{cr} of 0.1 Pa (Lick et al. 1995). A Sedflume study conducted in the Grand River yielded estimates of τ_{cr} ranging from approximately 0.1 to 1.6 Pa (Jepsen et al. 2001). Another Sedflume study examined Boston Harbor sediments, with values between approximately 0.1 and

5 Pa (Roberts et al. 2001). Generally, the higher critical shear stresses reported in the two Sedflume studies are for deeper sediment; surficial sediment typically has critical shear stresses in the lower portion of the range. Because uncertainty exists in the value of τ_{cr}, lower- and upper-bound estimates of 0.1 and 0.5 Pa, respectively, are used in this study. Areas of potential bed scour are determined using upper ($\tau_{cr,up}$ = 0.5 Pa) and lower ($\tau_{cr,low}$ = 0.1 Pa) bounds of critical shear stress. Areas where the bottom shear stress is less than the critical shear stress for erosion are conducive to deposition.

While the critical shear stress analysis provides information on areas of potential scour, comparing current velocity to a critical velocity may be used to identify areas of potentially significant scour (i.e., scour depth greater than approximately 1-2 cm). The 2 ft/s criterion is used as a threshold because it represents a current velocity above which significant bed scour may be expected (Graf 1971, USACE 1991); this criterion was used during a sediment stability study on the Grasse River (Alcoa 2002).

The second method uses predicted bottom shear stress to estimate scour depth in the two ponds. This approach will apply the Lick equation (Ziegler 2002):

$$\varepsilon = A\,(\tau/\tau_{cr} - 1)^n, \qquad \tau > \tau_{cr} \qquad (3\text{-}7)$$

where ε is resuspension potential (i.e., mass eroded per unit area); τ is bottom shear stress; τ_{cr} is critical bottom shear stress, assumed to be 0.1 Pa for this analysis (Ziegler 2002); A is site-specific constant; and n is site-specific exponent. A field study would be required to determine site-specific values of A and n for the study area, but a field study was not carried out as part of the present study. Results from studies carried out in other river systems provide sufficient data to make reasonable estimates of A and n for the Woonasquatucket River (Ziegler 2002). These approximate values (i.e., average values of A and n of 0.21 mg/cm^2 and 2.6, respectively) produce order-of-magnitude estimates of scour depths during a flood. Uncertainty in the values of A and n exists, but 95% CI for these two parameters have been determined (Ziegler 2002); lower- and upper-bound estimates of A and n were specified using information presented in Ziegler (2002), see Table 3-2.

Table 3-2. Resuspension Parameters Used in Scour Depth Analysis.

Type of Estimate	Eq. (3-3) Parameter: A (mg/cm^2)	Eq. (3-3) Parameter: n
Average	0.21	2.6
Lower-Bound	0.01	2.3
Upper-Bound	0.41	2.9

Scour depth is calculated using:

$$T = \varepsilon / \rho \qquad (3\text{-}8)$$

where T is scour depth (cm) and ρ is dry density of sediment (g/cm^3). As discussed in Section 2.1, 95% CI for dry density in Allendale and Lyman Mill Ponds are 0.63 to 0.89 g/cm^3 and 0.47 to 0.71 g/cm^3, respectively.

3.2.3 Allendale Pond Results

The spatial distribution of current velocity for the 100-year flood in Allendale Pond is shown on Figure 3-1. Similar velocity patterns are predicted for the 5-, 10-, 25, and 50-year floods except that current magnitude decreases with decreasing flow rate. Relatively high velocities occur in the upstream (inlet)

portion of the pond due to shallower depths and smaller cross-sectional area. Generally, higher velocities are found in the deeper central area of the pond.

Areas in the pond where bottom shear stress exceeds the upper- and lower-bound estimates of τ_{cr} (i.e., 0.1 and 0.5 Pa) for the five floods are presented on Figures 3-2 and 3-3. As is expected, areas of potential scour (i.e., $\tau > \tau_{cr}$) increase with increasing flow rate. Potential scour areas for each flood in Allendale Pond are tabulated in Table 3-3. Current velocities exceeding the critical velocity criterion for significant scour (i.e., 2 ft/s) are predicted in the areas shown on Figures 3-4 and 3-5. These areas are quantified and listed in Table 3-4. Note that total area of Allendale Pond is 4.49 hectares. The portion of Allendale Pond with shear stress greater than 0.1 and 0.5 Pa ranges from 37 to 63 and 6 to 21 percent, respectively, over the range of flow discharges. While erosion may occur in these areas, less than 5 percent of the pond will potentially experience significant scour due to velocities greater than 2 ft/s; these elevated velocities occur near the river inlet in the upstream portion of the pond.

Table 3-3. Potential Scour Areas in Allendale Pond.

Flood Return Period (years)	Area with $\tau > 0.1$ Pa (hectares)	% of Pond Area with $\tau > 0.1$ Pa	Area with $\tau > 0.5$ Pa (hectares)	% of Pond Area with $\tau > 0.5$ Pa
5	1.67	37	0.26	6
10	2.19	49	0.37	8
25	2.57	57	0.56	13
50	2.72	61	0.75	17
100	2.84	63	0.95	21

Table 3-4. Areas of Potential Significant Scour in Allendale Pond.

Flood Return Period (years)	Area with u > 2 ft/s (hectares)	% of Pond Area with u > 2 ft/s
5	0.06	1
10	0.11	2
25	0.17	4
50	0.20	4
100	0.25	5

Scour depths in Allendale Pond are estimated using Equations (3-7) and (3-8) with these average parameter values: $A = 0.21$ mg/cm^2, $n = 2.6$ and $\rho = 0.76$ g/cm^3. Spatial distributions of predicted scour depths for the five floods are illustrated on Figures 3-6 and 3-7. Scour impacts are quantified by examining two metrics: 1) area with scour depths > 1 cm and 2) mass of eroded sediment (see Table 3-5). Areas with scour depth greater than 1 cm appear to correlate with areas experiencing velocities greater than 2 ft/s; a rare flood will cause 1 cm or more of erosion in less than approximately 4 percent of the pond area. Mass of eroded sediment is predicted to be 200 metric tons or less for this range of floods; most of the erosion occurs in the region where velocities exceed 2 ft/s.

Table 3-5. Impacts of Bed Scour in Allendale Pond.

Flood Return Period (years)	Area with Scour > 1 cm (hectares)	% of Pond Area with Scour > 1 cm	Mass of Eroded Sediment (metric tons)
5	0.05	1	14
10	0.06	1	33
25	0.11	2	75
50	0.13	3	125
100	0.16	4	195

3.2.4 Lyman Mill Pond Results

Predicted velocities for the 100-year flood in Lyman Mill Pond are shown on Figures 3-8 and 3-9. Current patterns for the four floods with lower flow rates are similar to the 100-year flood results. Relatively high velocities occur in the northern portion of the pond due to shallower depths and smaller cross-sectional area, with recirculation zones (which may be conducive to deposition) occurring along the western shoreline. Current velocities tend to decrease in the southern portion of the pond due to deeper water and larger cross-sectional area.

Areas in the pond where bottom shear stress exceeds the upper- and lower-bound estimates of τ_{cr} for the five floods are presented on Figures 3-10 and 3-11 and tabulated in Table 3-6. Current velocities exceeding the critical velocity criterion for significant scour (i.e., 2 ft/s) are predicted in the areas shown on Figures 3-12 and 3-13. These areas are quantified and listed in Table 3-7. Total area of Lyman Mill Pond is 9.08 hectares. The area of potential scour is larger in Lyman Mill Pond than in Allendale Pond, with velocities greater than 2 ft/s occurring over 3 to 15 percent of Lyman Mill Pond.

Table 3-6. Potential Scour Areas in Lyman Mill Pond.

Flood Return Period (years)	Area with $\tau > 0.1$ Pa (hectares)	% of Pond Area with $\tau > 0.1$ Pa	Area with $\tau > 0.5$ Pa (hectares)	% of Pond Area with $\tau > 0.5$ Pa
5	3.99	44	1.58	17
10	4.48	49	2.02	22
25	4.81	53	2.44	27
50	4.97	55	2.71	30
100	5.09	56	3.01	33

Table 3-7. Areas of Potential Significant Scour in Lyman Mill Pond.

Flood Return Period (years)	Area with u > 2 ft/s (hectares)	% of Pond Area with u > 2 ft/s
5	0.29	3
10	0.44	5
25	0.67	7
50	1.01	11
100	1.32	15

Lyman Mill Pond scour depths are estimated using these average parameter values: A = 0.21 mg/cm^2, n = 2.6 and ρ = 0.59 g/cm^3. Spatial distributions of predicted scour depths for the five floods are illustrated on Figures 3-14 and 3-15. Scour impacts are quantified by examining two metrics: 1) area with scour

depths > 1 cm and 2) mass of eroded sediment (see Table 3-8). Similar to Allendale Pond, areas of velocity greater than 2 ft/s and scour greater than 1 cm appear to be correlated in Lyman Mill Pond. For the five floods simulated, approximately five times more bed area has scour depths greater than 1 cm in Lyman Mill Pond than the scour area predicted in Allendale Pond. Mass of eroded sediment is about 10 times greater in Lyman Mill Pond than in Allendale Pond for all flow rates.

Table 3-8. Impacts of Bed Scour in Lyman Mill Pond.

Flood Return Period (years)	Area with Scour > 1 cm (hectares)	% of Pond Area with Scour > 1 cm	Mass of Eroded Sediment (metric tons)
5	0.26	3	120
10	0.35	4	310
25	0.50	5	880
50	0.60	7	1,500
100	0.73	8	2,400

3.3 Sensitivity Analysis

The model results presented in Section 3.2 were developed using 'best' estimates of key model parameters. Due to a lack of site-specific data to specify these model parameters, combined with the fact that no model calibration was performed, uncertainty exists in the model predictions. An effort is made in this section to quantify this uncertainty by investigating the sensitivity of model results to variations in key parameters.

The parameters that are varied between upper- and lower-bound estimates are: 1) effective bottom roughness (Z_o); 2) resuspension potential parameters (A and n); and 3) dry density. The range of Z_o used in the sensitivity analysis is 0.5 Z_o (lower-bound) and 2 Z_o (upper-bound). Lower- and upper-bound values of A and n are provided in Table 3-2. Bounding estimates of dry density are based on the 95% CI values for each pond: 0.63 to 0.89 g/cm^3 (Allendale Pond) and 0.47 to 0.71 g/cm^3 (Lyman Mill Pond). The sensitivity analyses are conducted using the 100-year flood flow rate; sensitivity results are compared to results from the 'base case' simulation, which is the 100-year flood using the model parameter values discussed in Sections 3.1 and 3.2.

3.3.1 Sensitivity Analysis: Bottom Roughness

Increasing and decreasing bottom roughness (Z_o) by factors of two has minimal effect on model predictions. The four metrics based on areal fraction of each pond (i.e., percentage of pond area for which: 1) $\tau > 0.1$ Pa; 2) $\tau > 0.5$ Pa; 3) u > 2 ft/s; and 4) scour > 1 cm) changed by less than one percent due to the factor-of-two variation in Z_o (Figure 3-16, Tables 3-9 and 3-10). Similarly, eroded mass of sediment in Allendale Pond changed by about one percent. In Lyman Mill Pond, however, variation in Z_o caused a change of about ± 7 percent in mass of eroded sediment, relative to the base case results.

Table 3-9. Sensitivity to Bottom Roughness Variation: Allendale Pond, 100-Year Flood.

Value of Z_o With Respect to Base Case	% of Pond Area with u > 2 ft/s	% of Pond Area with Scour > 1 cm	Mass of Eroded Sediment (metric tons)
Base Case	5	4	195
0.5 Z_o	5	4	196
2 Z_o	6	4	193
10 Z_o	5	4	189
100 Z_o	5	3	176

Table 3-10. Sensitivity to Bottom Roughness Variation: Lyman Mill Pond, 100-Year Flood.

Value of Z_o With Respect to Base Case	% of Pond Area with u > 2 ft/s	% of Pond Area with Scour > 1 cm	Mass of Eroded Sediment (metric tons)
Base Case	15	8	2,400
0.5 Z_o	15	8	2,500
2 Z_o	14	8	2,200
10 Z_o	14	7	1,700
100 Z_o	12	5	720

The reason that model results are negligibly affected by factor-of-two changes in Z_o is that this magnitude of variation in bottom roughness only causes an approximately 10 percent change in bottom friction factor (C_f) and, hence, shear stress. One to two order-of-magnitude increases in Z_o are necessary to increase C_f by factors of two to five. The relatively small value of Z_o, due to the fine-grained composition of the bed in both ponds, causes this situation.

Due to the relative insensitivity of the model to factor-of-two changes in Z_o, further investigation was conducted by increasing Z_o by factors of 10 and 100. Increasing Z_o caused a decrease in current velocity, shear stress and, hence, bed erosion; the increased bottom friction caused slower velocities and less erosion. In Allendale Pond, minimal variations in areas with velocity greater than 2 ft/s and scour greater than 1 cm occurred when Z_o was increased by up to a factor of 100; erosion mass decreased by a maximum of 10 percent, with respect to the base case (Table 3-9). For Lyman Mill Pond, impacts of Z_o variation were more apparent than in Allendale Pond, but still minor for increases in Z_o up to a factor of 10 (Table 3-10).

3.3.2 Sensitivity Analysis: Erosion Potential Parameters

Bounding estimates of erosion potential parameters (i.e., A and n in Equation (3-7), see Table 3-2 for values) may cause large changes in predicted scour depth and erosion mass due to the nonlinear nature of the Lick equation. For Allendale and Lyman Mill Ponds, model results are sensitive to the bounding variations in A and n. In both ponds, the mass of eroded sediment varied by about a factor of 800 between the lower- and upper-bound estimates (see Table 3-11). The upper-bound estimates of eroded mass are about eight times greater than the mass predicted for the base case in each pond for the 100-year flood. Over the range of flood flow rates (i.e., 5-year to 100-year flood), the upper-bound estimates of erosion mass range between five and eight times greater than the base case results in both ponds.

Table 3-11. Sensitivity of Erosion Mass to Erosion Parameters (100-Year Flood).

Pond	Base Case (metric tons)	Lower-Bound (metric tons)	Upper-Bound (metric tons)
Allendale	195	2	1,500
Lyman Mill	2,400	25	21,300

3.3.3 Sensitivity Analysis: Dry Density

Uncertainty in dry density affects predicted scour depth, see Equation (3-8). For Allendale Pond, bed area with scour greater than 1 cm varies by about 10 percent, with respect to the base case, with the specified variation in dry density. In Lyman Mill Pond, the variation in scour depth area (> 1 cm) is about 20 percent.

3.4 Summary of Model Results

The potential impacts of rare floods on bed stability in the two ponds were evaluated using a hydrodynamic model as discussed in the preceding sections. Primary results of the modeling are:

- In Allendale Pond, significant scour will occur over less than 5 percent of the bed area in the pond during a rare flood. Significant erosion, i.e., greater than approximately 1 cm, will generally occur in the northern portion of the pond, near the upstream inlet.

- Significant scour will occur over a larger area in Lyman Mill Pond than in Allendale Pond, with up to 10 to 15 percent of the Lyman Mill Pond bed having erosion greater than approximately 1 cm. Bed scour generally occurs in the northern portion of Lyman Mill Pond, with maximum erosion near the upstream inlet.

- Model predictions are most sensitive to estimated values of resuspension potential parameters, i.e., A and n in Equation (3-7). Lack of site-specific data is the primary cause of this sensitivity.

- The most useful model metrics for evaluating potential impacts on bed stability are areas with u > 2 ft/s and scour depth > 1 cm. Not surprisingly, these two metrics appear to be correlated (Figure 3-17). Comparison of bottom shear stress to critical shear stress values is less useful because of the nonlinear relationship between scour depth (or resuspension potential) and shear stress for cohesive sediment. Generally, minimal erosion of a cohesive bed occurs for applied shear stress near the critical value; in contrast to noncohesive sediment, where significant erosion can happen once the critical shear stress is exceeded.

- Absolute magnitude of model predictions is more uncertain than relative magnitude. For example, predictions of 195 and 2,400 metric tons of erosion in Allendale and Lyman Mill Ponds, respectively, during a 100-year flood have an order-of-magnitude accuracy, at best. The relative difference between the two predictions, i.e., Lyman Mill erosion is much larger than Allendale erosion, is probably more accurate and reliable.

Comparison of potential impacts of rare floods on bed scour between the two ponds provides additional insights concerning bed stability in the study area. Generally, a larger area of the sediment bed is impacted by a rare flood in Lyman Mill Pond than in Allendale Pond (Figure 3-18). About five times more bed area in Lyman Mill Pond will experience significant bed scour during a flood than in the upstream pond. Similarly, the mass of eroded sediment is greater in Lyman Mill Pond, with about 10 times more sediment being scoured during a 100-year flood in the downstream pond than in Allendale Pond (Figure 3-19).

3.5 Model Limitations

The modeling analysis provides useful information for evaluating bed stability in the two ponds. Limitations exist in the model, however, primarily due to lack of site-specific data for specifying model parameters and inputs. Specific model limitations are:

- The assumption that the sediment bed in each pond is composed of cohesive sediment. This assumption is necessary because of a lack of bed-type data, e.g., side-scan sonar data that delineates areas of cohesive (fine) and noncohesive (coarse) sediment. Even though assuming that the bed is entirely cohesive is a reasonable first-approximation, model results may be impacted. For example, noncohesive sediment may exist in the inlet areas of the ponds, where the model presently predicts maximum erosion depths, due to higher velocities routinely occurring in those areas. The erosion properties of cohesive and noncohesive sediments are significantly different and, hence, model predictions may change if bed type is switched to noncohesive in a particular area.

- No site-specific data on the resuspension properties of sediments in Allendale and Lyman Mill Ponds is a definite limitation of the model. Even though resuspension parameters were estimated from data collected at different sites, model predictions of scour depth and erosion mass are probably only order-of-magnitude estimates.

- Inability to calibrate the hydrodynamic model using stage height and current velocity data collected in the ponds introduces uncertainty into the results. The model, however, is based on relatively solid physical principles, e.g., conservation of mass and momentum, and the geometry/bathymetry of the ponds are specified with reasonable accuracy. Thus, the primary parameter affecting model performance is effective bottom roughness (Z_0). Sensitivity tests indicate that model results are relatively insensitive to this parameter. Therefore, this limitation (i.e., no calibration) is relatively minor when compared to the two limitations discussed above.

- Other potential limitations include: estimation of stage height at the dams using Equation (3-1); neglecting effects of floodplains during overbank flow conditions; and neglecting impact of vegetation on hydrodynamic drag. Neglecting floodplain and vegetation effects tends to produce conservative results; predicted current velocity and bottom shear stress are maximized when the effects of floodplains and vegetation are not incorporated into the model.

4.0 CONCEPTUAL SITE MODEL FOR SEDIMENT TRANSPORT

Results of the data-based analyses in Section 2 may be used to develop a CSM for sediment transport. A CSM is an important component of a sediment stability analysis because consistency must be maintained between the CSM and the results of quantitative and qualitative sediment stability analyses. A sediment transport CSM is a detailed component of the overall CSM that is typically developed for risk assessment at a contaminated sediment site. The sediment transport CSM is a qualitative description of the processes (e.g., deposition and erosion) and system characteristics (e.g., upstream and tributary sediment loads, spatial distribution of bed properties) that control sediment dynamics within the study area.

Based on the data-based analyses presented earlier in the report, the following CSM for sediment transport is proposed:

- The surficial layer of the sediment bed in each pond, i.e., approximately upper 1-2 ft, is generally composed of cohesive sediment. Relatively small areas of noncohesive sediment exist in each pond, typically in locations where higher current velocities exist.

- The composition of surficial sediment is finer in the downstream pond (Lyman Mill Pond) due to selective deposition of coarser sediment in the upstream pond (Allendale Pond).

- The two ponds, which are dammed and serve as run-of-the-river impoundments, are net depositional environments for most flow rates. Significant erosion during a high-flow event is expected to occur over small areas within each pond.

- The river channel upstream of each pond is composed of coarse, noncohesive sediment and is typically non-depositional. The river channels serve as conduits for suspended sediment into and between the ponds.

The model-based analyses presented in Section 3 appear to be consistent with the proposed CSM. The impacts of rare floods on bed scour are predicted to be restricted to a relatively small portion (i.e., less than approximately 5 to 15 percent of pond area) of the sediment bed in each pond. The modeling results suggest that deposition occurs over large portions of Allendale and Lyman Mill Ponds during high-flow events; deposition rates during a flood will be spatially variable within each pond due to variations in sediment load and bottom shear stress. In addition, sediment eroded in the upstream portions of each pond during a flood will be transported downstream by river currents. A portion of the eroded sediment will be re-deposited within the pond; current velocity and bottom shear stress tend to decrease in the downstream portions of each pond, making those areas conducive to re-deposition of eroded material from upstream locations.

5.0 CONCLUSIONS RELATED TO BED STABILITY

The data- and model-based analyses conducted during this study provide information that may be used to develop conclusions regarding bed stability within Allendale and Lyman Mill Ponds. These conclusions, along with the supporting data and analysis results, may prove to be helpful when considering potential remedial alternatives for the two ponds. Specific conclusions based on the results of the analyses are:

- A representative sedimentation rate for Allendale Pond varies from 0.5 to 0.8 cm/yr, which corresponds to a range for depositional mass in the pond of 170 to 270 metric tons/yr (assuming a dry density of 0.76 g/cm^3 and an area of 4.49 hectares).

- Insufficient data are available in Lyman Mill Pond for estimating a representative sedimentation rate. Assuming that a range of 0.5 to 0.8 cm/yr is valid for that pond, it is estimated that 270 to 430 metric tons/yr are deposited in Lyman Mill Pond (assuming a dry density of 0.59 g/cm^3 and an area of 9.08 hectares).

- A representative depth range for the 1940 time horizon in the sediment bed of Allendale Pond is between 1 and 2 feet. An estimate of the 1940-TH could not be made for Lyman Mill Pond due to insufficient data.

- Minimal net export of dioxin from the two ponds occurs during low-flow, non-resuspending conditions; the water-column load of dioxin entering the study area (i.e., background load) is approximately equal to the load over Lyman Mill Dam during low-flow periods.

- In Allendale Pond, significant scour will occur over less than 5 percent of the bed area in the pond during a rare flood. Significant erosion, i.e., greater than approximately 1 cm, will generally occur in the northern portion of the pond, near the upstream inlet.

- Significant scour will occur over a larger area in Lyman Mill Pond than in Allendale Pond, with up to 10 to 15 percent of the Lyman Mill Pond bed having erosion greater than approximately 1 cm. Bed scour generally occurs in the northern portion of Lyman Mill Pond, with maximum erosion near the upstream inlet. Note that bed erosion in Lyman Mill Pond may be over-predicted because the effects of floodplains are neglected in the model; incorporating floodplain effects into the model may significantly decrease predicted current velocity and bottom shear stress in the vicinity of the pond inlet.

The validity of these conclusions is dependent on the uncertainty in the data and model. Attempts were made to incorporate the effects of uncertainty in the data-based analyses, which are discussed in Section 2. Uncertainty in the data-based analyses is reflected in the conclusions through use of ranges of results, rather than specific numbers.

Uncertainty in the model-based conclusions is due to these primary sources: 1) lack of model calibration; 2) insufficient data to develop a detailed bed map for the ponds; and 3) lack of site-specific erosion potential data. Not performing a calibration of the hydrodynamic model introduces uncertainty into the model predictions. This uncertainty, however, does not significantly affect conclusions developed from the modeling analyses for the following reason. Calibrating the hydrodynamic model involves adjusting the effective bottom roughness (Z_0) such that agreement between observed and predicted stage height and/or current velocity is optimized; a unique value of bottom roughness, i.e., $Z_{0,cal}$, is determined during calibration. The sensitivity analysis, however, demonstrated that (see Section 3.3.1): 1) model results are

relatively insensitive to variations in Z_o of up to a factor of 100; and 2) base case values of Z_o produce conservative results. While determining $Z_{o.cal}$ through model calibration will reduce uncertainty in hydrodynamic model results (e.g., predicted stage height and current velocity), it is doubtful that scour-related results from the calibrated model will be significantly different from results produced by the uncalibrated model. In addition, the uncalibrated model is generating conservative, i.e., worse case, results. Thus, calibrating the hydrodynamic model will not significantly improve the reliability of the modeling results.

The largest improvement in the reliability of the modeling analyses can be achieved through collection of additional bed data. Bed probing data obtained from the areas of each pond where significant erosion is predicted by the model will make it possible to delineate cohesive and noncohesive zones and create a bed-type map. Conducting a shaker study will provide site-specific erosion potential parameters, i.e., values of A and n in the Lick equation for each pond.

6.0 REFERENCES

Alcoa, 2002. *Analysis of Alternatives Report. Grasse River Study Area. Massena, New York.* Alcoa report. June 12, 2002.

Battelle, 2003. Data Summary Report, Interim Data Collection, Remedial Investigation and Feasibility Study, Centredale Manor Restoration Project Superfund Site, North Providence, Rhode Island. Prepared for U.S. Army Corps of Engineers, New England District. June 2003.

Corcoran, M., 2004. *Geomorphic Assessment of the Woonasquatucket River, RI.* USGS report, Engineer Research and Development Center, Vicksburg, MS.

Graf, W.H. 1971. *Hydraulics and Sediment Transport.* McGraw-Hill, Inc., New York, NY. 513 p.

Jepsen, R., Roberts, J., Langford, R. and Gailani, J., 2001. *Rio Grande Erosion Potential Demonstration, Report for the National Border Technology Partnership Program.* Sandia National Laboratories report SAND2001-3611.

Lick, W., Xu, Y.J., and McNeil, J., 1995. Resuspension properties of sediments from the Fox, Saginaw and Buffalo Rivers. *J. Great Lakes Res.*, 21(2):257-274.

Olsen, C.R., Simpson H.J., Bopp R.F., Williams S.C., Peng T.H. and Deck B.L., 1978. Geochemical analysis of the sediments and sedimentation of the Hudson River Estuary. *J Sed Petrol* 48:401-418.

Orson R.A., Simpson R.L. and Good E.E., 1990. Rates of sediment accumulation in a tidal freshwater marsh. J. Sediment Petrology. *J Sed Petrol* 19:849-869.

Quantitative Environmental Analysis, 2004. Final Work Plan, Centredale Manor Sediment Stability Study. Prepared for USACE, New England District, June 2004.

Robbins, J.A., 1978. Geochemical and geophysical applications of radioactive lead isotopes. In: Nriagu JO, ed, *Biogeochemistry of lead.* Elsevier, Amsterdam, pp 285-393.

Roberson, J.A., Cassidy, J.J. and Chaudhry, M.H., 1998. *Hydraulic Engineering.* John Wiley & Sons, New York, 204 p.

Roberts, J., Jepsen, R., Bryan, C. and Chapin, M., 2001. *Boston Harbor Sediment Study.* Sandia National Laboratories, report SAND2001-2226.

Shields, G., 2003. Waterborne geophysical surveys and sediment coring, Centredale Manor site, Work Assignment R1A00270 – trip report. Lockheed Martin Technology Services, October 21, 2003.

Simpson, H.J., Olsen C.R., Trier R.M. and Williams S.C., 1976. Manmade radionuclides and sedimentation in the Hudson River Estuary. *Science* 194:179-183.

TTNUS, Inc., 2000. *Final Technical Memorandum, Volume I Text, Woonasquatucket River Sediment Investigation, Centredale Manor Restoration Project Site, North Providence, Rhode Island.* Prepared for U.S. Environmental Protection Agency, Region 1. June 2000.

U.S. Army Corps of Engineers (USACE), 1991. *Hydraulic Design of Flood Control Channels.* EM-1110-2-1601. Vicksburg, MS.

U.S. Geological Survey (USGS), 1996. *Water Resources Data, Massachusetts and Rhode Island, Water Year 1996*. USGS water-data report MA-RI-96-1.

Van Rijn, L.C., 1993. *Principles of Sediment Transport in Rivers, Estuaries and Coastal Seas*. Aqua Publications, Amsterdam.

Ziegler, C.K., 2002. Evaluating sediment stability at sites with historic contamination. *Environmental Management*, 29(3):409-427.

Ziegler, C.K. and Nisbet, B.S., 1994. Fine-grained sediment transport in Pawtuxet River, Rhode Island. *ASCE J. Hydr. Engr.*, 121(11):773-781.

APPENDIX A

FIGURES

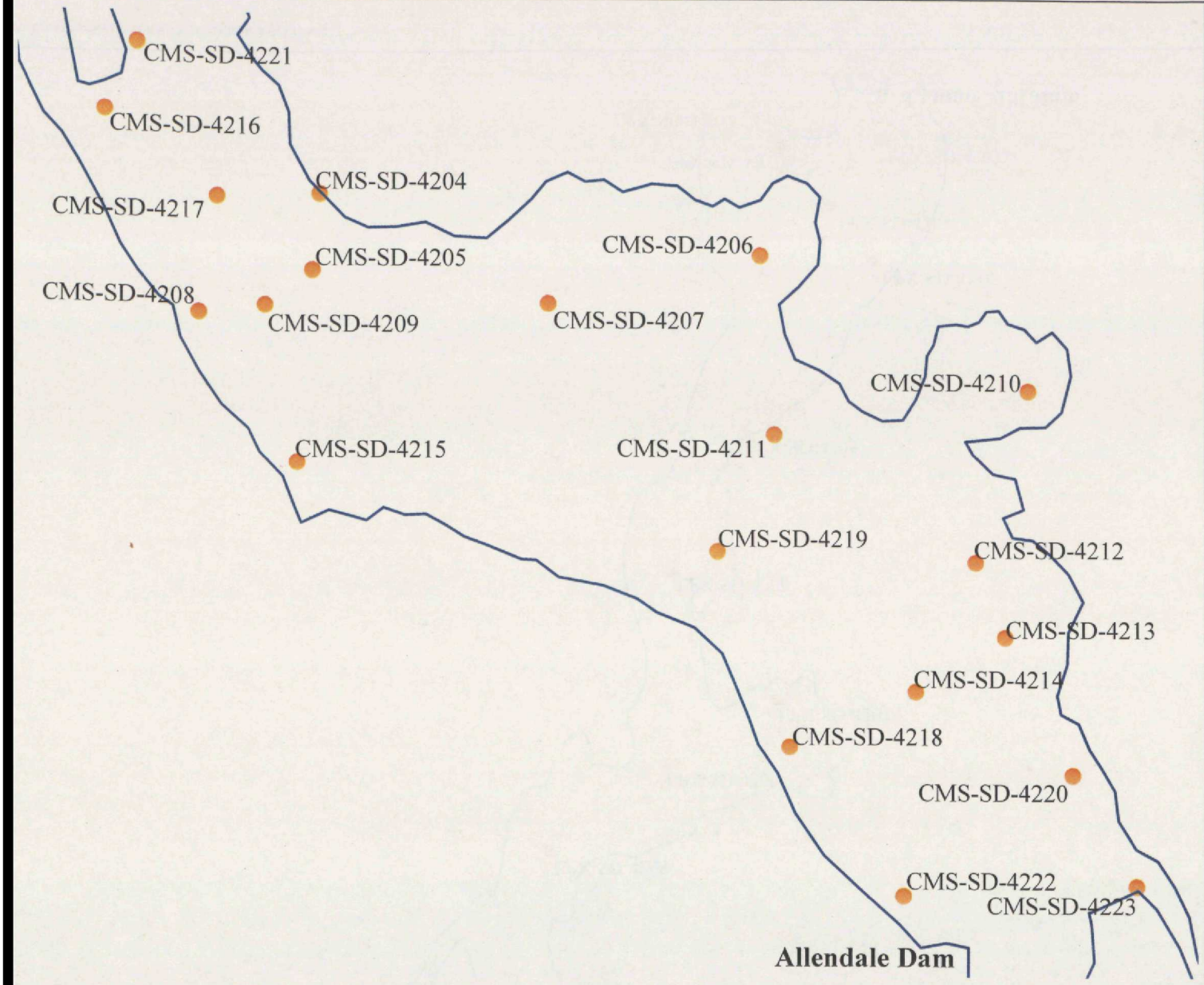

Locator Map

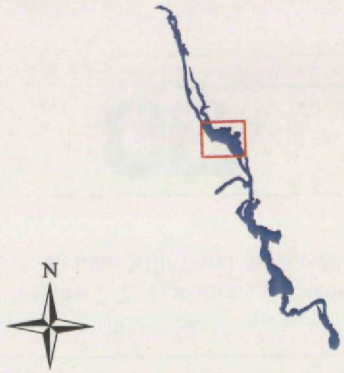

Legend

1997 Shoreline

May 2003 Core Locations

Figure 2-1. Locations of cores collected in Allendale Pond during May 2003.

QEA Quantitative Environmental Analysis, LLC

BATcen:120 August 2004

C:\BATman\Maps\ArcGIS\May2003r\batcen_allendale_may03_loc.mxd

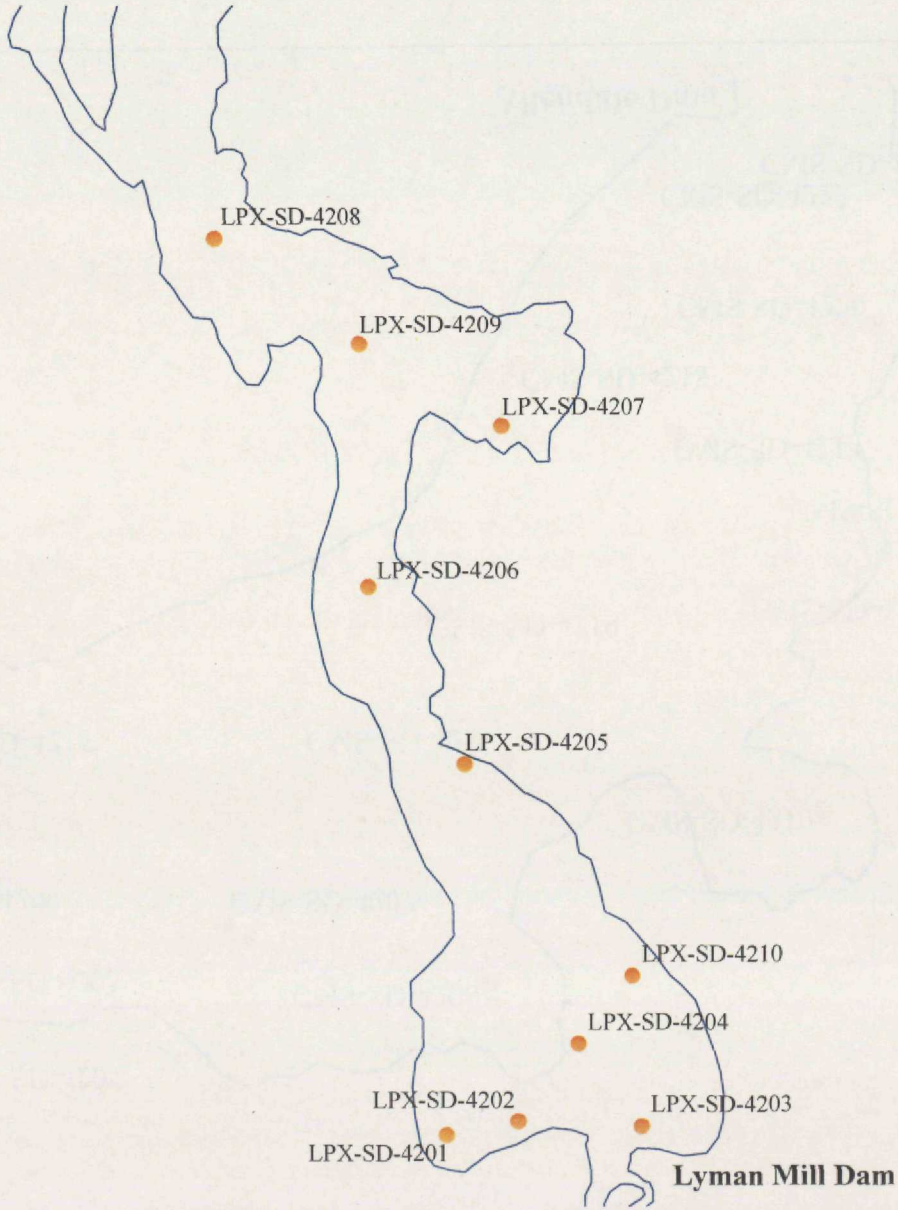

Locator Map

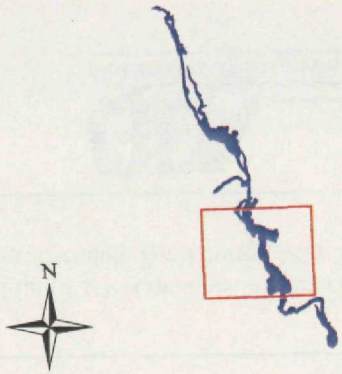

Legend

1997 Shoreline

May 2003 Core Locations

Figure 2-2. Locations of cores collected in Lyman Mill Pond during May 2003.

QEA Quantitative Environmental Analysis, LLC

BATcen:120 **August 2004**

CO- C:\BATman\Maps\ArcGIS\May2003\batcen_lyman_may03_loc.mxd

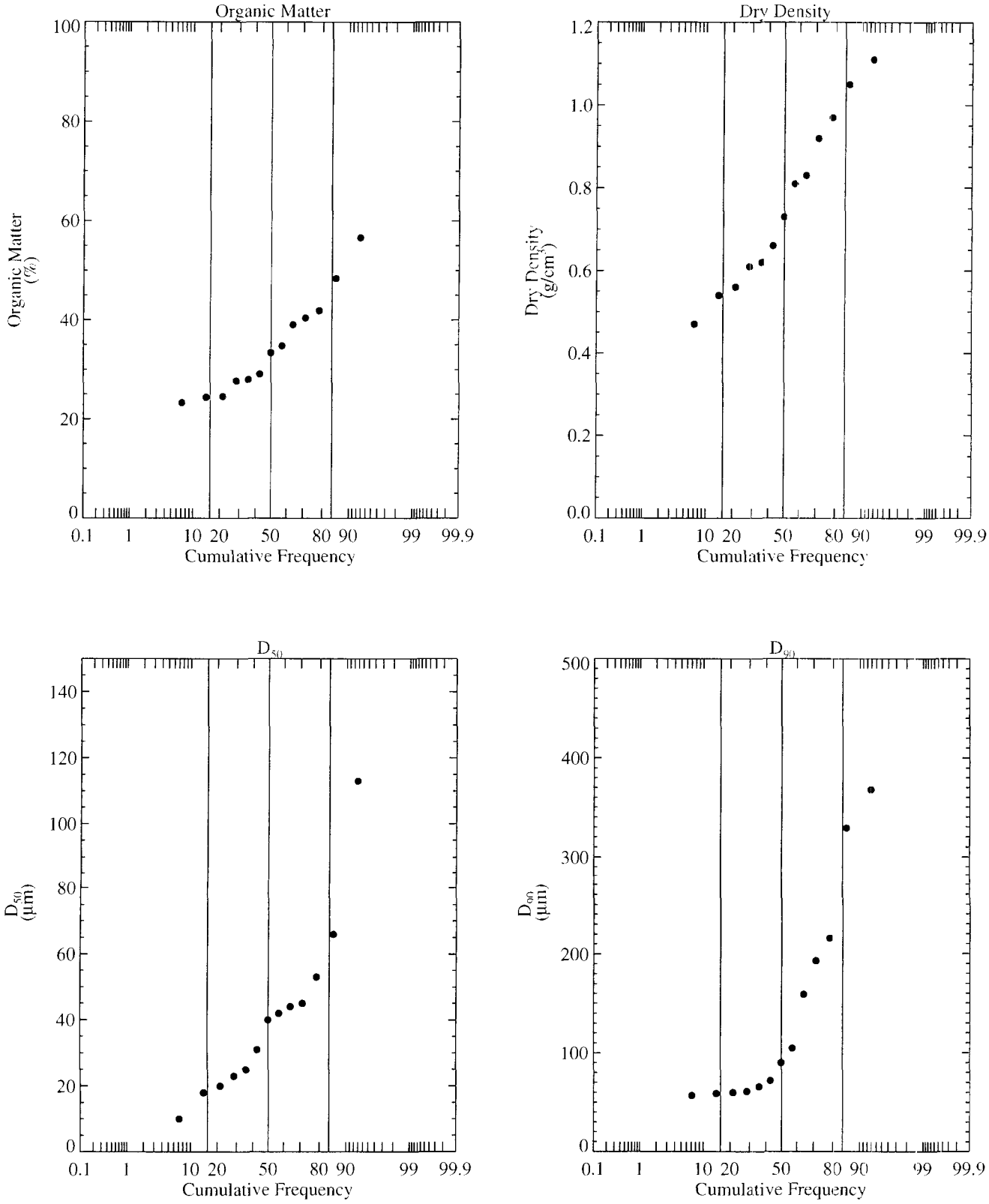

Figure 2-3. Frequency distributions of bulk bed properties in Allendale Pond (May 2003 data).

cfo - C:\BATman\Analysis\Sediment_Investigations\May2003\plot_bedproperties_040823.pro
Thu Aug 26 15:18:29 2004

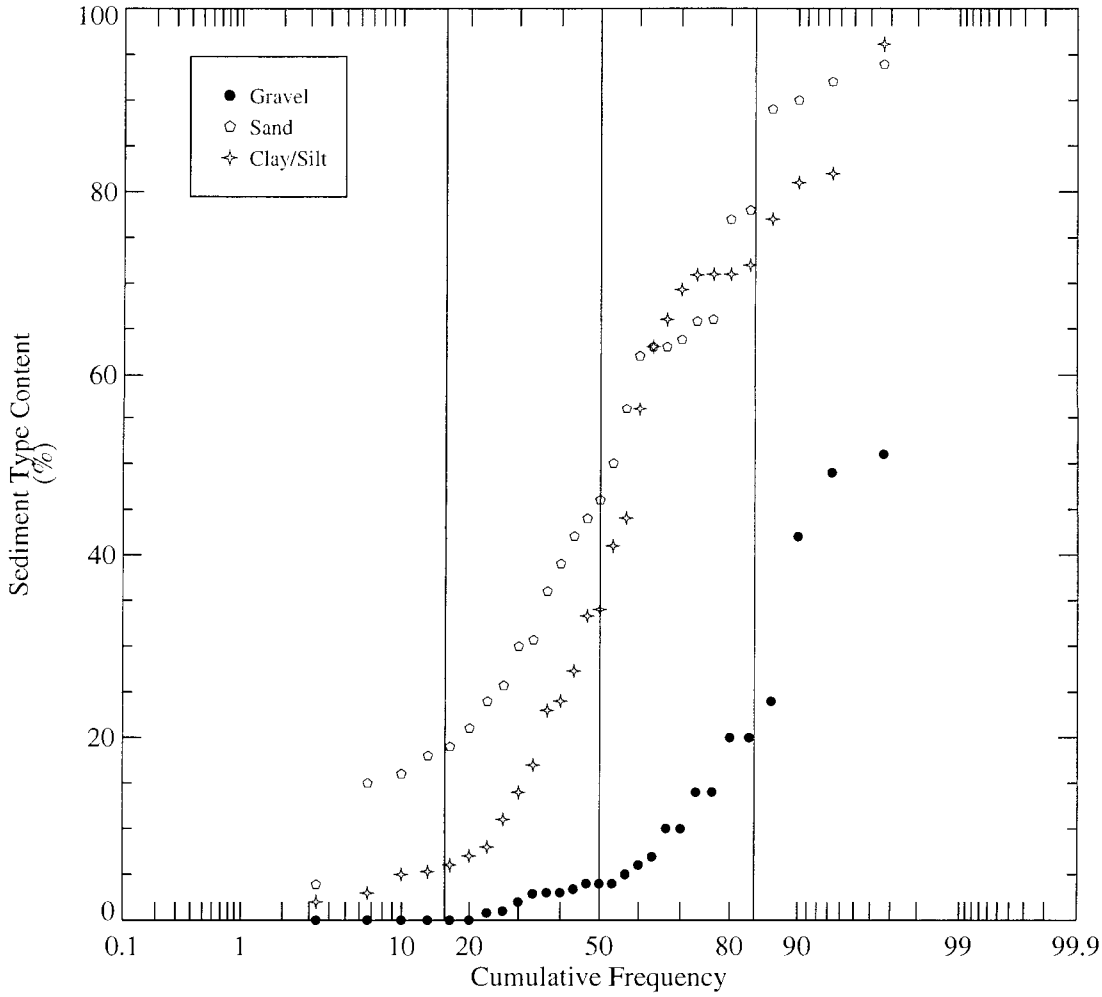

Figure 2-4. Frequency distributions of clay/silt, sand and gravel content in Allendale Pond sediment (May 2003 data).

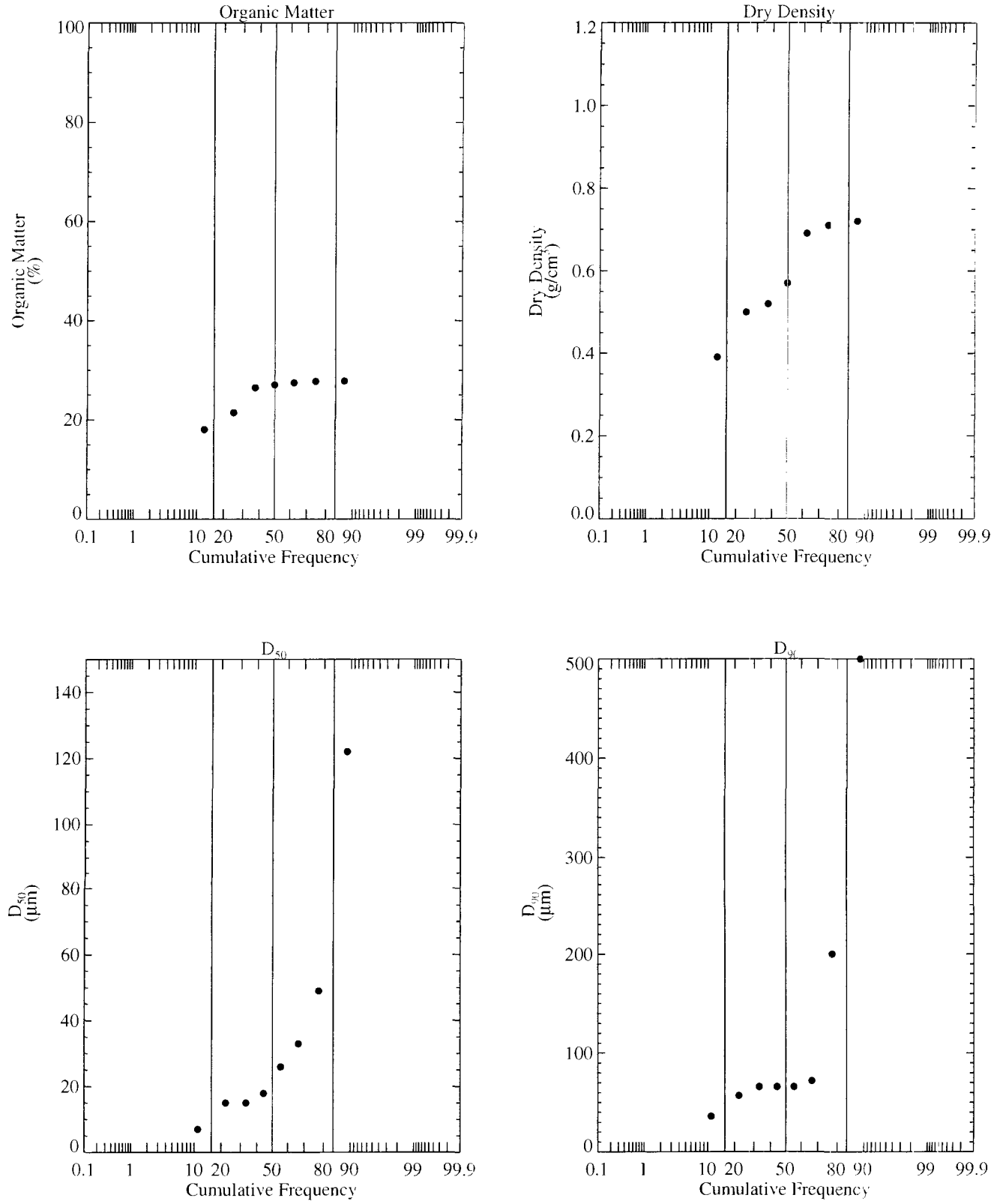

Figure 2-5. Frequency distributions of bulk bed properties in Lyman Mill Pond (May 2003 data).

cfo - C:\BATman\Analysis\Sediment_Investigations\May2003\plot_bedproperties_040823.pro
Thu Aug 26 15:18:29 2004

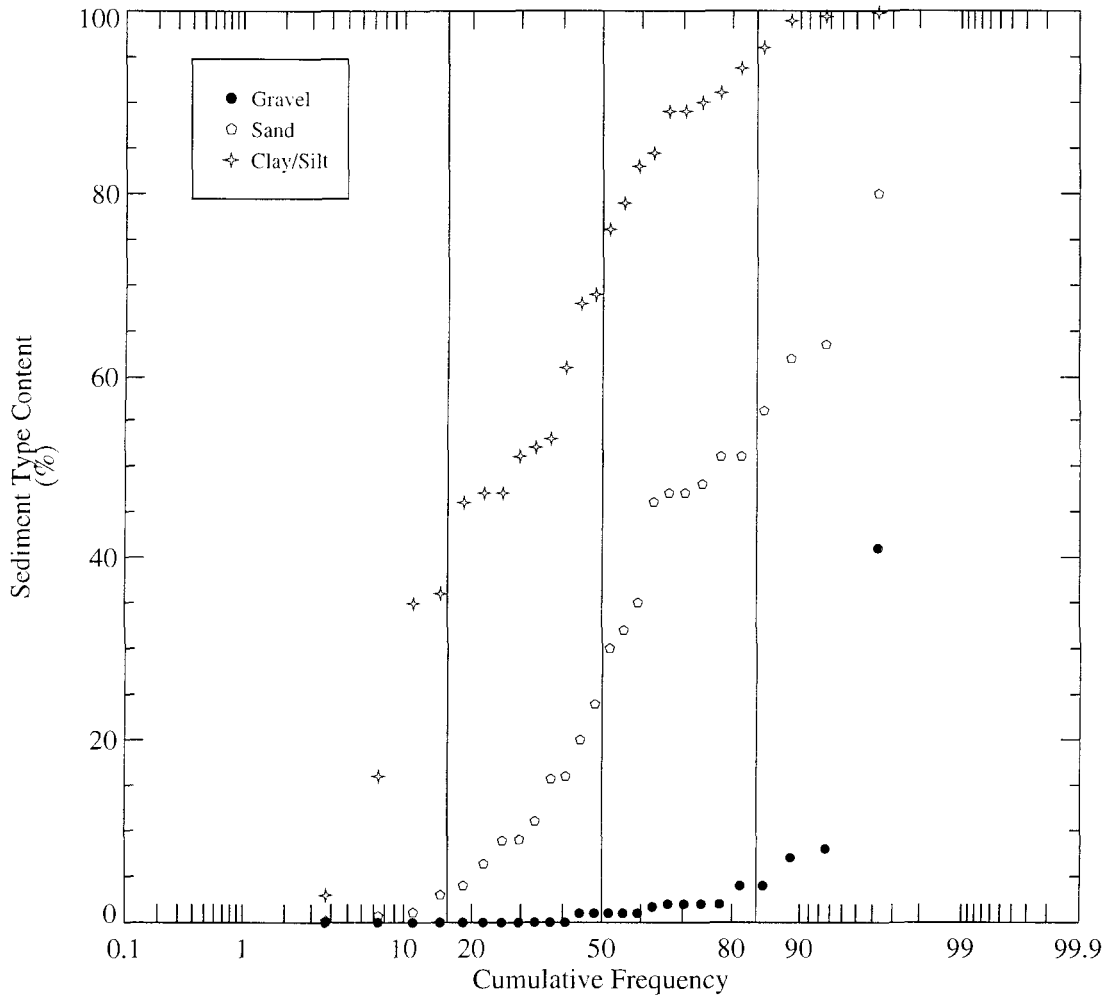

Figure 2-6. Frequency distributions of clay/silt, sand and gravel content in Lyman Mill Pond sediment (May 2003 data).

cfo - C:\BATman\Analysis\Sediment_Investigations\June1999\probplot_grainsize_040823.pro
Thu Aug 26 15:15:06 2004

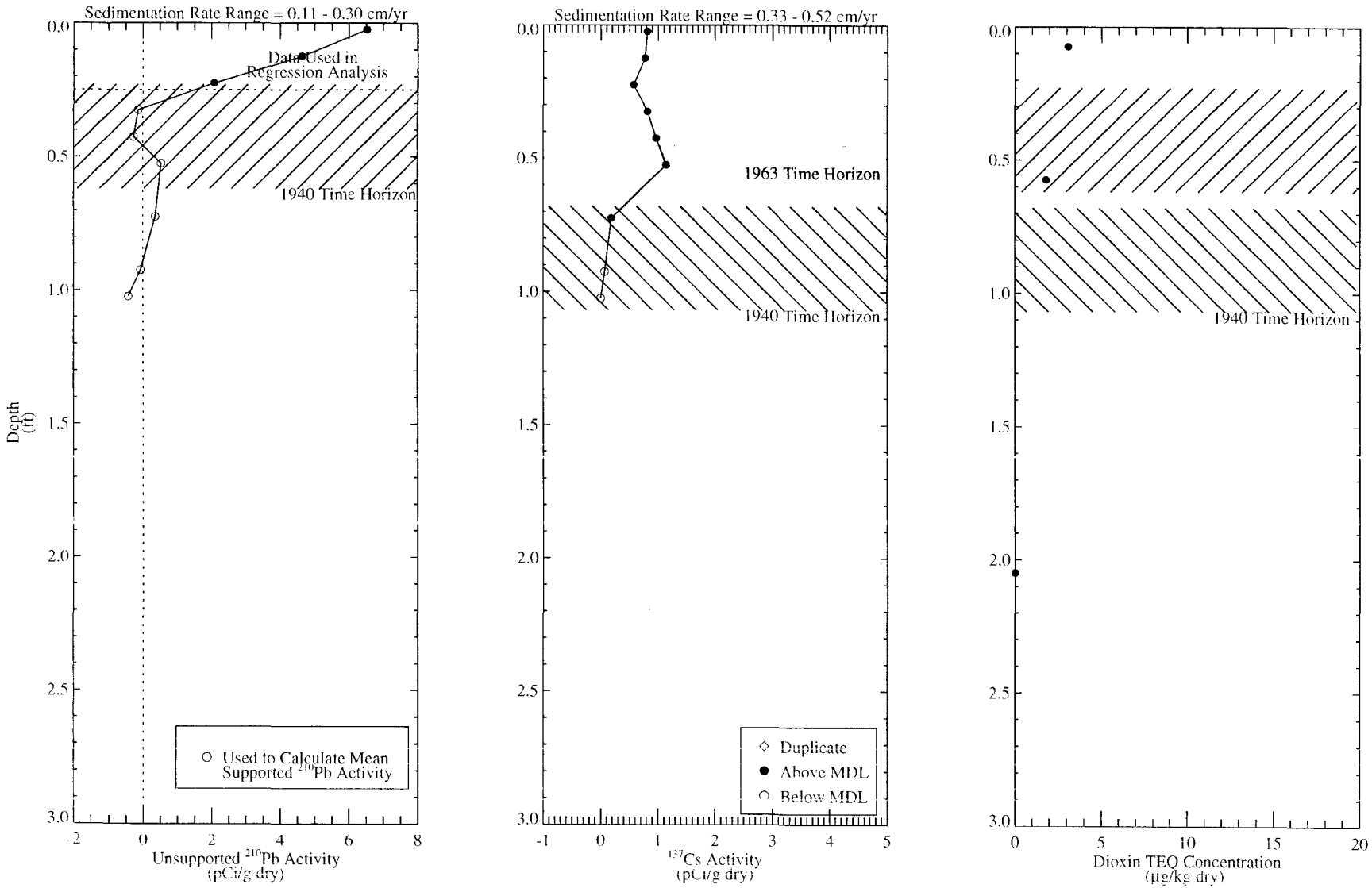

Figure 2-7. Vertical profiles of Pb-210 activity, Cs-137 activity and dioxin TEQ concentration for core CMS-SD-4204 in Allendale Pond (May 2003 data).

cfo - C:\BATman\Analysis\Sedimentation_rates\plot_pb_cs_profiles_3panel_040721.pro
Thu Aug 26 16:02:04 2004

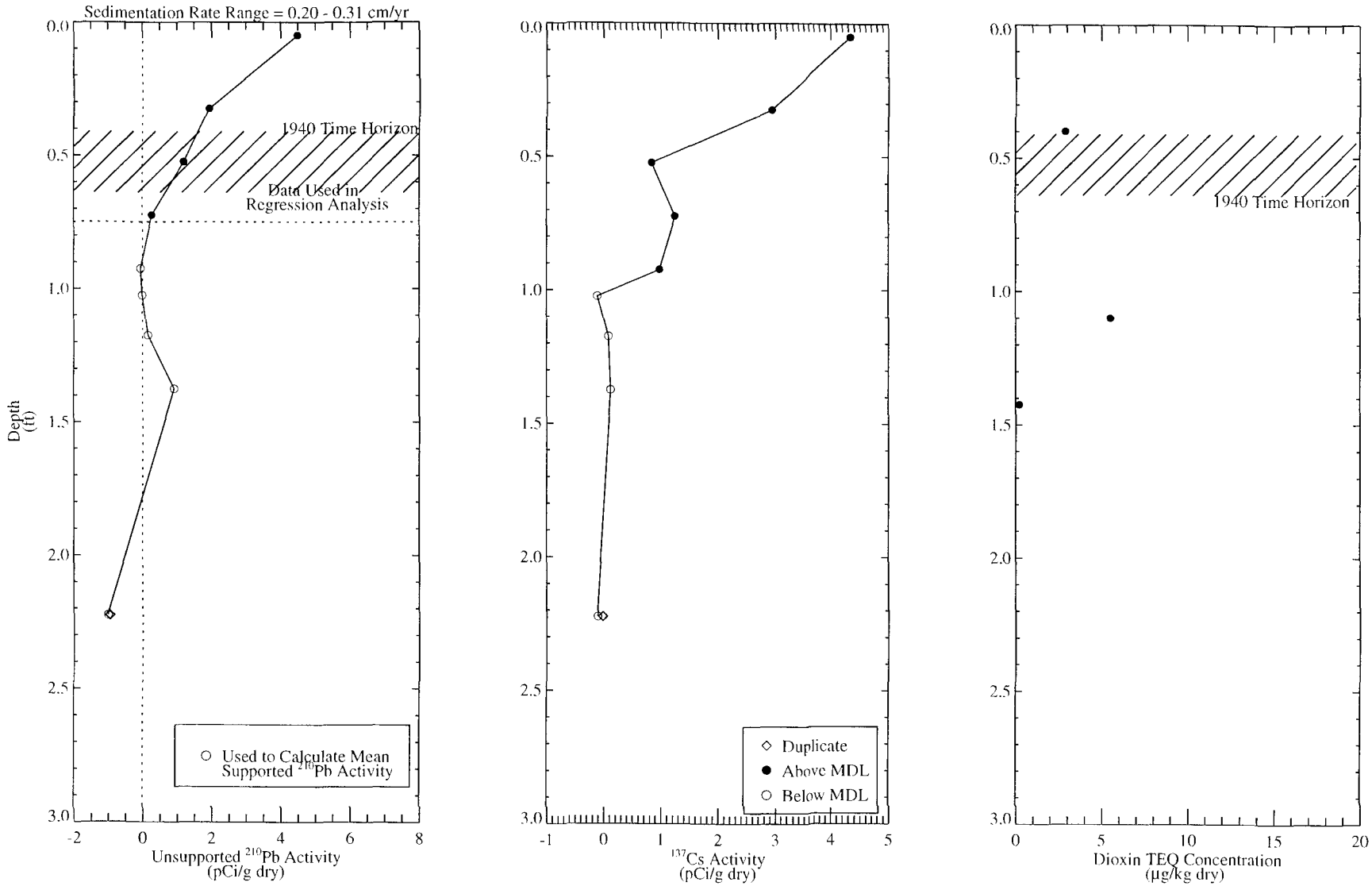

Figure 2-8. Vertical profiles of Pb-210 activity, Cs-137 activity and dioxin TEQ concentration for core CMS-SD-4206 in Allendale Pond (May 2003 data).

cfo - C:\BATman\Analysis\Sedimentation_rates\plot_pb_cs_profiles_3panel_040721.pro
Thu Aug 26 16:02:0[illegible]

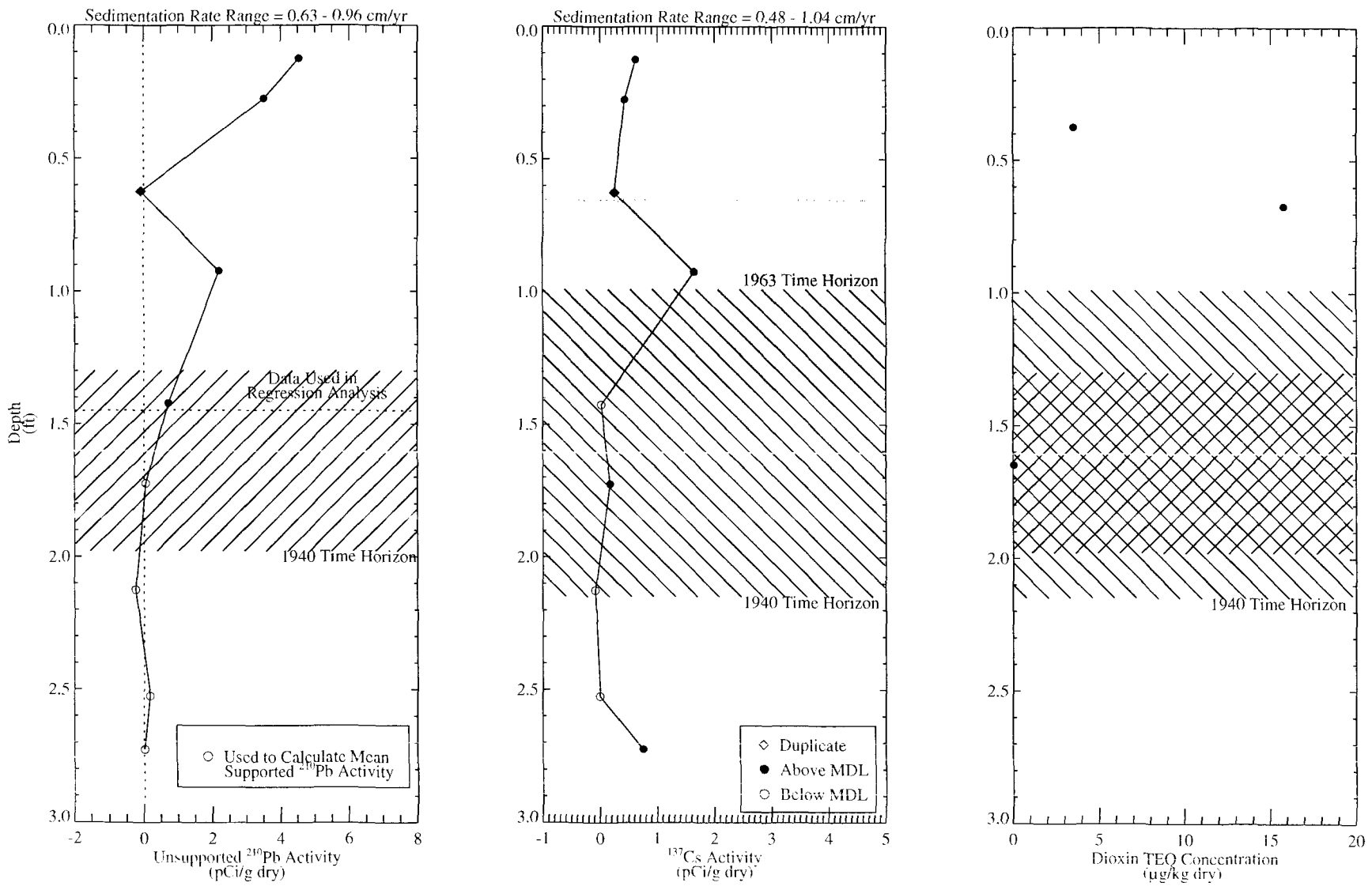

Figure 2-9. Vertical profiles of Pb-210 activity, Cs-137 activity and dioxin TEQ concentration for core CMS-SD-4209 in Allendale Pond (May 2003 data).

cfo - C:\BATman\Analysis\Sedimentation_rates\plot_pb_cs_profiles_3panel_040721.pro
Thu Aug 26 16:02:04 2004

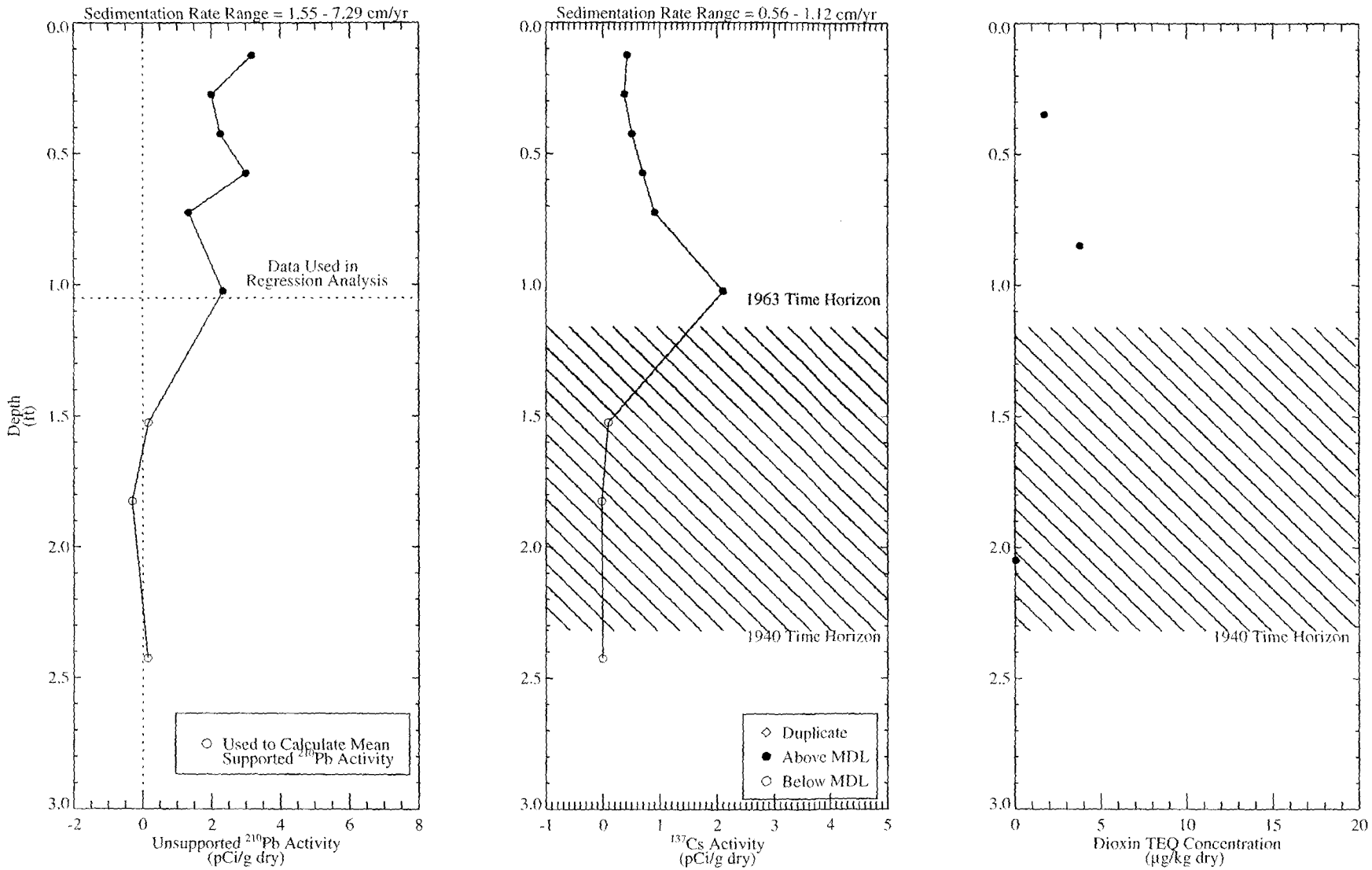

Figure 2-10. Vertical profiles of Pb-210 activity, Cs-137 activity and dioxin TEQ concentration for core CMS-SD-4210 in Allendale Pond (May 2003 data).

cfo - C:\BATman\Analysis\Sedimentation_rates\plot_pb_cs_profiles_3panel_040721.pro
Thu Aug 26 16:02:0

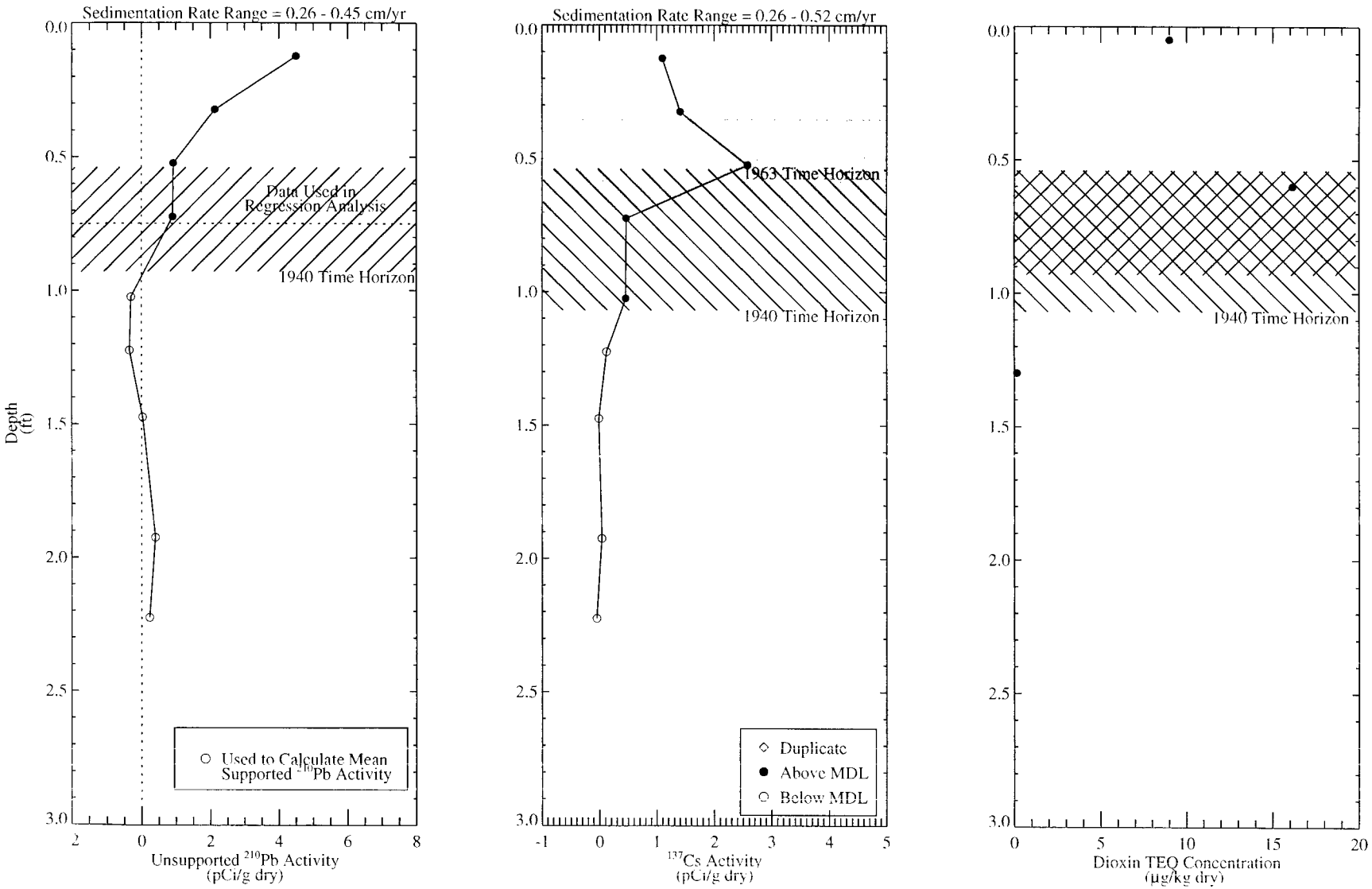

Figure 2-11. Vertical profiles of Pb-210 activity, Cs-137 activity and dioxin TEQ concentration for core CMS-SD-4212 in Allendale Pond (May 2003 data).

cfo - C:\BATman\Analysis\Sedimentation_rates\plot_pb_cs_profiles_3panel_040721.pro
Thu Aug 26 16:02:04 2004

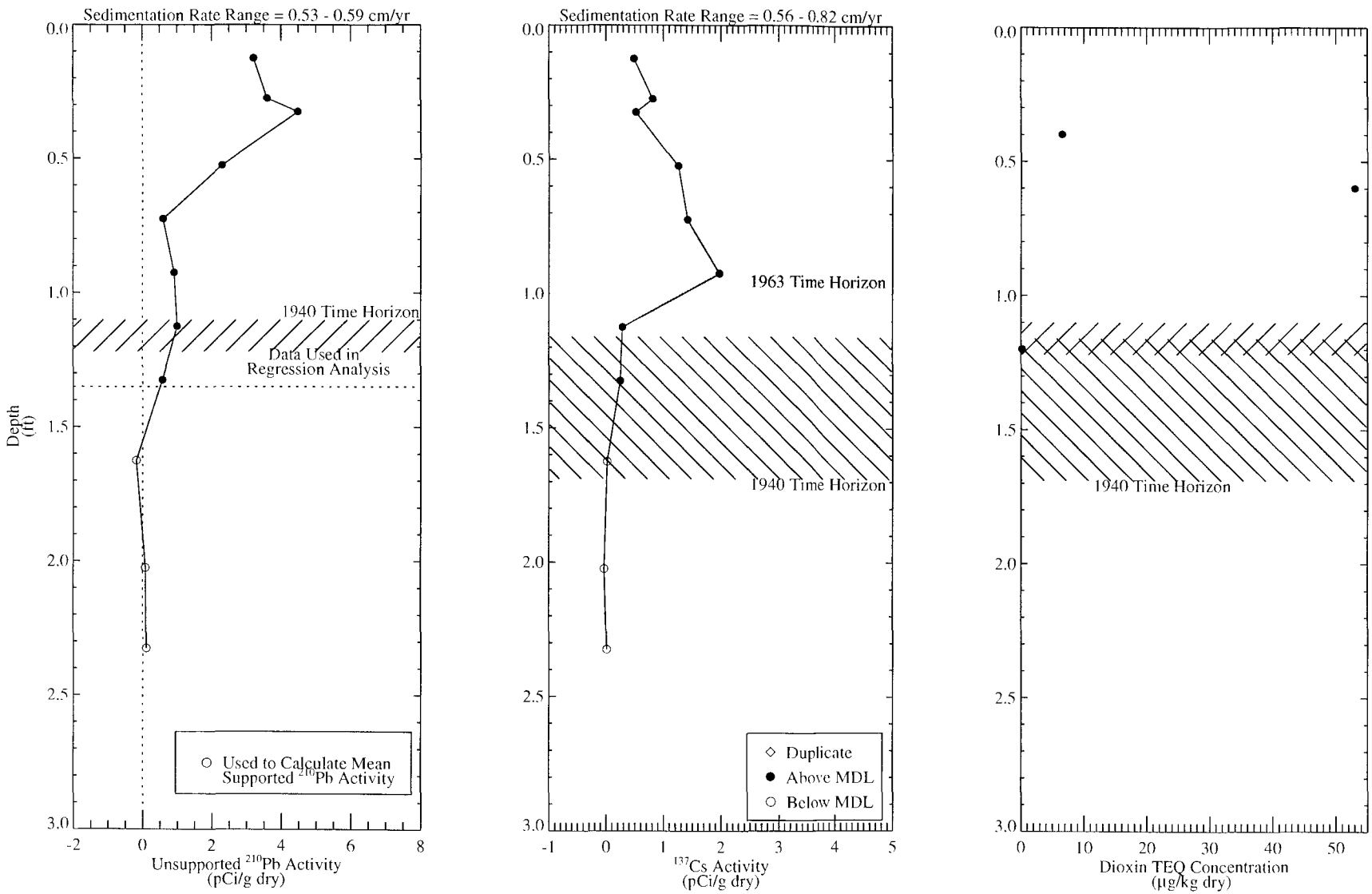

Figure 2-12. Vertical profiles of Pb-210 activity, Cs-137 activity and dioxin TEQ concentration for core CMS-SD-4213 in Allendale Pond (May 2003 data).

cfo - C:\BATman\Analysis\Sedimentation_rates\plot_pb_cs_profiles_3panel_040721.pro
Thu Aug 26 16:02:0[illegible]04

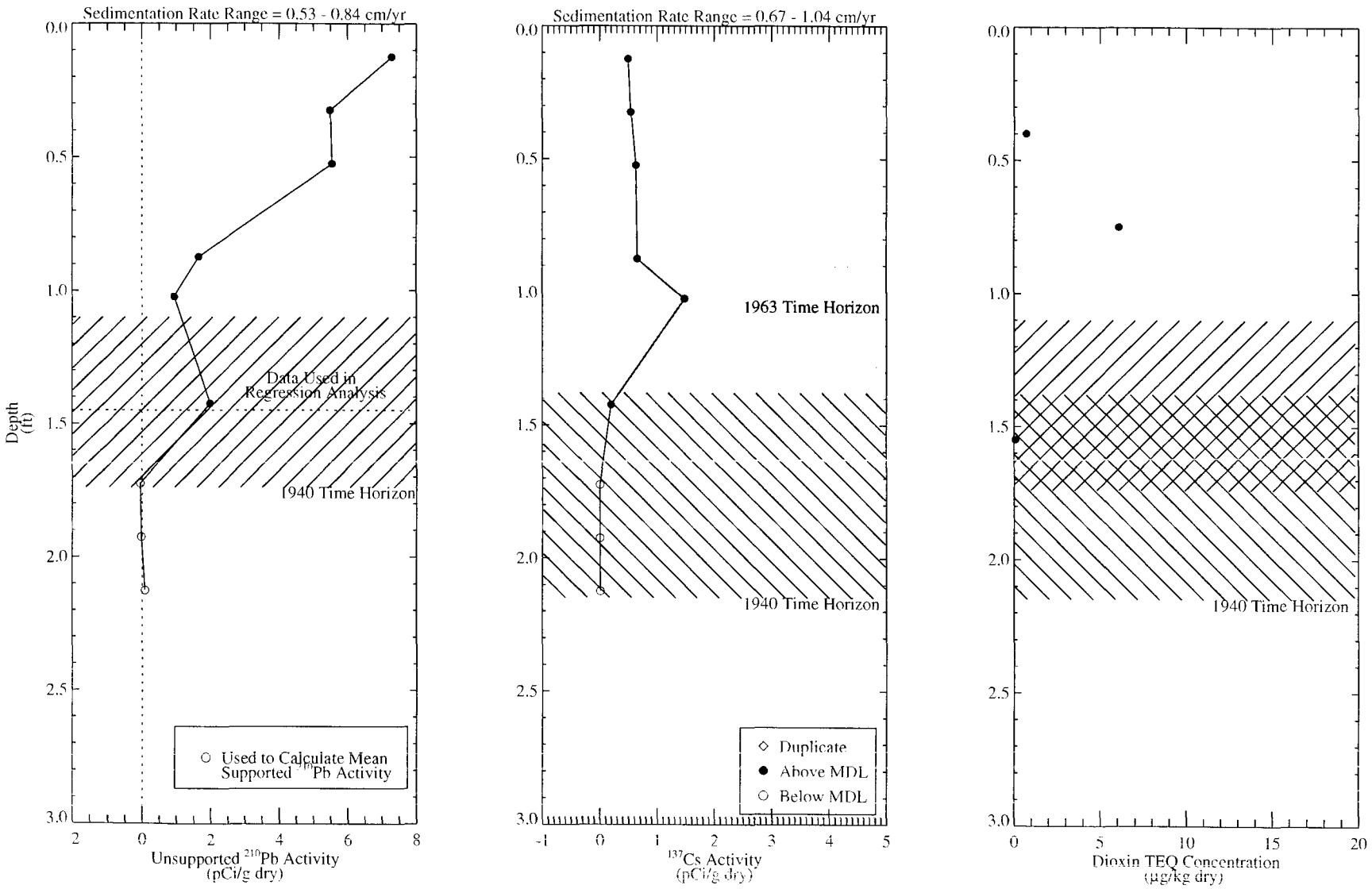

Figure 2-13. Vertical profiles of Pb-210 activity, Cs-137 activity and dioxin TEQ concentration for core CMS-SD-4218 in Allendale Pond (May 2003 data).

cfo - C:\BATman\Analysis\Sedimentation_rates\plot_pb_cs_profiles_3panel_040721.pro
Thu Aug 26 16:02:04 2004

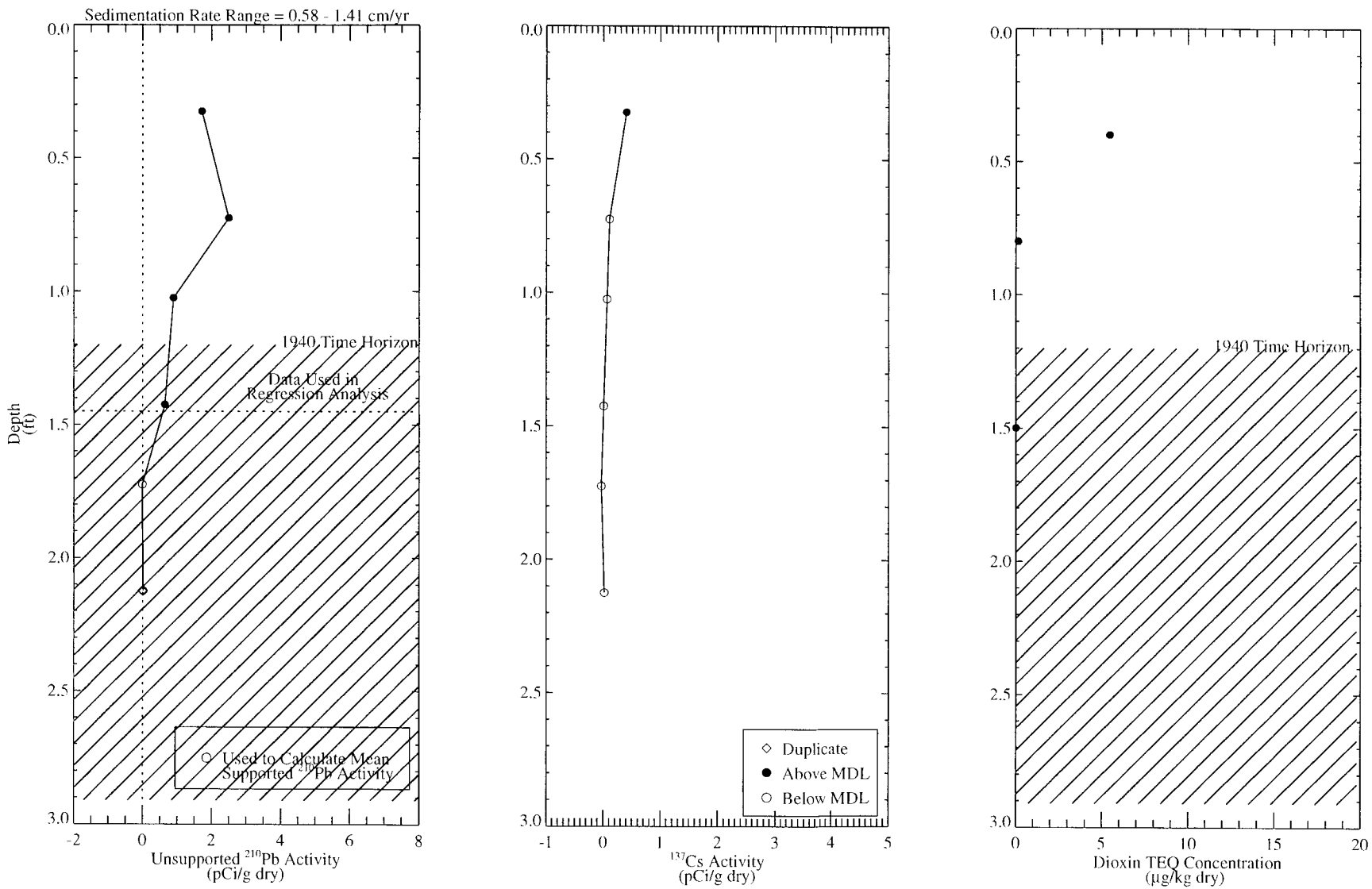

Figure 2-14. Vertical profiles of Pb-210 activity, Cs-137 activity and dioxin TEQ concentration for core CMS-SD-4219 in Allendale Pond (May 2003 data).

cfo - C:\BATman\Analysis\Sedimentation_rates\plot_pb_cs_profiles_3panel_040721.pro
Thu Aug 26 16:02:04

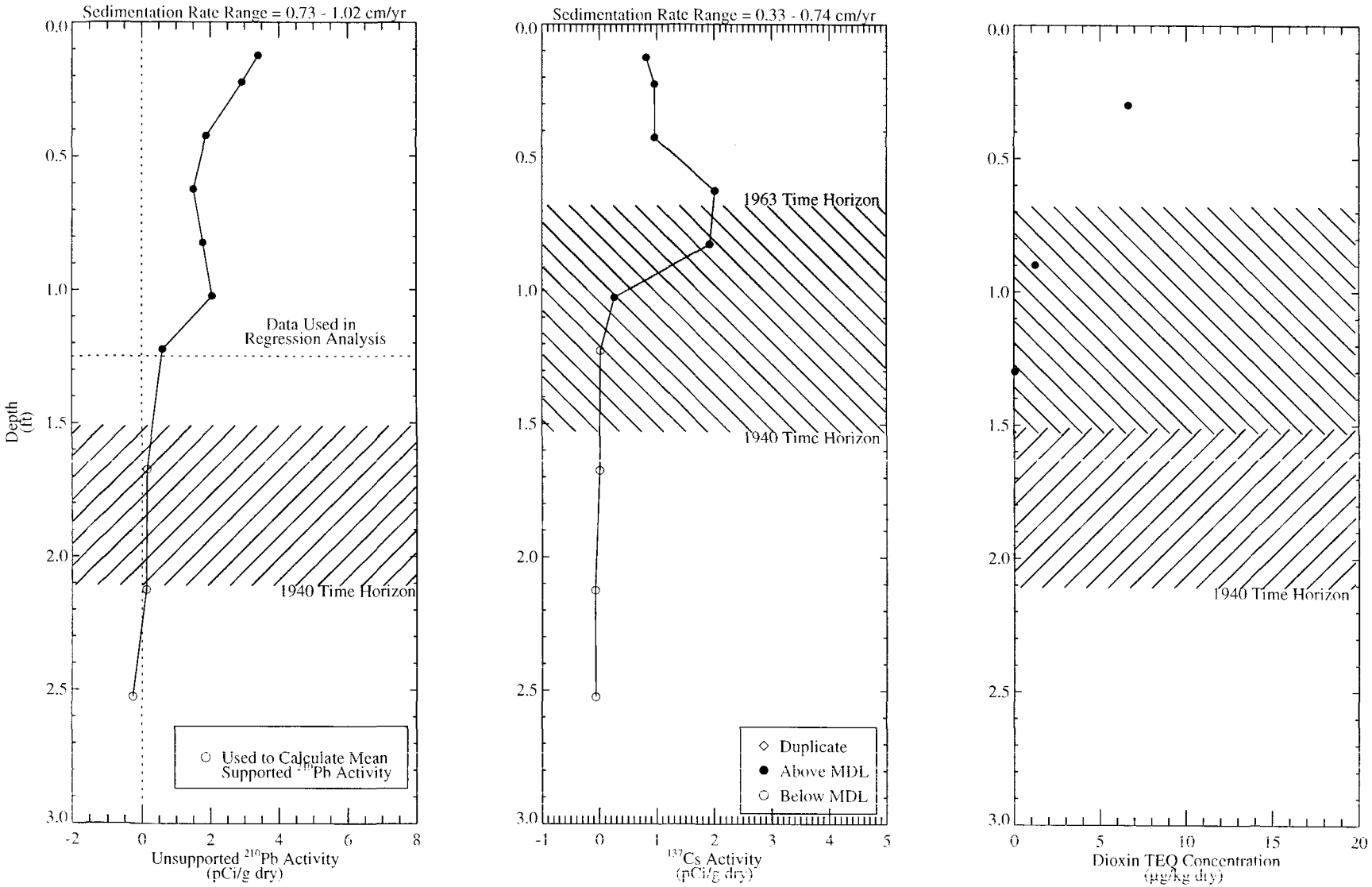

Figure 2-15. Vertical profiles of Pb-210 activity, Cs-137 activity and dioxin TEQ concentration for core CMS-SD-4222 in Allendale Pond (May 2003 data).

cfo - C:\BATman\Analysis\Sedimentation_rates\plot_pb_cs_profiles_3panel_040721.pro
Thu Aug 26 16:02:04 2004

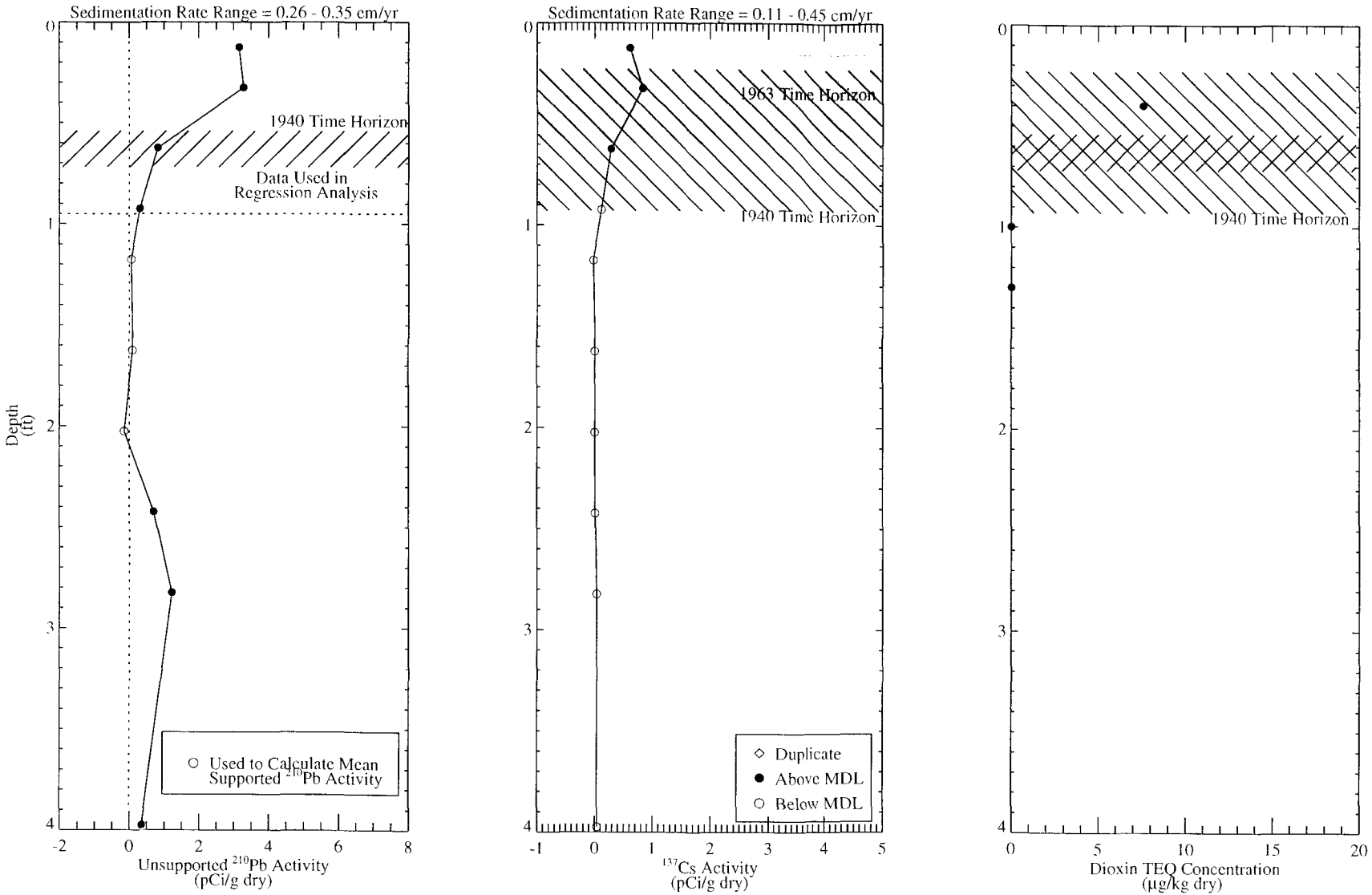

Figure 2-16. Vertical profiles of Pb-210 activity, Cs-137 activity and dioxin TEQ concentration for core LPX-SD-4201 in Lyman Mill Pond (May 2003 data).

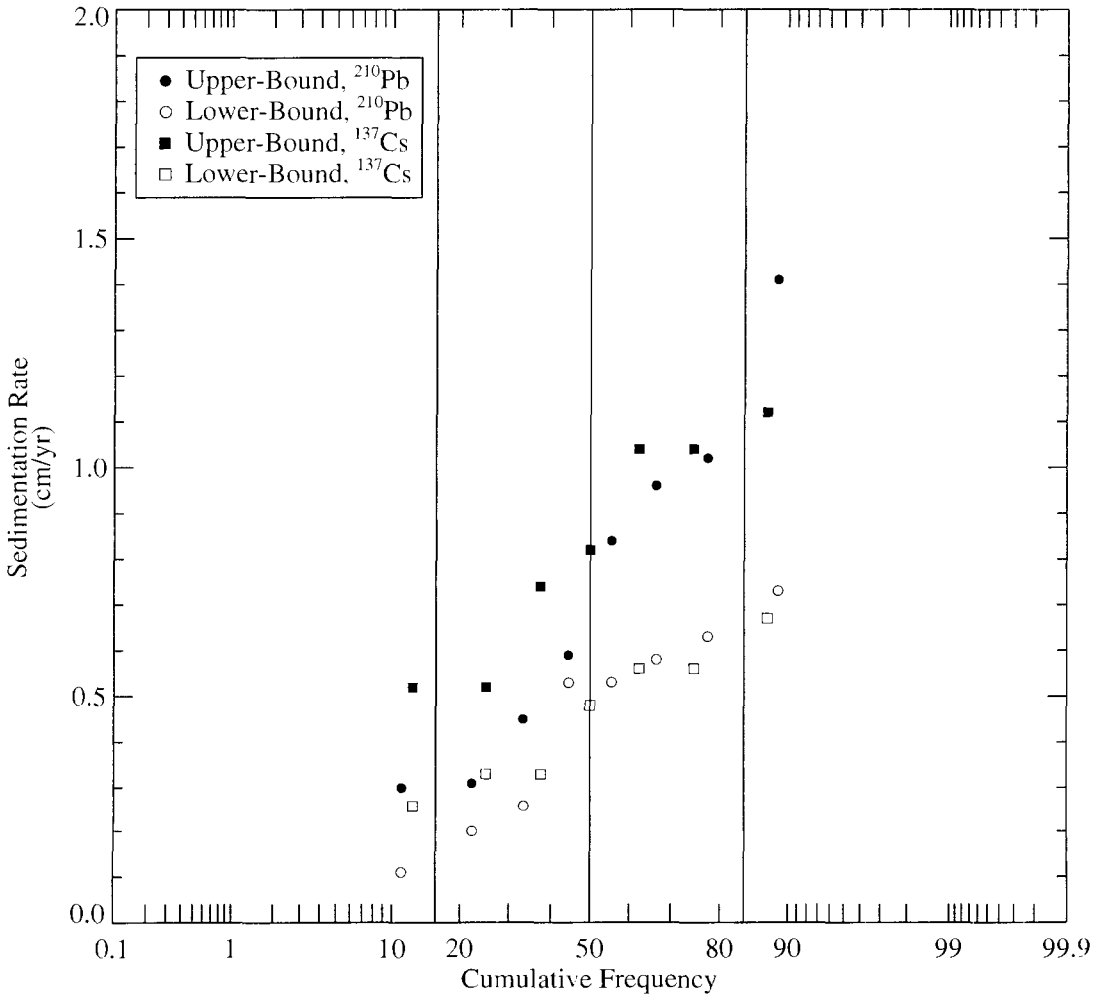

Figure 2-17. Frequency distributions of upper- and lower-bound estimates of Allendale Pond sedimentation rates based on analysis of Pb-210 and Cs-137 activity data.

cfo - C:\BATman\Analysis\Sedimentation_rates\probplot_pb_cs_sedrate_bounds_040823.pro
Thu Aug 26 15:20:44 2004

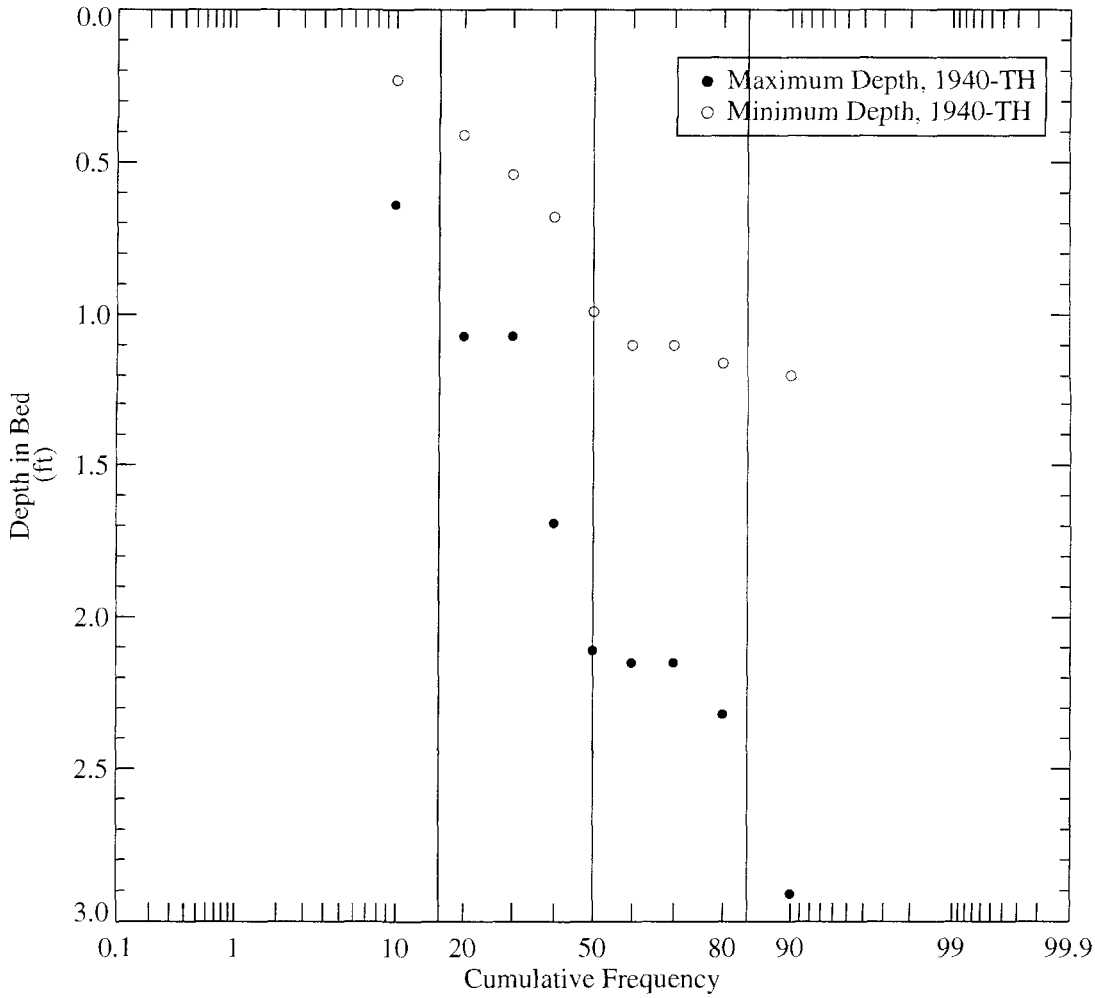

Figure 2-18. Frequency distributions of minimum and maximum depths of 1940-TH in Allendale Pond sediment cores.

cfo - C:\BATman\Analysis\Sedimentation_rates\probplot_pb_cs_sedrate_bounds_040823.pro
Thu Aug 26 15:20:44 2004

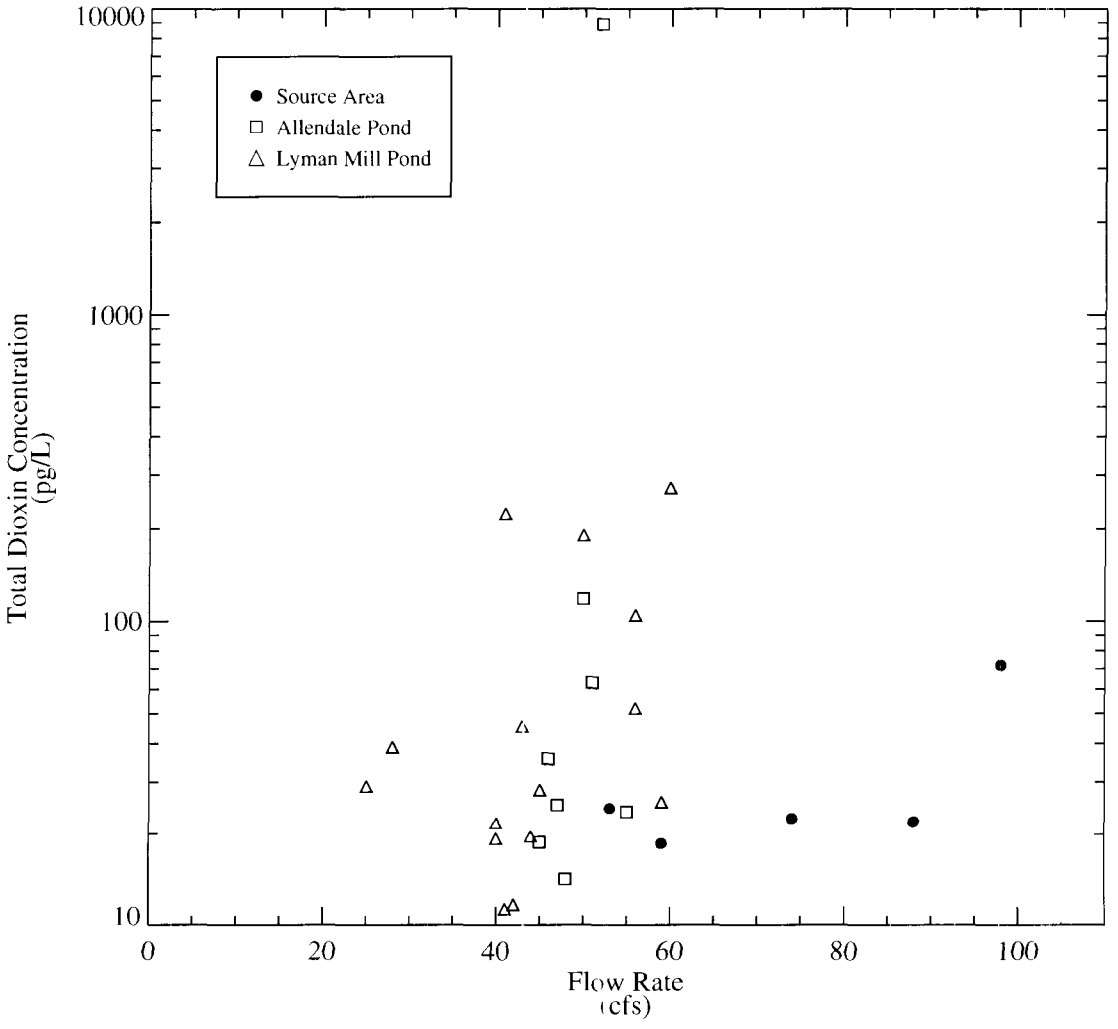

Figure 2-19. Correlation between total dioxin water-column concentration and flow rate during October-November 1999 sampling period.

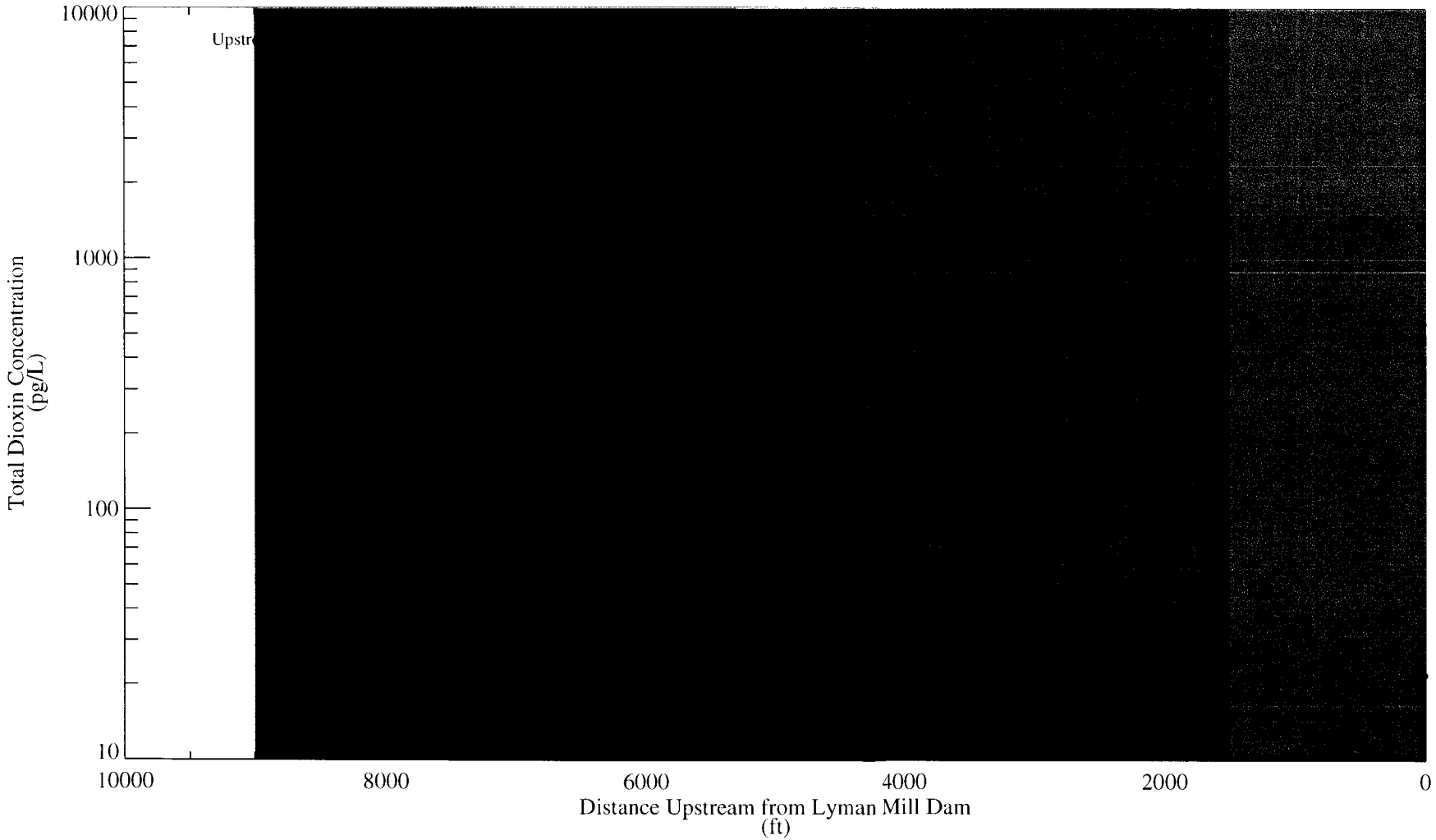

Figure 2-20. Spatial distribution of total dioxin water-column concentration during October-November 1999 sampling period.

Locator Map

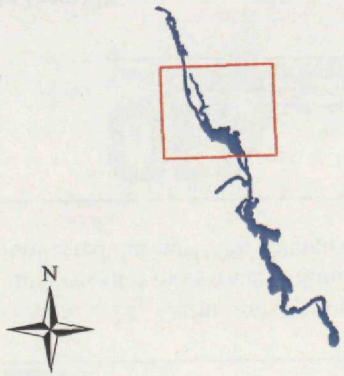

Legend

1997 Shoreline

1999 WQ Sampling Locations

Zones

1

2

3

4

5

Figure 2-21. Definitions of zones used in analysis of dioxin water-column data collected during 1999: Allendale Pond.

QEA
Quantitative Environmental Analysis, LLC

BATcen:120 August 2004

CO- C:\BATman\Maps\ArcGIS\vector\batcen_allendale_tau.mxd

Locator Map

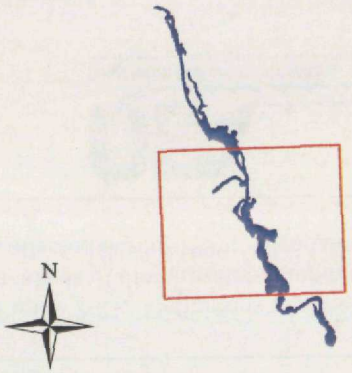

Legend

- 1997 Shoreline
- 1999 WQ Sampling Locations

Zones

- 1
- 2
- 3
- 4
- 5

Figure 2-22. Definitions of zones used in analysis of dioxin water-column data collected during 1999: Lyman Mill Pond.

QEA
Quantitative Environmental Analysis, LLC

BATcen:120 **August 2004**

CO- C:\BATman\Maps\ArcGIS\vector\batcen_vectors.mxd

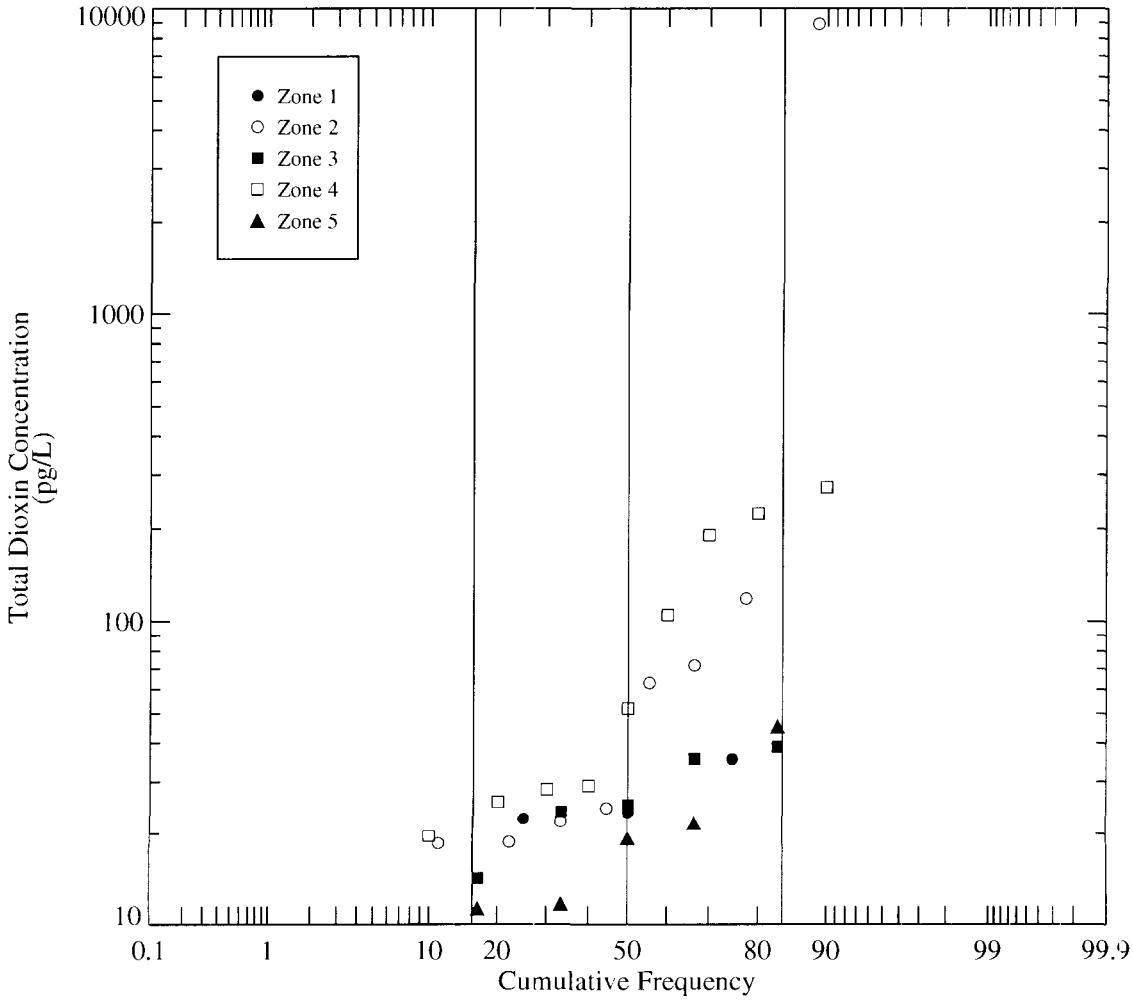

Figure 2-23. Frequency distributions of total dioxin water-column concentration in Zones 1, 2, 3, 4 and 5 during October-November 1999 sampling period.

cfo - C:\BATman\Analysis\WQ_spatial\wq_spatial_040820.pro
Fri Aug 27 08:38:51 2004

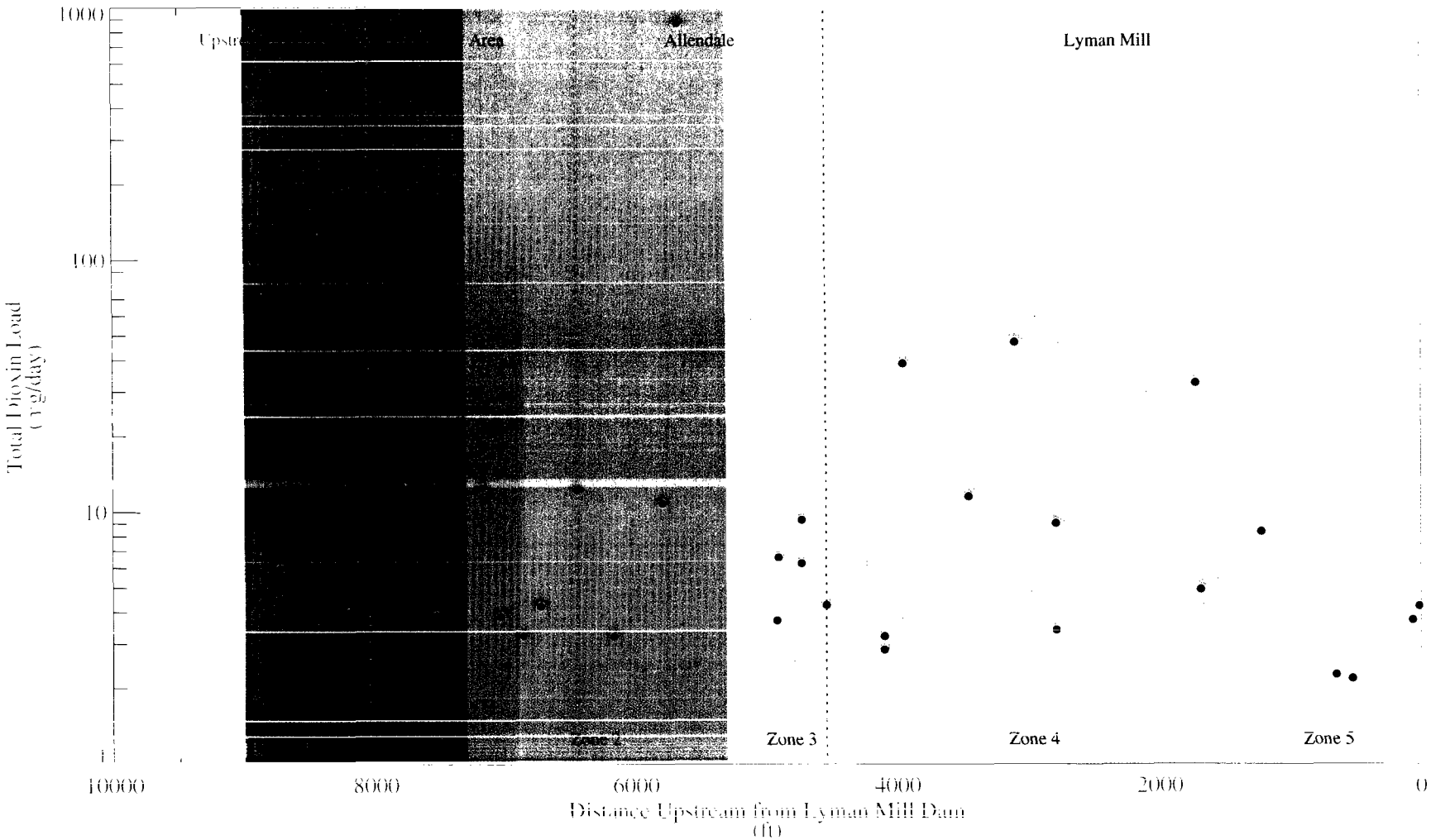

Figure 2-24. Spatial distribution of total dioxin water-column load during October-November 1999 sampling period.

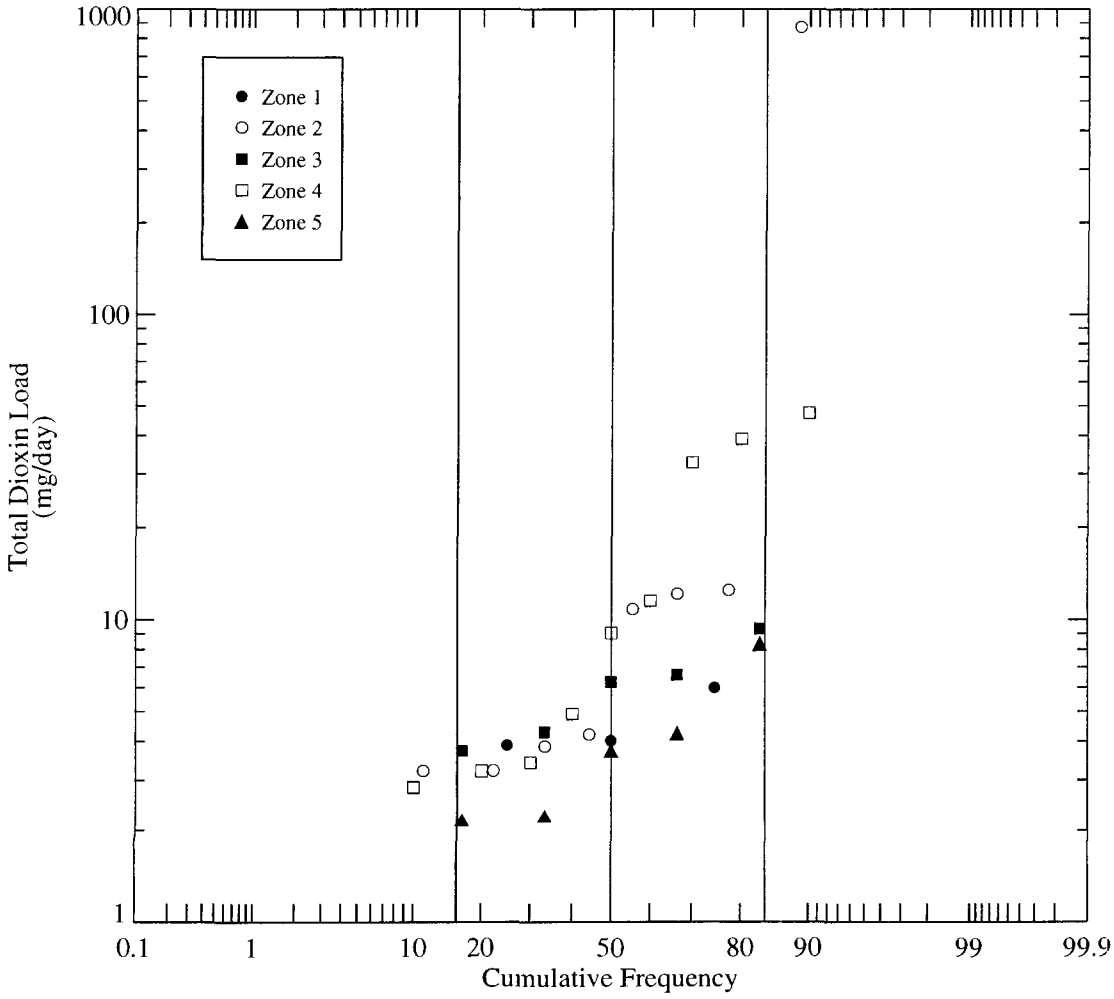

Figure 2-25. Frequency distributions of total dioxin water-column load in Zones 1, 2, 3, 4 and 5 during October-November 1999 sampling period.

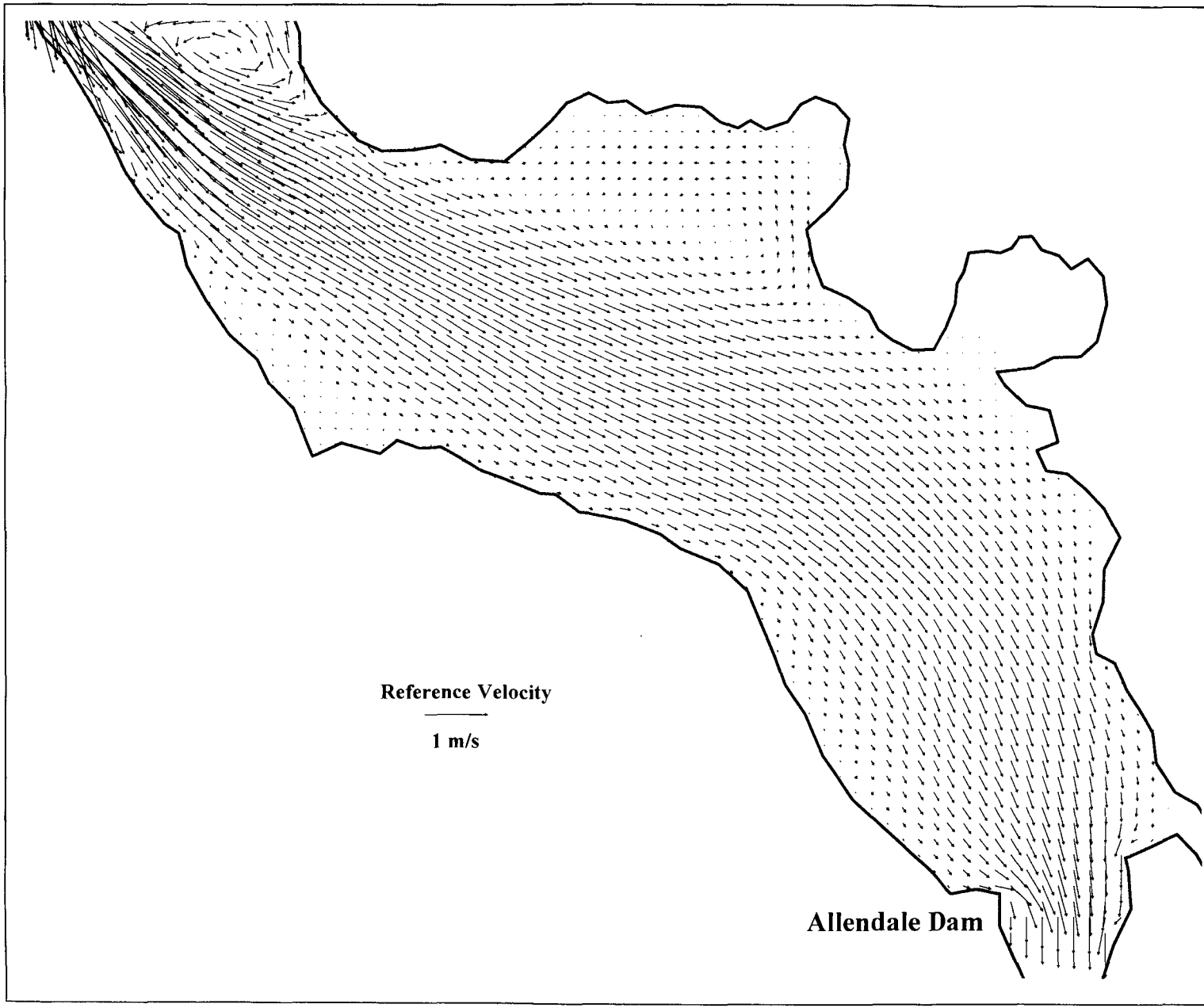

Locator Map

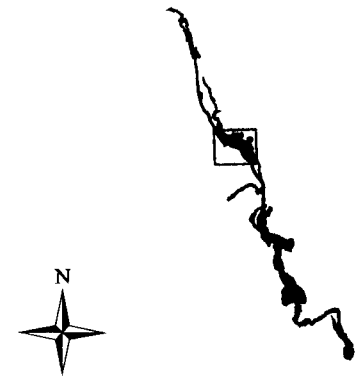

Legend

1997 Shoreline
Velocity Vector

Figure 3-1. Predicted current velocities during 100-year flood in Allendale Pond.

QEA
Quantitative Environmental Analysis, LLC

BATcen:120 **August 2004**

CO- C:\BATman\Maps\ArcGIS\vector\batcen_vectors.mxd

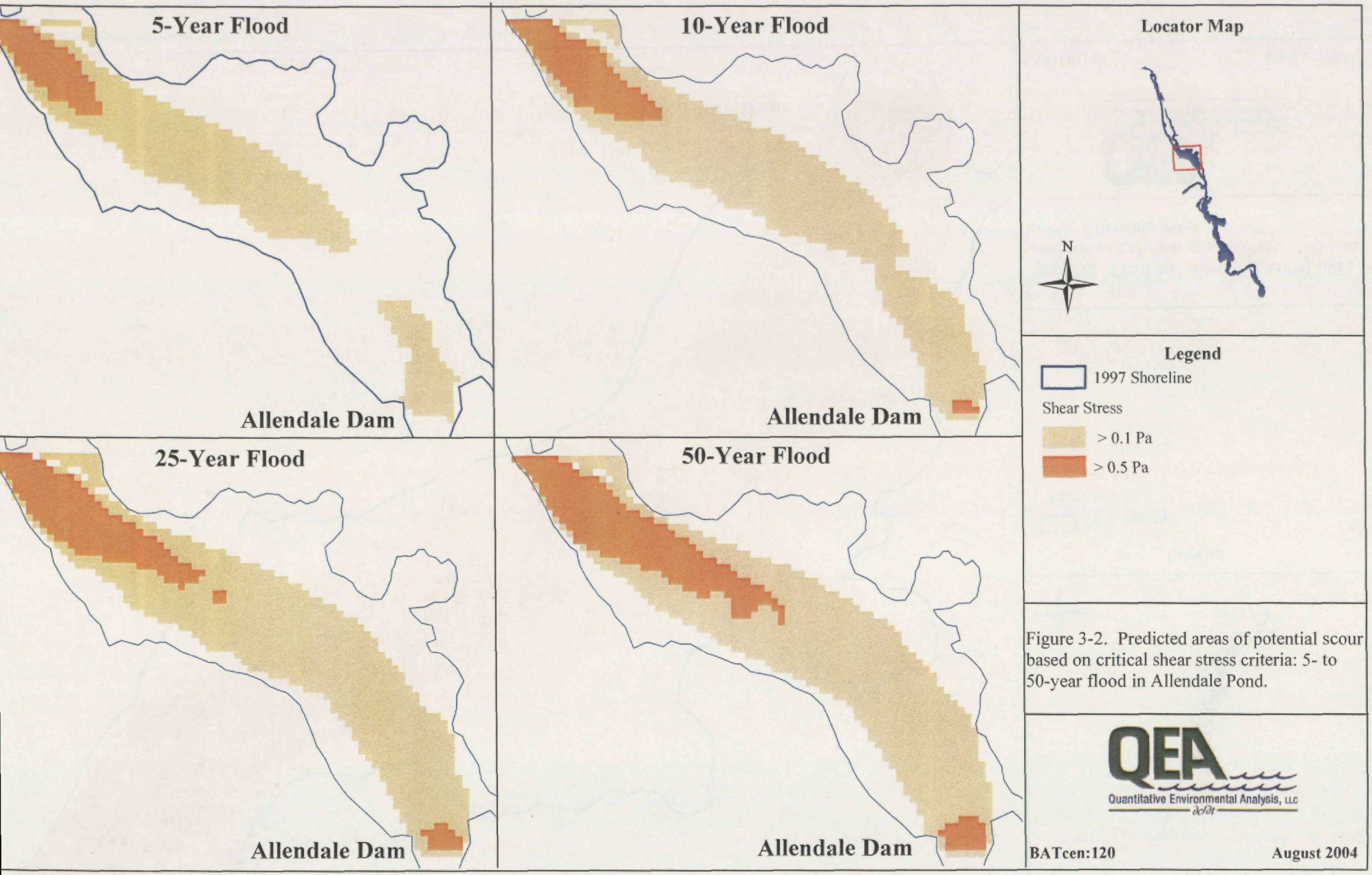

Figure 3-2. Predicted areas of potential scour based on critical shear stress criteria: 5- to 50-year flood in Allendale Pond.

C:\BATman\Maps\ArcGIS\shear_stress\batcen_allendale_tau_4panel.mxd

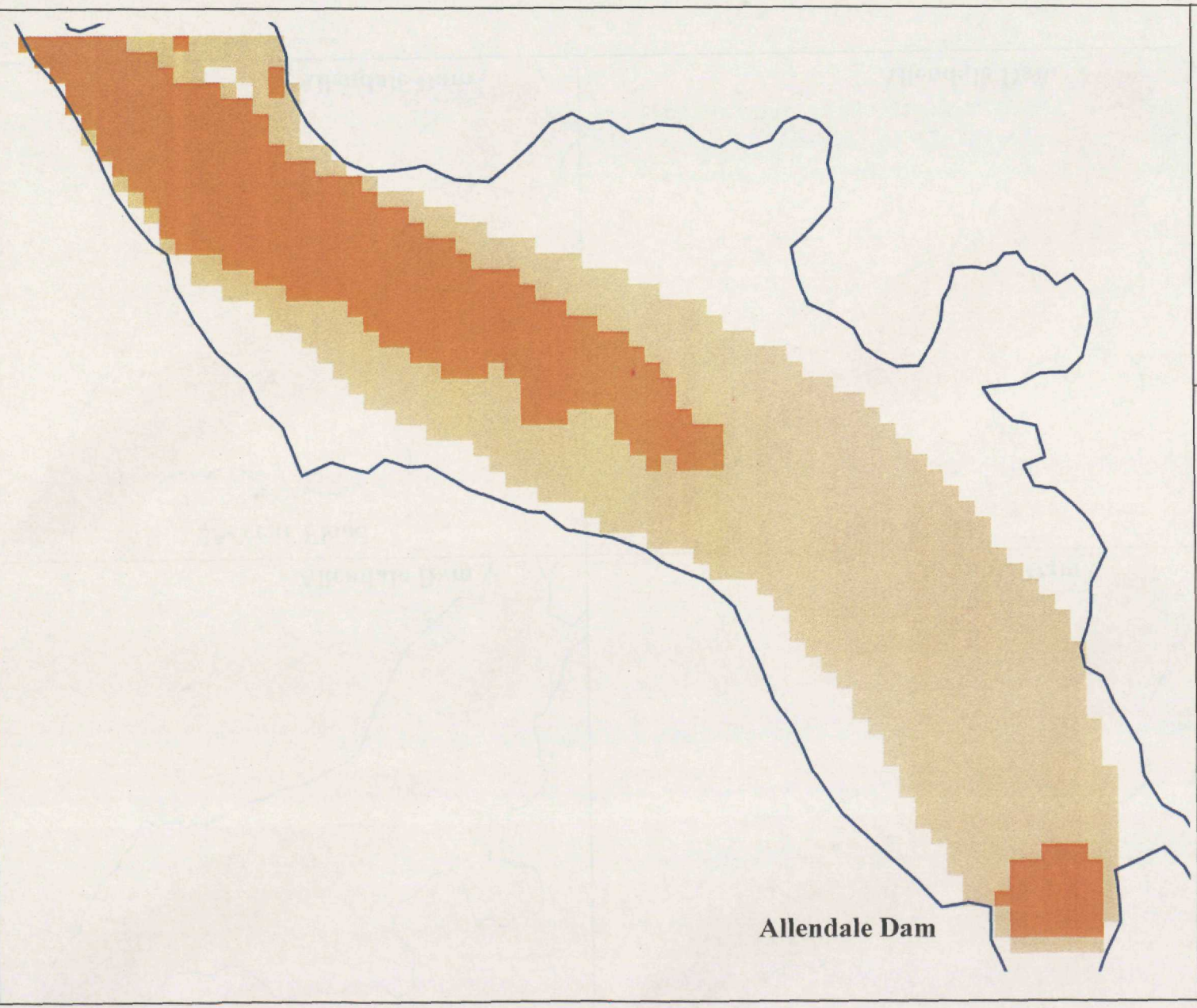

Locator Map

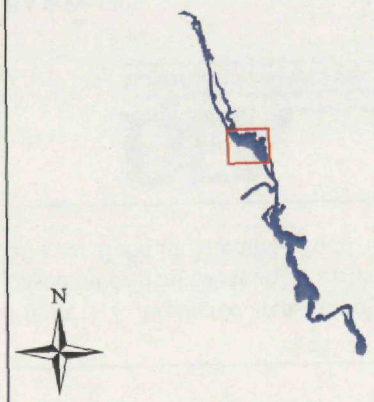

Legend

1997 Shoreline

Shear Stress

> 0.1 Pa

> 0.5 Pa

Figure 3-3. Predicted areas of potential scour based on critical shear stress criteria: 100-year flood in Allendale Pond.

QEA
Quantitative Environmental Analysis, LLC

BATcen:120 **August 2004**

CO- C:\BATman\Maps\ArcGIS\vector\batcen_allendale_tau.mxd

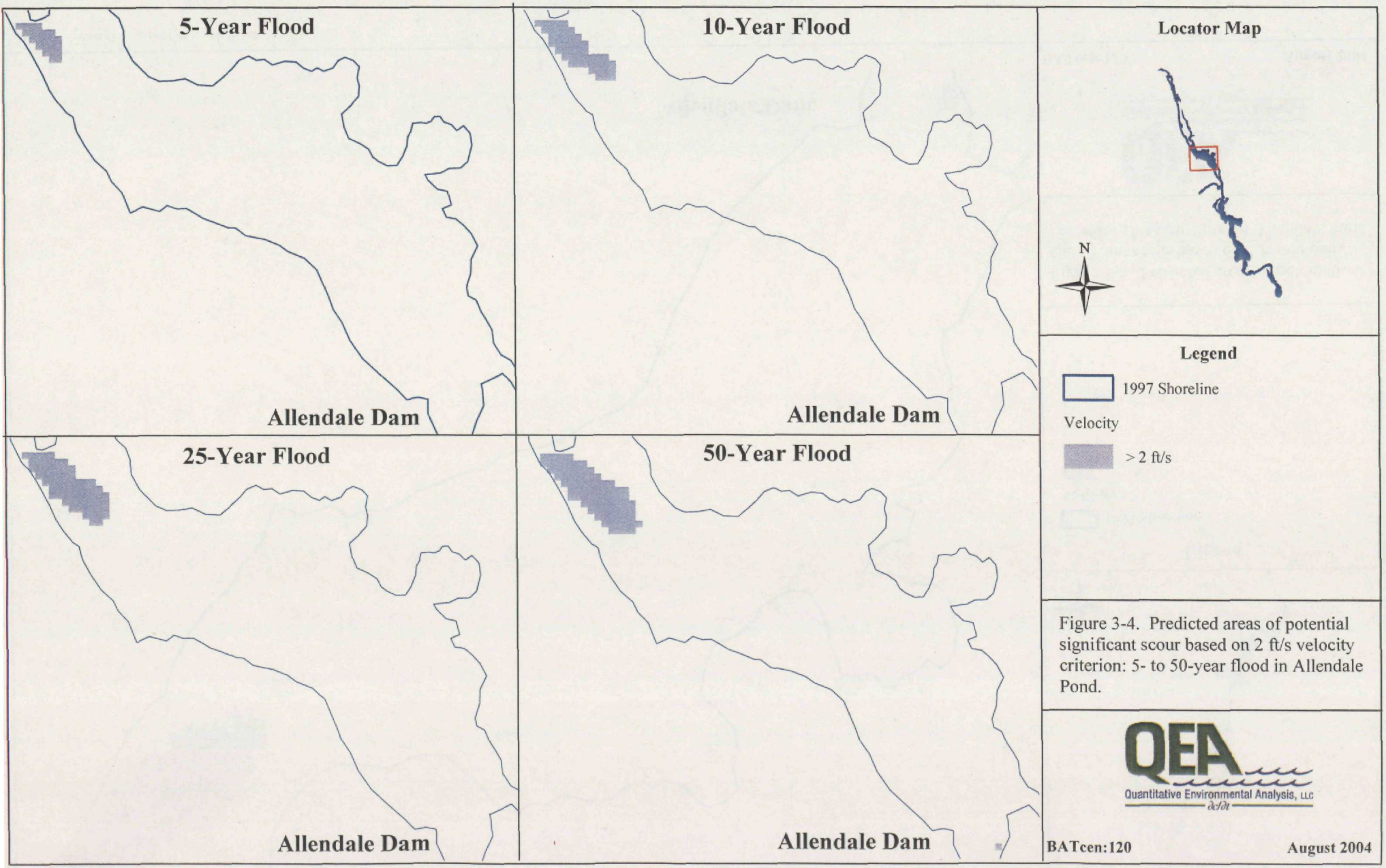

Figure 3-4. Predicted areas of potential significant scour based on 2 ft/s velocity criterion: 5- to 50-year flood in Allendale Pond.

CO- C:\BATman\Maps\ArcGIS\velocity\batcen_allendale_velocity_4panel.mxd

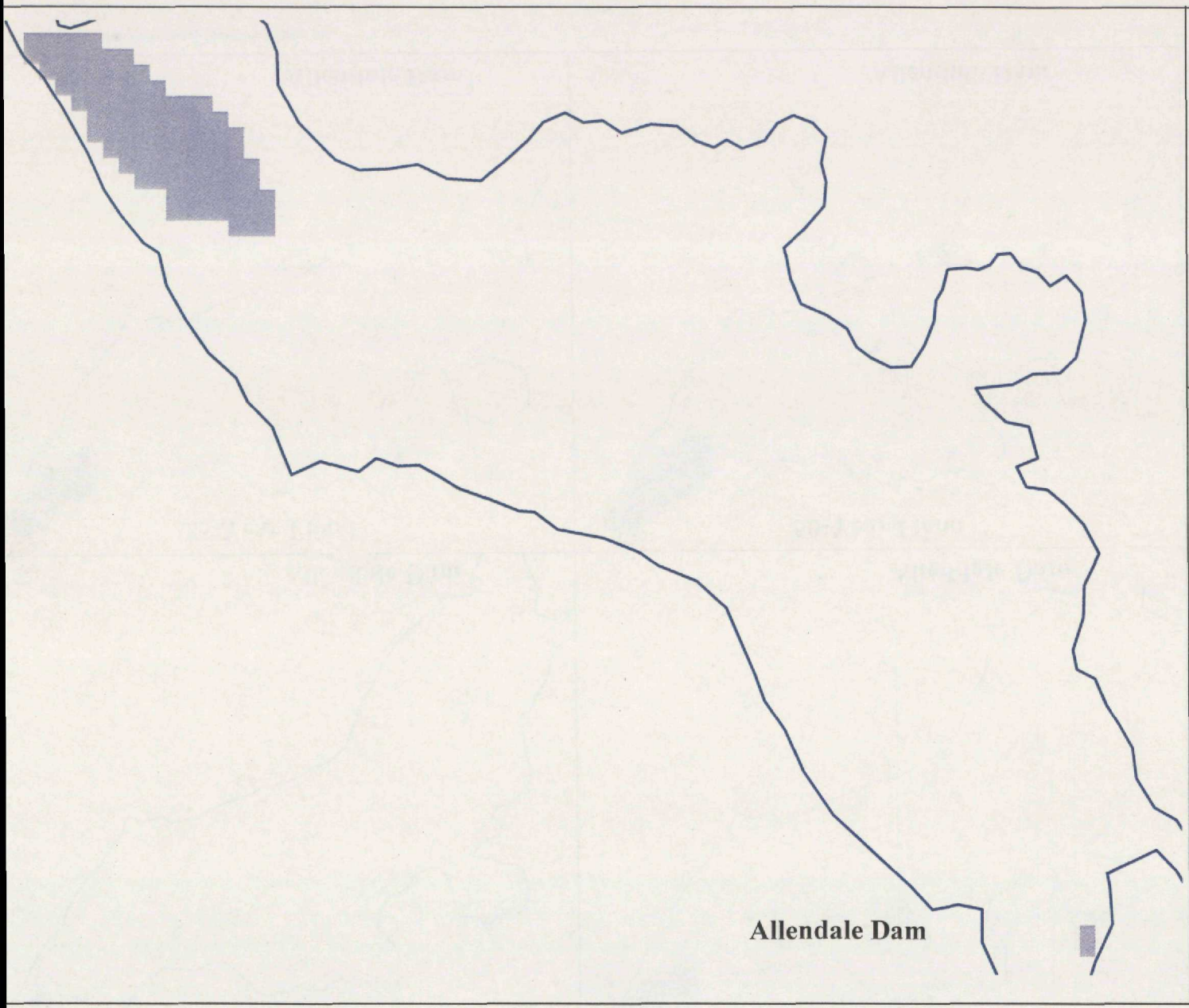

Locator Map

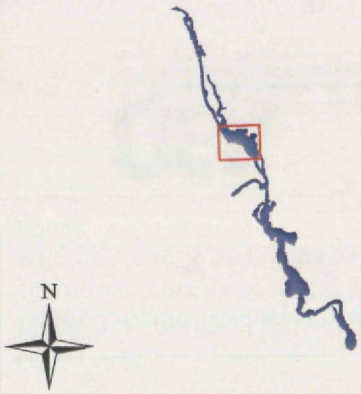

Legend

1997 Shoreline

Velocity

> 2 ft/s

Figure 3-5. Predicted areas of potential significant scour based on 2 ft/s velocity criterion: 100-year flood in Allendale Pond.

QEA
Quantitative Environmental Analysis, LLC

BATcen:120 **August 2004**

Q- C:\BATman\Maps\ArcGIS\vector\batcen_allendale_tau.mxd

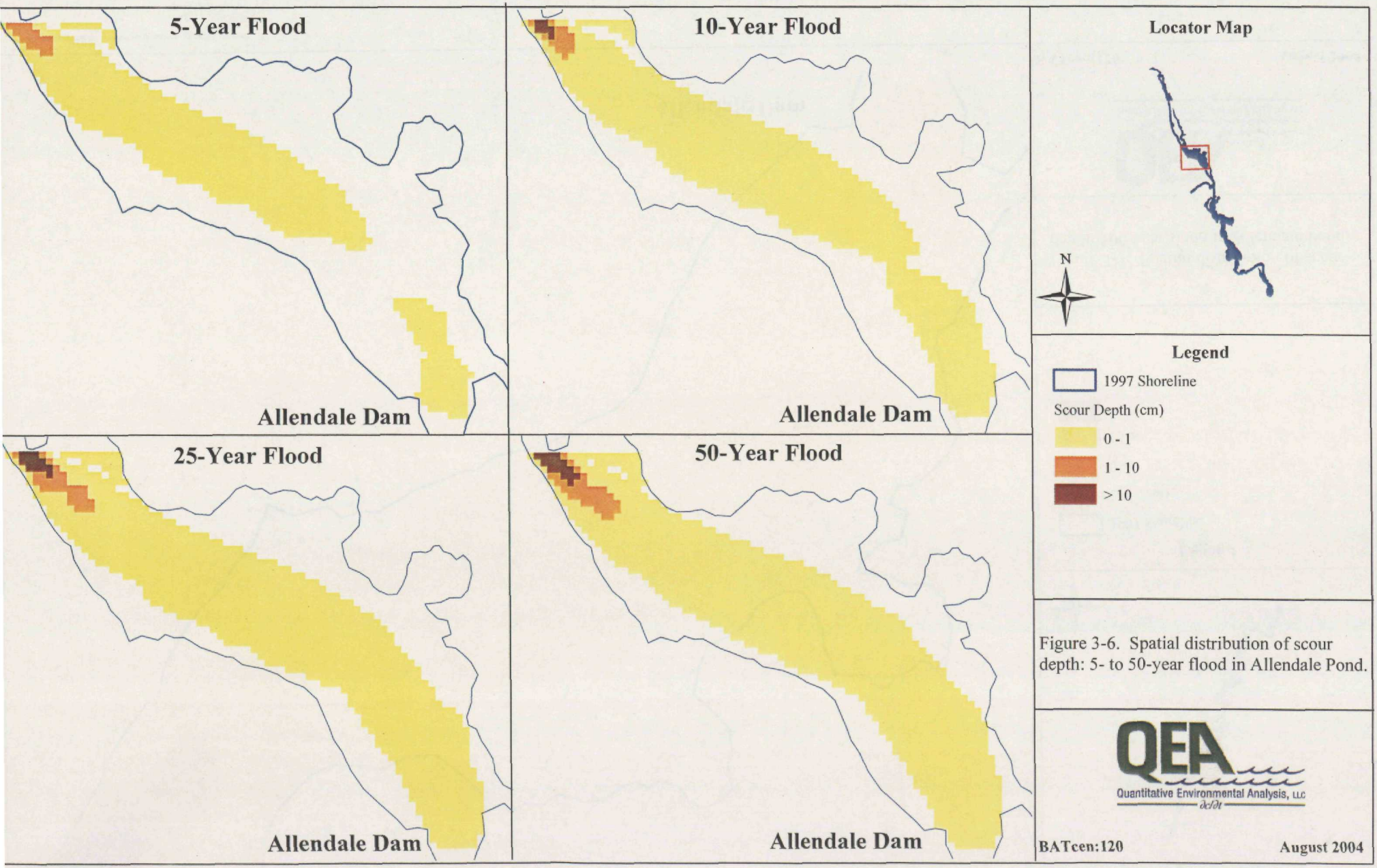

Figure 3-6. Spatial distribution of scour depth: 5- to 50-year flood in Allendale Pond.

CO- C:\BATman\Maps\ArcGIS\scour\batcen_allendale_scour_4panel.mxd

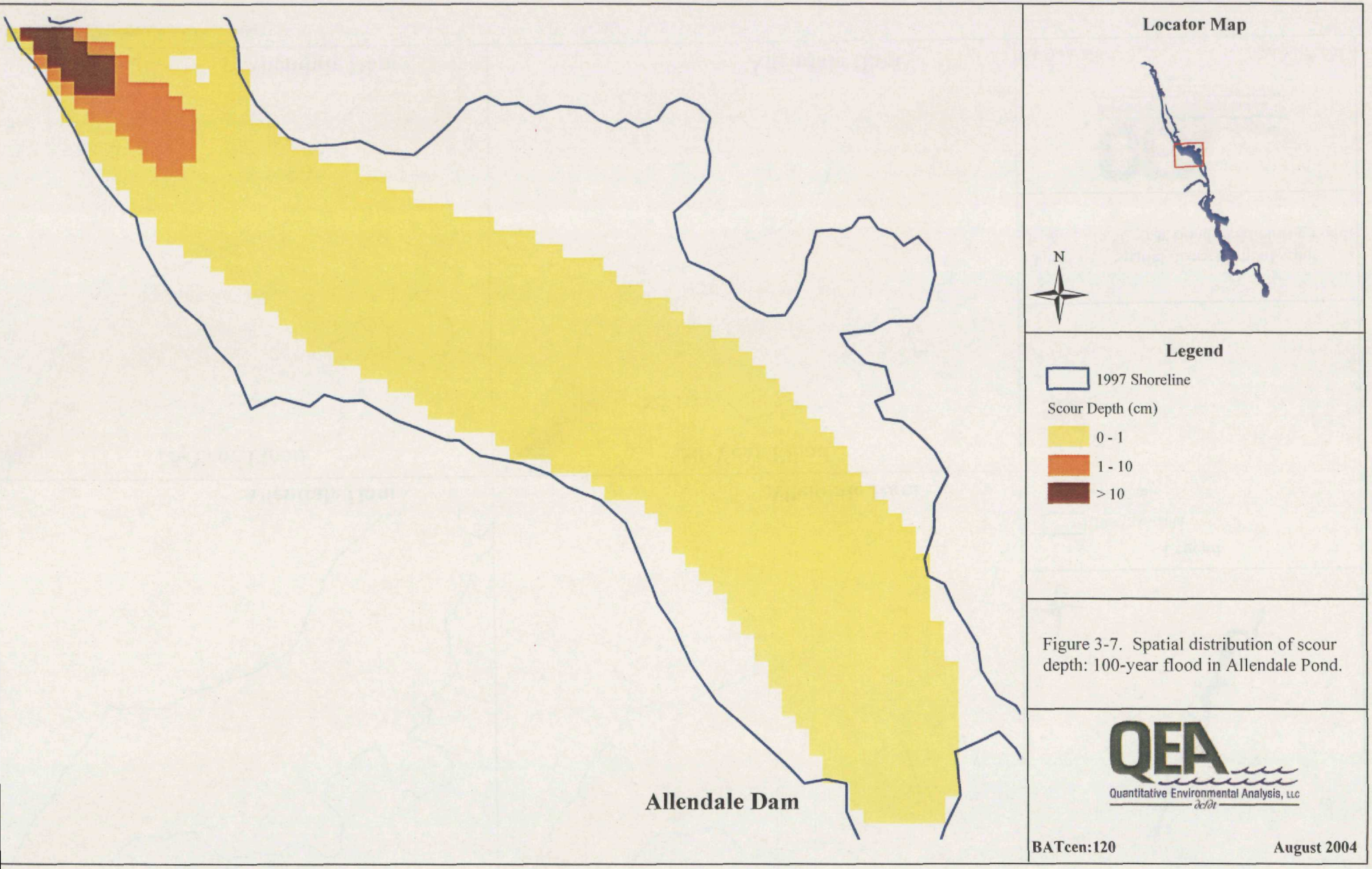

Figure 3-7. Spatial distribution of scour depth: 100-year flood in Allendale Pond.

CO- C:\BATman\Maps\ArcGIS\vector\batcen_allendale_tau.mxd

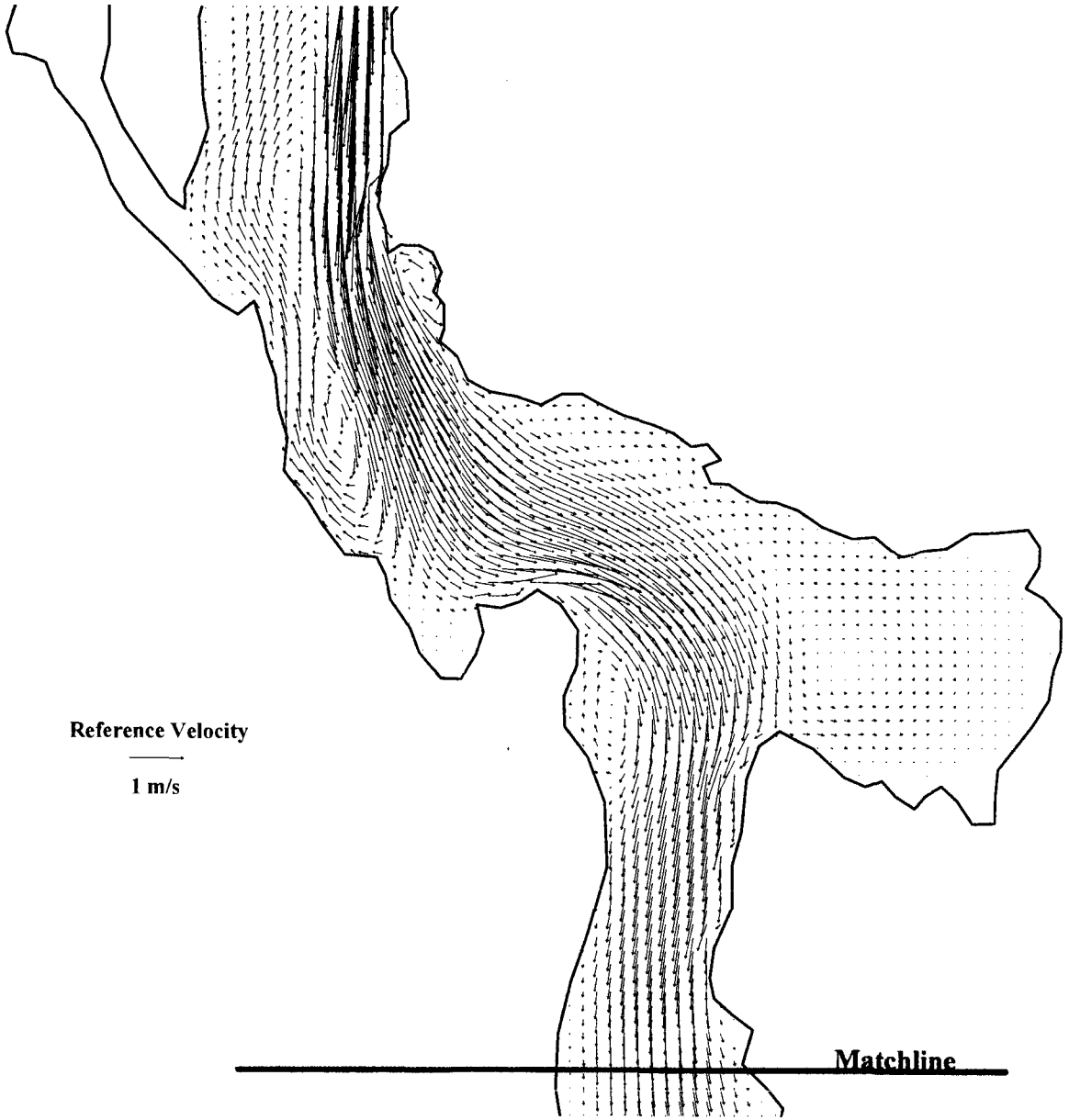

Locator Map

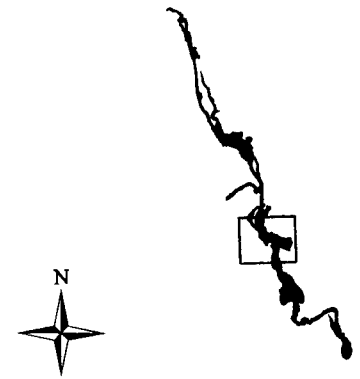

Legend

1997 Shoreline
Velocity Vector

Figure 3-8. Predicted current velocities during 100-year flood in Lyman Mill Pond: northern portion.

QEA
Quantitative Environmental Analysis, LLC

BATcen:120 August 2004

CO- C:\BATman\Maps\ArcGIS\vector\batcen_vectors.mxd

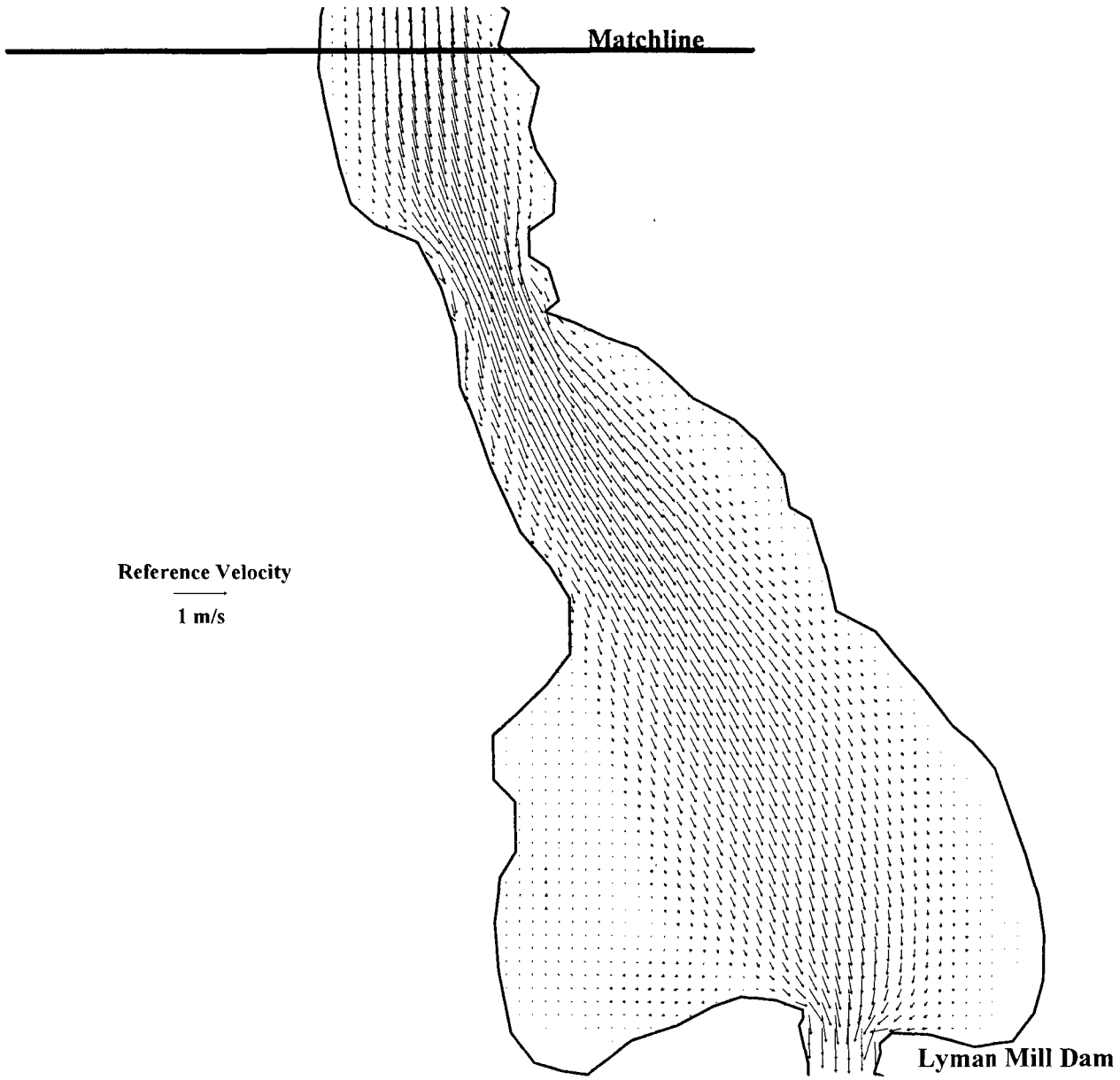

Locator Map

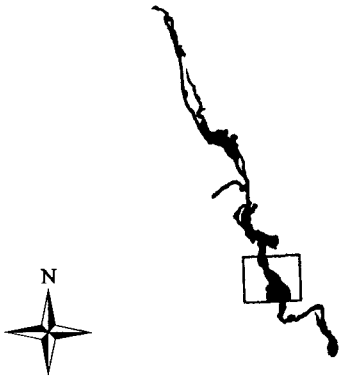

Legend

1997 Shoreline
Velocity Vector

Figure 3-9. Predicted current velocities during 100-year flood in Lyman Mill Pond: southern portion.

QEA
Quantitative Environmental Analysis, LLC

BATcen:120 **August 2004**

CO- C:\BATman\Maps\ArcGIS\vector\batcen_vectors.mxd

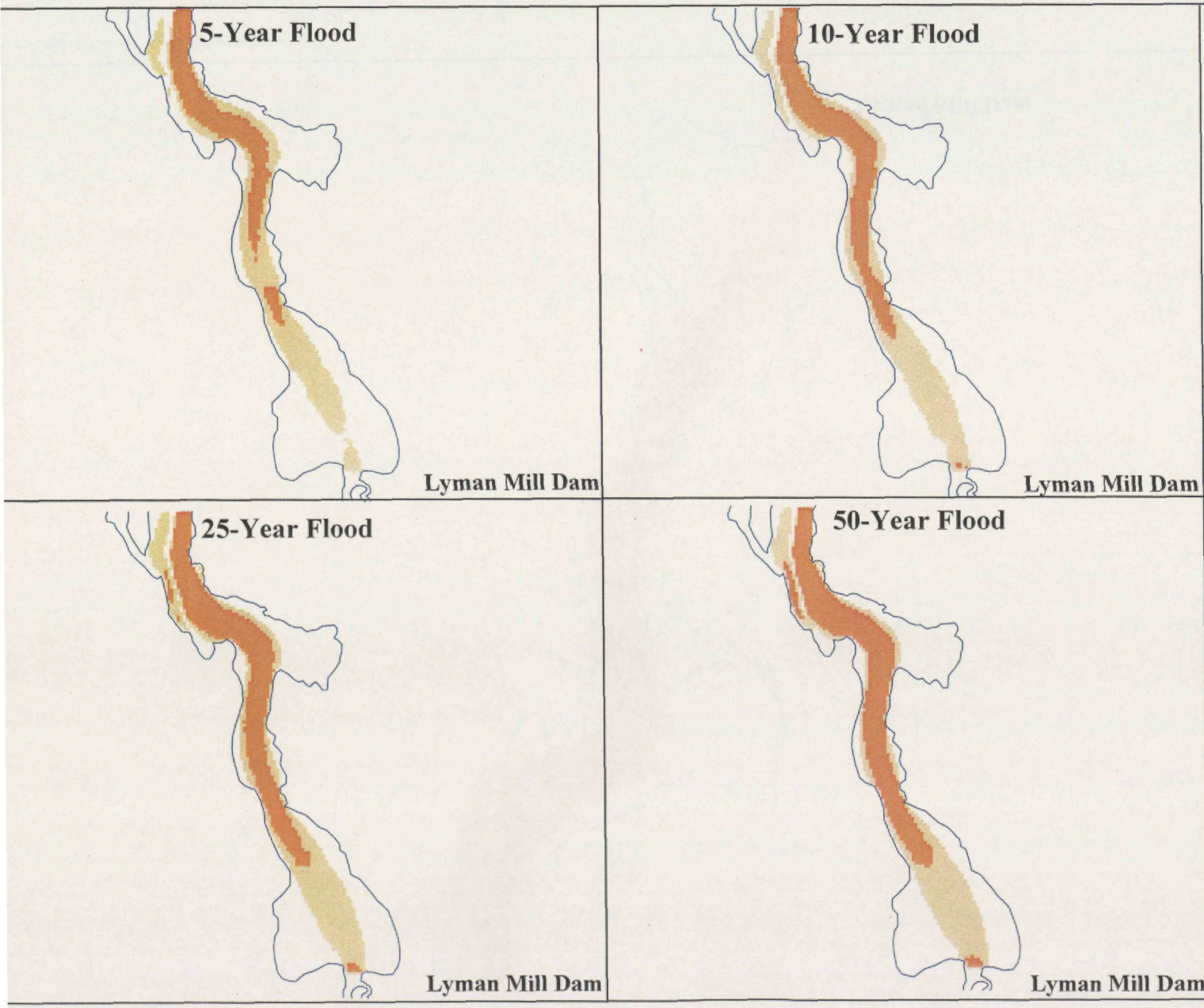

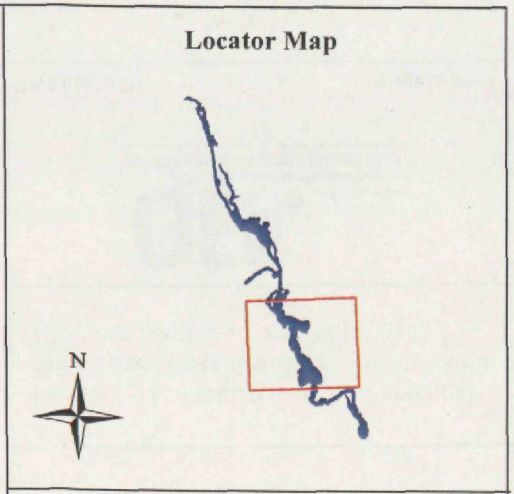

Legend

1997 Shoreline

Shear Stress

> 0.1 Pa

> 0.5 Pa

Figure 3-10. Predicted areas of potential scour based on critical shear stress criteria: 5- to 50-year flood in Lyman Mill Pond.

QEA
Quantitative Environmental Analysis, LLC

BATcen:120

August 2004

CO- C:\BATman\Maps\ArcGIS\shear_stress\batcen_lyman_tau_4panel.mxd

Locator Map

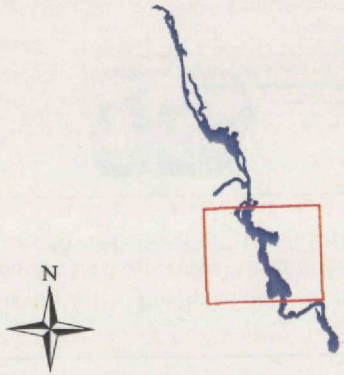

Legend

1997 Shoreline

Shear Stress

> 0.1 Pa

> 0.5 Pa

Figure 3-11. Predicted areas of potential scour based on critical shear stress criteria: 100-year flood in Lyman Mill Pond.

QEA Quantitative Environmental Analysis, LLC

BATcen:120 **August 2004**

CO- C:\BATman\Maps\ArcGIS\vector\batcen_vectors.mxd

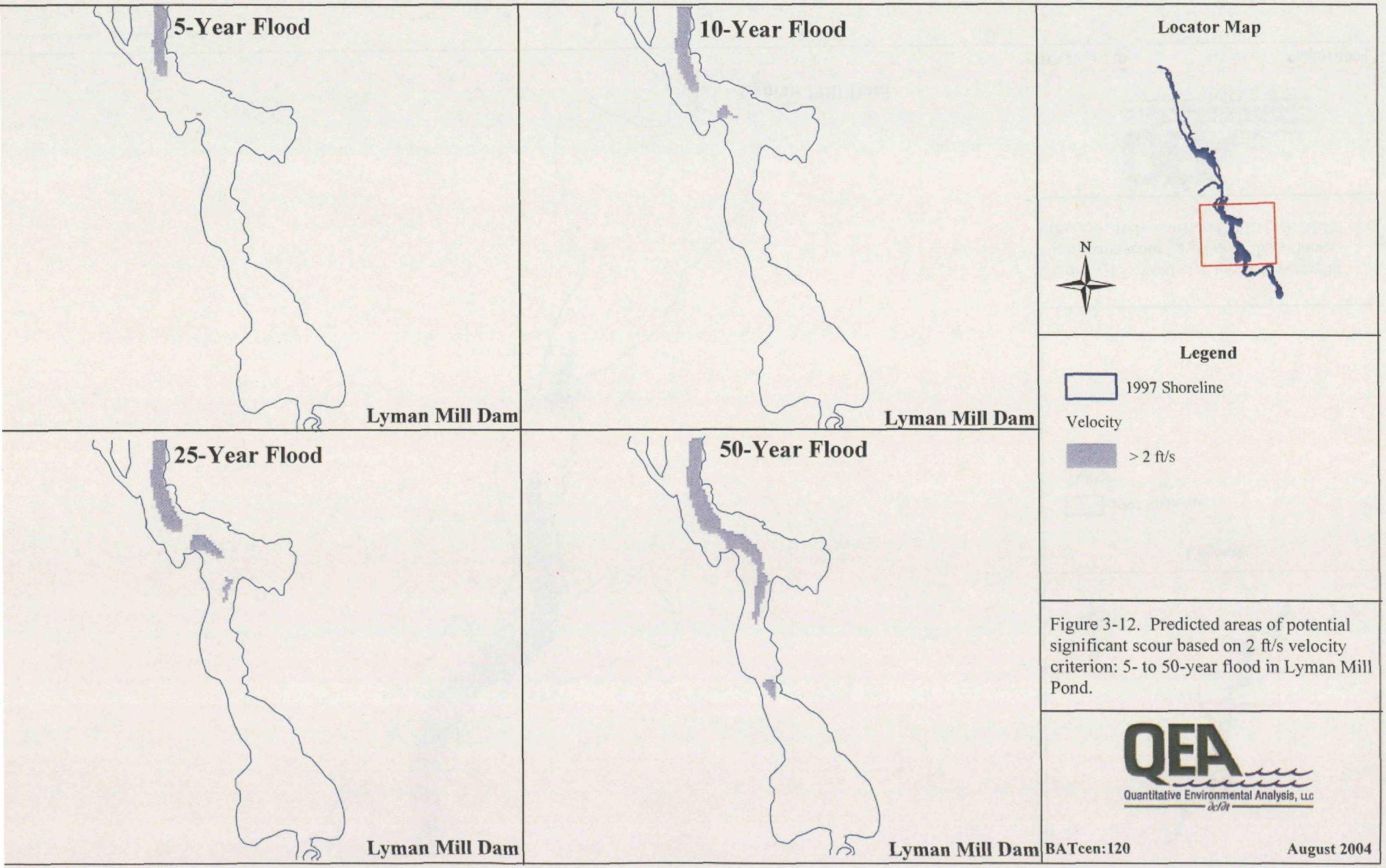

Figure 3-12. Predicted areas of potential significant scour based on 2 ft/s velocity criterion: 5- to 50-year flood in Lyman Mill Pond.

CO- C:\BATman\Maps\ArcGIS\velocity\batcen_lyman_velocity_4panel.mxd

Locator Map

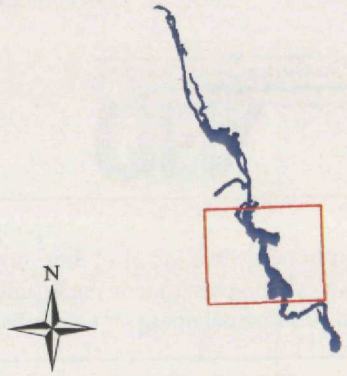

Legend

1997 Shoreline

Velocity

> 2 ft/s

Figure 3-13. Predicted areas of potential significant scour based on 2 ft/s velocity criterion: 100-year flood in Lyman Mill Pond.

QEA
Quantitative Environmental Analysis, LLC

BATcen:120 **August 2004**

C:\BATman\Maps\ArcGIS\vector\batcen_vectors.mxd

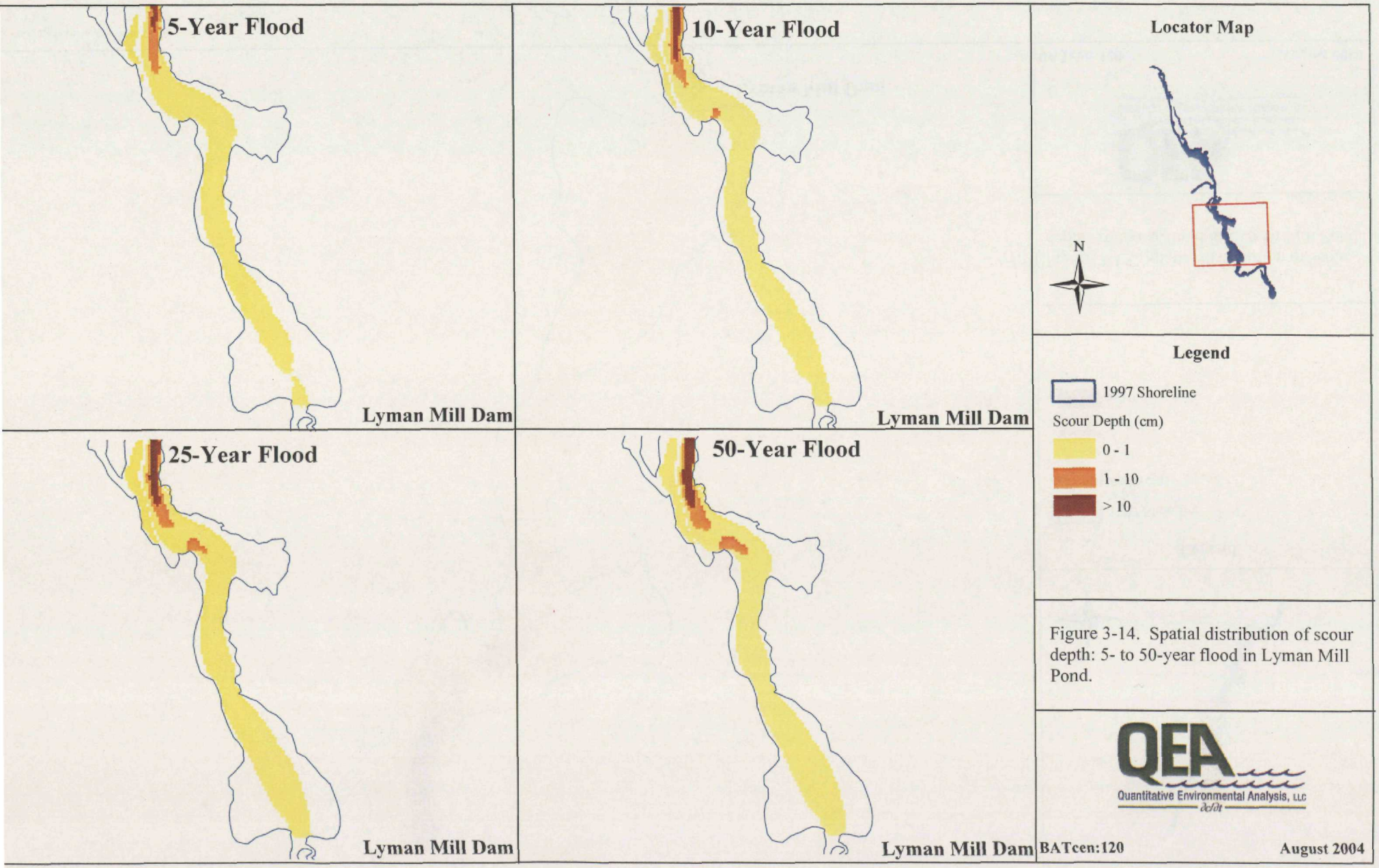

Figure 3-14. Spatial distribution of scour depth: 5- to 50-year flood in Lyman Mill Pond.

CO- C:\BATman\Maps\ArcGIS\scour\batcen_lyman_scour_4panel.mxd

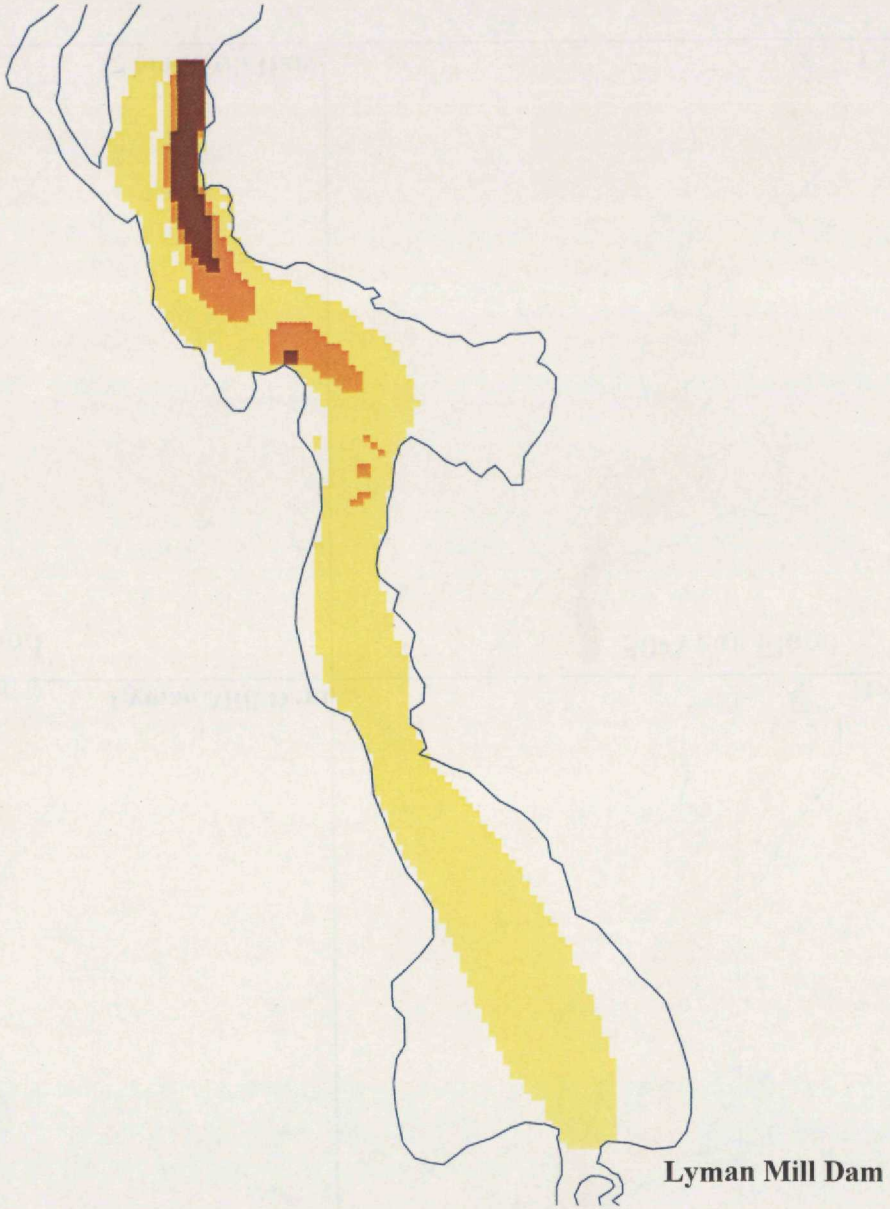

Locator Map

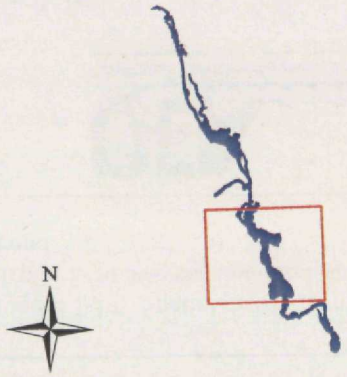

Legend

1997 Shoreline

Scour Depth (cm)

- 0 - 1
- 1 - 10
- > 10

Figure 3-15. Spatial distribution of scour depth: 100-year flood in Lyman Mill Pond.

QEA
Quantitative Environmental Analysis, LLC

BATcen:120 **August 2004**

CO- C:\BATman\Maps\ArcGIS\vector\batcen_vectors.mxd

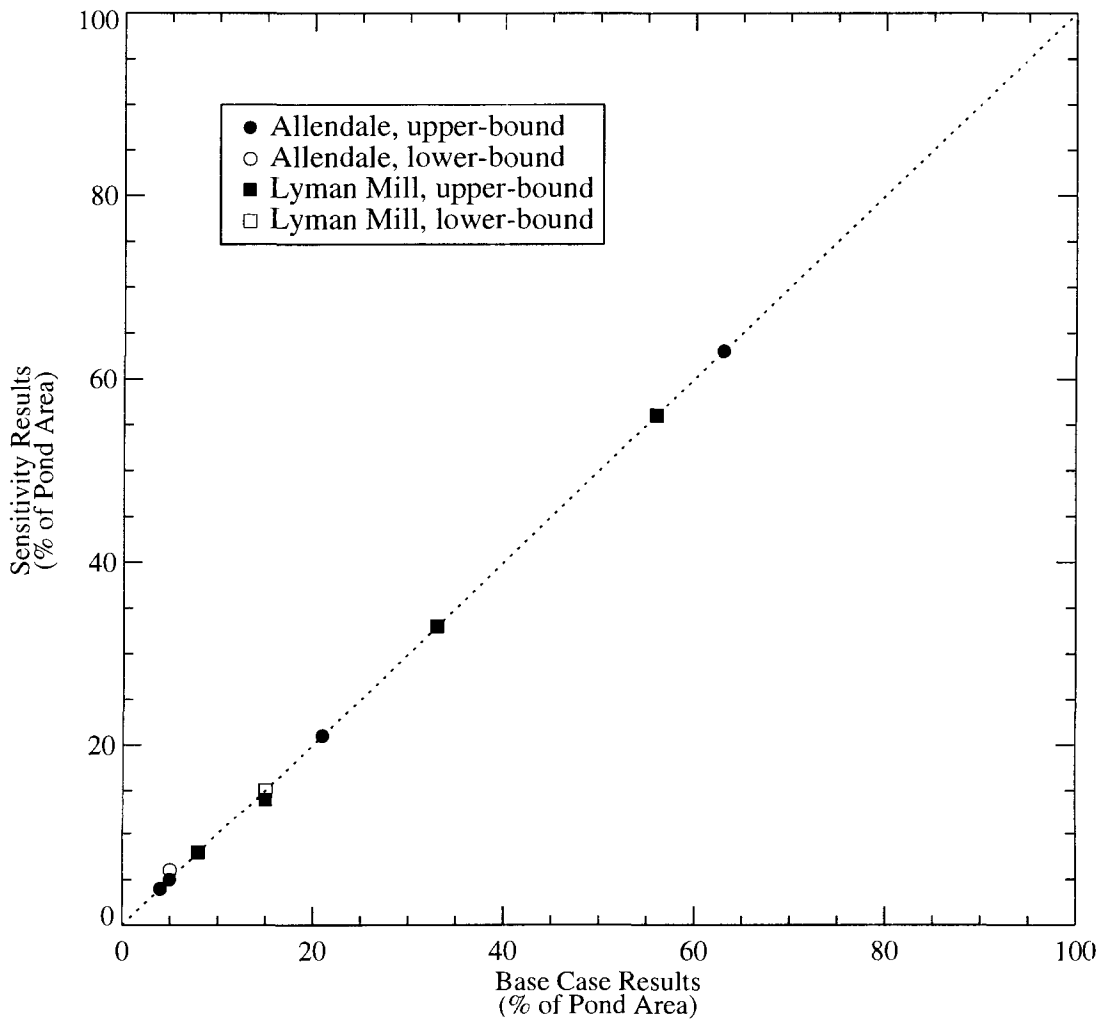

Figure 3-16: Sensitivity analysis results for bottom roughness: % of pond area with $\tau > 0.1$ Pa, $\tau > 0.5$ Pa, $u > 2$ ft/s, and scour depth > 1 cm.

lz - C:\BATman\Analysis\Model_outputs\Sensitivity_plots\plot_fig_3_34.pro
Thu Aug 26 16:08:29 2004

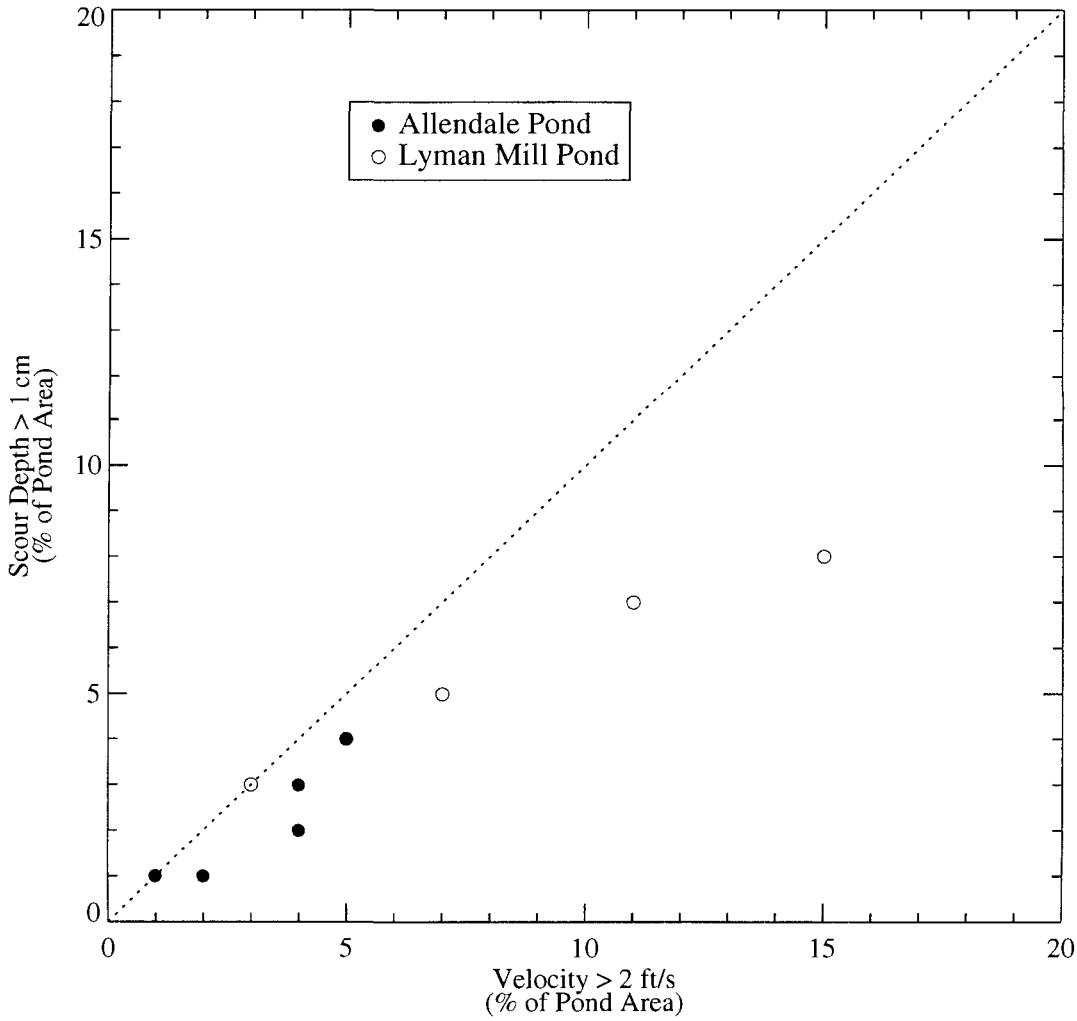

Figure: 3-17: Correlation between area of scour depth > 1 cm and velocity > 2 ft/s (expressed as % of pond area).

lz - C:\BATman\Analysis\Model_outputs\Sensitivity_plots\plot_fig_3_35.pro
Thu Aug 26 16:09:26 2004

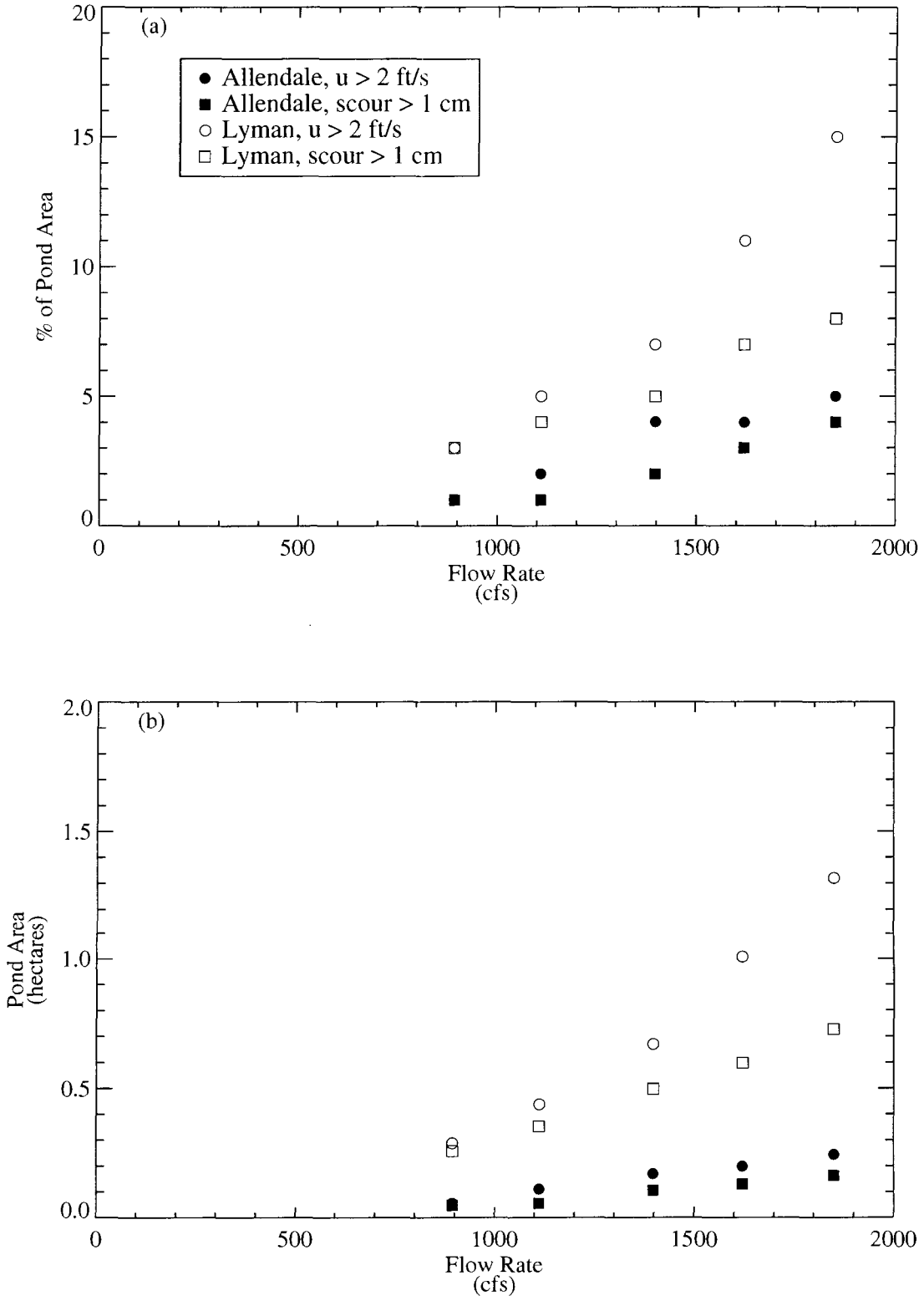

Figure 3-18: Comparison of areas of scour depth > 1 cm and velocity > 2 ft/s between the two ponds: (a) % of pond area vs. flow rate and (b) pond area vs. flow rate.

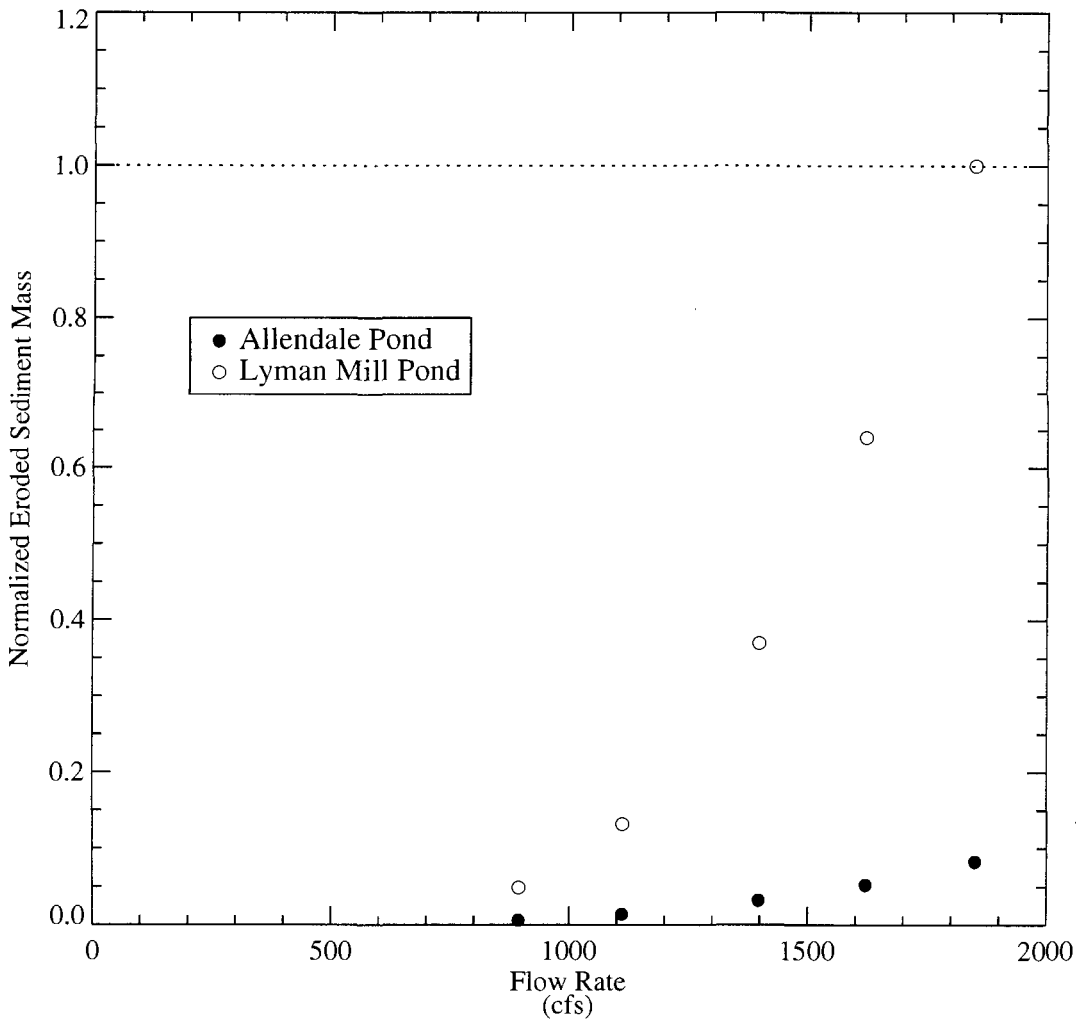

Figure 3-19: Comparison of variation in erosion mass with flow rate between the two ponds. Erosion mass is normalized with respect to the predicted mass for Lyman Mill Pond during a 100-year flood.

lz - C:\BATman\Analysis\Model_outputs\Sensitivity_plots\plot_fig_3_37.pro
Thu Aug 26 16:11:14 2004